Imperial College London

Characterisation of the Type III Secretion System EspO effector family in enteric pathogens

Ph.D. Thesis

Submitted to the Division of Cell and Molecular Biology,
Department of Life Sciences, Imperial College, London
in partial fulfillment of the requirements for the degree of
Doctor of Philosophy

By

Nicholas Constantinou

Imperial College, London

I hereby declare that the work shown in this thesis was performed by the author unless stated otherwise. Any information taken from the literature is appropriately referenced.

“And if you find her poor, Ithaca has not deceived you. Wise as you have become, with so much experience, you must already have understood what these Ithacas mean.” Constantine Cavafy

“The greatest obstacle to discovery is not ignorance; it is the illusion of knowledge.” Daniel J. Boorstin

“The most beautiful thing we can experience is the mysterious. It is the source of all true art and all science. He to whom this emotion is a stranger, who can no longer pause to wonder and stand rapt in awe, is as good as dead: his eyes are closed.” Albert Einstein

Acknowledgements

The commitment and time invested into a Ph.D. research project needs to be appropriately acknowledged and as the Ph.D. candidate and author of this thesis, I would like to express my sincere gratitude to Professor Gadi Frankel who invested in me and my project. Much of this work has resulted from an invaluable help recieved by a great mentor, Dr Abigail Clements. Work done for this project would have been impossible without Dr Cedric Berger who showed a great interest in the project and the input of Dr Valerie Crepin-Sevenou who performed much of the *in-vivo* work. Many thanks to Dr Benoit Reymond, Dr Gunnar Schroeder, Dr Michael Bright, Dr Mariella Lomma, Dr Aurelie Mousnier, Dr Ana Arbeloa, Dr Diana Munera and Dr James Collins for being very helpful in many cases throughout. Dr Alex Wong, Dr Scott Robinson, Leah Ensell, Joanna Young and Clare Harding were all great lab friends.

I would also like to show my appreciation towards the Centre for Molecular Bacteriology and Infection (CMBI) and in general the prestigious establishment of Imperial College for a great research opportunity, full of experiences, challenges but also support when needed. Many thanks should also go to BBSRC and the CASE partner that jointly funded my research. A number of other colleagues, CMBI members and friends are appreciated for their support. Finally, much of my appreciation goes to my family who supported me while going through this experience.

Abstract

Many enteric pathogens employ a type III secretion system to translocate effector proteins directly into the host cell cytoplasm, where they subvert signalling pathways of the intestinal epithelium. Once inside the cell, effector proteins may interact with host cell proteins to control various cellular processes. This enables enteric pathogens to establish their infective niche within the human host.

The T3SS effectors EspO of enterohaemorrhagic *Escherichia coli* and *Citrobacter rodentium*, OspE of *Shigella flexnerie* and SopO of *Salmonella enterica* Serovar Typhimurium are known to interact with integrin-linked kinase to enhance cellular attachment to the substratum. In this project we demonstrate that the EspO family of effectors also interacts with the anti-apoptotic regulator Hax-1 and the co-chaperone DnaJB6.

Employing fluorescence microscopy we found that ectopically expressed EspO resides on large cytosolic vacuoles, which stained positive for the endoplasmic reticulum marker CREB3. Moreover, ectopic expression of EspO changed the cellular distribution of endogenous Hax-1, which co-localized with the EspO vacuoles. We found that the EspO orthologs are anti apoptotic, protecting cells from apoptosis triggered by multiple inducers including staurosporine (a global kinase inhibitor), tunicamycin (induces unfolded protein response) and thapsigargin (interferes with Ca^{2+} homeostasis). Additionally, EspO protects HeLa cells from the apoptosis induced in EPEC infections. Hax-1 depleted HeLa cells by siRNA showed that the anti apoptotic activity of the EspO orthologs is Hax-1 dependent.

Using the *C. rodentium in-vivo* model of EHEC / EPEC infections, we found that deletion of *espO* results in decreased levels of hyperplasia similar to the uninfected control. The mutant strain also showed low levels of neutrophils and CD4+T cells, whereas the EspO complemented strain showed a dramatic increase in both inflammatory cells. These results suggest new mechanisms unique to the T3SS EspO family of effectors, which might shed new insights regarding the infection strategies followed by enteric pathogens. These results suggest new mechanisms unique to the T3SS EspO family of effectors, which might shed new insights regarding the infection strategies followed by enteric pathogens.

Contents

Figures and Tables

List of Abbreviations

A/E lesion	Attaching and Effacing lesion
AD	Activating domain
BD	DNA Binding domain
C. rodentium	*Citrobacter rodentium*
$CaCl_2$	Calcium chloride
DAPI	4',6-diamidino-2-phenylindole
DDO	Double Dropout medium (SD broth/-Leu/-Trp)
DnaJB6	DnaJ homolog, subfamily B, member 6
DMEM	Dulbecco's modified eagle medium
E2348/69	EPEC wild type strain E2348/69
EDL933	EHEC wild type strain EDL933
E. coli	*Escherichia coli*
EHEC	Enterohaemorrhagic *Escherichia coli*
EPEC	Enteropathogenic *Escherichia coli*
Hax-1	HCLS-associated protein X-1
ILK	Integrin-linked kinase
IPTG	Isopropyl β-D-1-thiogalactopyranoside
LB	Luria–Bertani broth
LEE	Locus of enterocyte effacement
LiAc	Lithium Acetate
MBP	Maltose-binding protein
OD_{600}	Optical density at 600 nm
PBS	Phosphate buffered saline
PCR	Polymerase chain reaction
PEG	Polyethylene glycol

RPM	Rotations per minute
RT	Room temperature
QDO	Quadruple Dropout medium (SD broth/-Leu/-Trp/-His/-Ade)
S. Typhimurium	*Salmonella enterica* Serovar Typhimurium
SDS-PAGE	Sodium Dodecyl Sulphate Polyacrylamide Gel Electrophoresis
S. flexneri	*Shigella flexnerie*
STS	Staurosporine
T3SS	Type Three Secretion System
TG	Thapsigargin
TUN	Tunicamycin
TUNEL	Terminal deoxynucleotidyl transferase mediated dUTP Nick End Labeling
Y2H	Yeast two-hybrid

1 Chapter 1 : Introduction

1.1 Enteric Bacterial Pathogens

Enteric bacteria comprise a group within the gamma Proteobacteria and share similar phenotypic characteristics with its members mainly being natural inhabitants of the intestinal tract of humans and animals. They are described as gram-negative, non-sporulating rods that can be motile or non-motile with peritrichous (uniformly distributed around the body) flagella. Escherichia, Salmonella and Shigella are closely related enteric bacteria (Figure 1) and the pathogenic strains within each genus have evolved many strategies to survive within an infected host and avoid the defence mechanisms to establish an efficient colonisation of the intestinal epithelium leading to specific disease outcomes.

Enteropathogenic *E. coli* (EPEC) was the first *E. coli* strain linked to human disease. Although, it is currently prevalent mainly in developing countries as a major cause of infantile diarrheal diseases, recent data may suggest its re-emergence in the UK [1]. EPEC outbreaks are often associated with high mortality rates, which range between 10% and 40%. Humans are considered the main host and outbreaks usually occur as a cause of close contact between children [1]. However, animals (e.g. dogs, cattle) may also act as EPEC reservoirs [2, 3]. The closely related enterohaemorrhagic *E. coli* (EHEC) are foodborne pathogens that cause diarrhoea, haemorrhagic colitis and the potentially lethal haemolytic uraemic syndrome - HUS [4]. Production of Shiga-like toxins (Stx) presents HUS, which is the leading cause of acute paediatric renal failure in the UK and USA. Approximately 1 in every 10 EHEC (particularly serotype O157) cases reported each year in the UK would be

HUS in children under 16. In adults, a complication similar to HUS may occur, which is known as thrombotic thrombocytopenic purpura (TTP) affecting the blood but the brain and nervous system can also be affected. Epidemiological data published by the Health Protection Agency (HPA) show 1182 *E. coli* O157 cases reported in England and Wales for 2011[http://www.hpa.org.uk/Topics/InfectiousDiseases/InfectionsAZ/EscherichiaColiO157/EpidemiologicalData/].

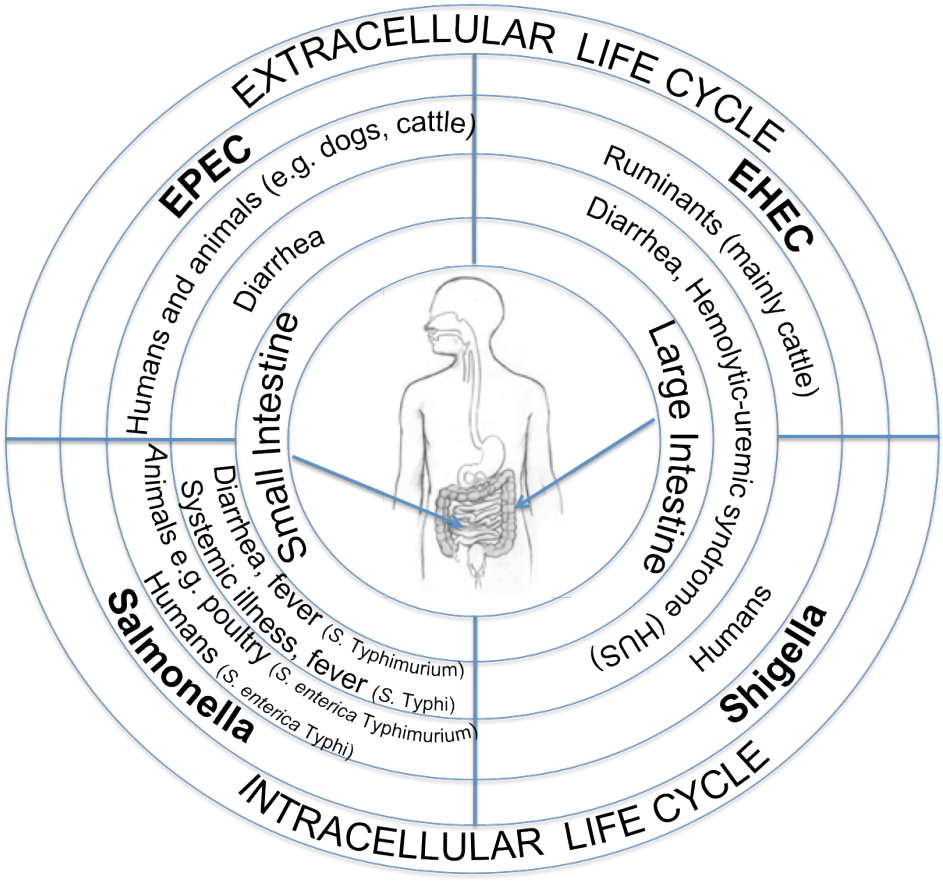

Figure 1. Targeting the intestine (Designed by author)
Diagram shows the relationship between enteropathogenic *E. coli* (EPEC) that infects the small intestine and presents the major cause of infantile diarrheal diseases in developing countries with its main host being humans and animals; enterohaemorrhagic *E. coli* (EHEC) with main reservoir being the cattle and similarly to Shigella, infects the large intestine with the disease outcomes ranging from diarrhea to hemolytic uremic syndrome (HUS) and Non-typhoidal *Salmonella enterica* (e.g. *S.* Typhimurium), which are food-borne pathogens that cause self-limiting gastroenteritis with diarrhea or *S.* Typhi that cause a systemic disease with high fever and headache. Diagram designed by the author for this study.

The genus *Salmonella* contains only the two species, *Salmonella enterica* and *Salmonella bongori,* according to the classification provided by the Centre of Disease Control (CDC) [CDC *Salmonella annual surveillance report summary:* Available at http://www.cdc.gov/ncidod/dbmd/phlisdata/salmonella.htm]. *S. enterica* further subdivides into six subspecies and based on the human clinical syndromes, these are limited to only two types of strains. These types are described as typhoidal or not depending on the specific infecting strain. *Salmonella enterica*, which is also a foodborne pathogen, is considered a significant burden in industrialised and under-developed countries [5, 6]. Non-typhoidal *Salmonella enterica* (NTS) is the cause of self-limiting gastroenteritis and is estimated to cause 1 billion cases (93.8 million cases leading to 155,000 deaths per year according to World Health Organisation – WHO) of foodborne gastroenteritis annually [5]. More recently, multiple antibiotic-resistant strains have emerged as important cause of fatal invasive bacteraemia, particularly in sub-Saharan regions [7, 8]. In epidemiological data provided by HPA for England and Wales, 2000-2010 indicate *S.* Typhimurium (1959 cases in 2010) and *S.* Enteritidis (2444 cases in 2010) the most infectious Salmonella strains [http://www.hpa.org.uk/Topics/InfectiousDiseases/InfectionsAZ/Salmonella/EpidemiologicalData/salmDataHuman/].

Shigella is a genus comprised of four species and these are subdivided into several serotypes. *S. sonnei,* which is the only *Shigella* species with just one serotype is more prevalent in developed countries whereas *S. flexneri* and *S. dysenteriae* are more common in developing countries. Shigellosis remains a global endemic disease responsible for 165 million cases of severe dysentery and 1 million deaths annually, particularly in children less than five years of age. Only in year 2002, the epidemiological data provided by WHO indicate an estimate of 4.5 billion diarrhoeal cases with 1.8 million deaths [http://www.who.int/topics/global_burden_of_disease/en/]. In addition, more than half a

million cases of shigellosis are reported among travellers and military personnel. HUS has been described as a complication of *Shigella* infections and it can be mild with easy recovery but it may also have the more severe outcome, which results in fatal kidney failure [WHO – Guidelines for the control of *Shigella* epidemics: WHO/CDR/95.4, http://www.who.int/csr/en/].

Similar strategies of infection are followed by enteric pathogens, which employ a type III secretion system (T3SS) to deliver bacterial proteins, known as effectors, into the cytosol of the mammalian host cell. These effectors hijack and subvert various host cell processes, including the function of Rho GTPases, actin dynamics, protein ubiquitination, phagocytosis, apoptosis and inflammatory signalling, which enable the pathogen to colonise, multiply, cause disease and spread within the infected host. Unlike EPEC or EHEC, Shigella and Salmonella sp. use their T3SS to invade gut epithelial cells.

Intracellular Shigella gains entry into the basolateral side of the intestinal epithelium by M cell transcytosis (Microfold or M cells are included in the group of epithelial cells and their specialty is the cellular mechanism of vesicular transport of molecules from one side of the cell to the other or from the gut lumen to the underlying mucosa) [9-11]. After release from M cells, Shigella is engulfed by macrophages where it resides within the phagosome very briefly and then escapes, induces cell death and eventually released into the basolateral side [12-14]. Using the T3SS encoded on the Mxi-Spa locus, the pathogen promotes uptake by the intestinal epithelium and soon after engulfment, Shigella escapes the phagosome to spread from cell to cell laterally with the aid of actin based-motility (Figure 2) [15-17]. The escape from the phagosomes also enables the replication of the intracellular organism within the infected host cell [18]. On the contrary, Salmonella invades the intestinal epithelium from the apical surface using the T3SS-1 harboured in Salmonella pathogenicity island 1

(SPI-1). The pathogen resides within the phagosome (Salmonella containing vacuole - SCV) where the SPI-2 T3SS mediates intracellular survival and replication (Figure 2).

EPEC and EHEC colonise the intestinal mucosa, while remaining extracellular, through formation of attaching and effacing (A/E) lesions (Figure 2). These lesions are induced following an interaction between the T3SS effector Tir and the outer membrane adhesin intimin, both of which are encoded on the LEE pathogenicity island. The focus of this project are the T3SS effector orthologs EspO of EHEC O157:H7, which contains two *espO* paralogs, and the A/E mouse pathogen *C. rodentium*, which encodes one copy of *espO*, OspE of *Shigella flexneri* and SopO *Salmonella enterica* serovar Typhimurium.

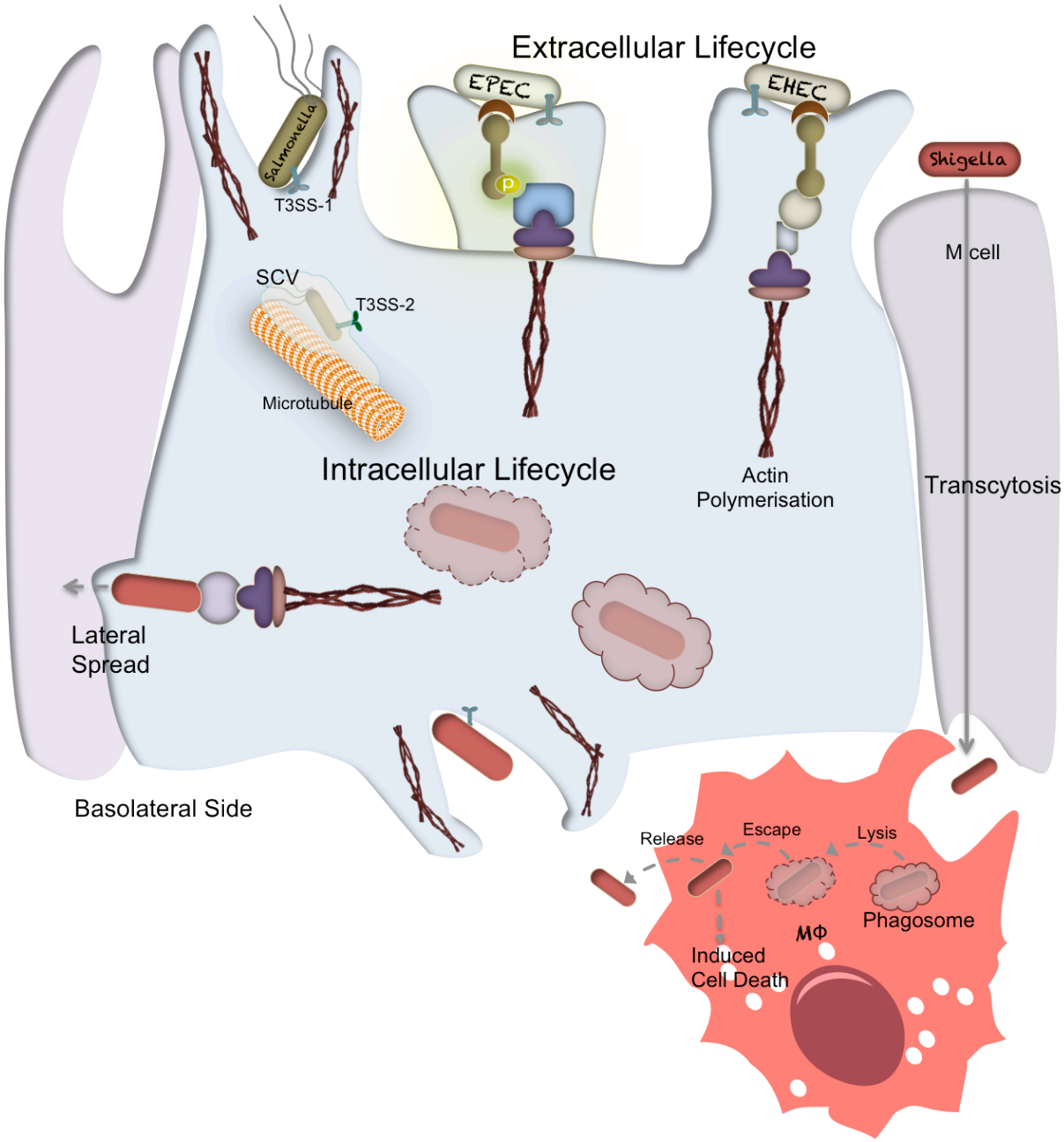

Figure 2. Life cycle of enteric bacteria (Designed by author)
EPEC and EHEC utilise their T3SS to form attaching and effacing lesions shown by the rise of pedestal-like structures on which the bacteria rest to establish their infective niche while remaining extracellular. Shigella and Salmonella invade the intestinal epithelium using their T3SS and further maintain an intracellular life cycle. Details of the host cell signalling processes and T3SS effectors involved in pathogenesis are explained later. Illustration was designed by the author for this study.

1.2 Pathogenic Escherichia coli

Firstly described by Theodor Escherich in 1885 as Gram-negative rod-shaped bacteria, *Escherichia coli* (*E. coli*) is now classified in the family Enterobacteriaceae of the gamma-proteobacteria. As the predominant aerobic bacterial commensal of the gastrointestinal tract of humans and other mammals, *E. coli* can coexist with its host without any disease onset [19]. However a number of *E. coli* clones have acquired virulence abilities, which enable them to cause a wide spectrum of human diseases such as diarrhoea, urinary tract infections, sepsis or meningitis.

Diarrhoeagenic *E. coli* have been traditionally divided into 6 pathotypes (Figure 3). The Enteropathogenic *E. coli* (EPEC) that targets the small bowel epithelium and along with Enterohaemorrhagic *E. coli* (EHEC), which is distinguished by the Stx production and targets the colon, introduced the family of A/E pathogens. Enterotoxigenic *E. coli* (ETEC) targets the small bowel and secretes enterotoxins, whereas Enteroaggregative *E. coli* (EAEC) commonly adheres to both small and large bowel forming biofilms and secreting enterotoxins and cytotoxins. Enteroinvasive *E. coli* (EIEC) similar to Shigella sp. enters the epithelium within a vacuole and moves intracellularly by actin-based motility. Diffusely adherent *E. coli* (DAEC) also acts in the small bowel but induces cellular projections of the microvilli to enclose the bacteria. Recently, another two pathotypes have emerged; Adherent Invasive *E.coli* (AIEC) and the Shiga Toxin producing Enteroaggregative *E.coli* (STEAEC), which was the main cause of the recent outbreak in Europe, 2011 [Published by WHO at http://www.euro.who.int/__data/assets/pdf_file/0009/144981/EHEC_outbreak_10_June_2011.pdf.]

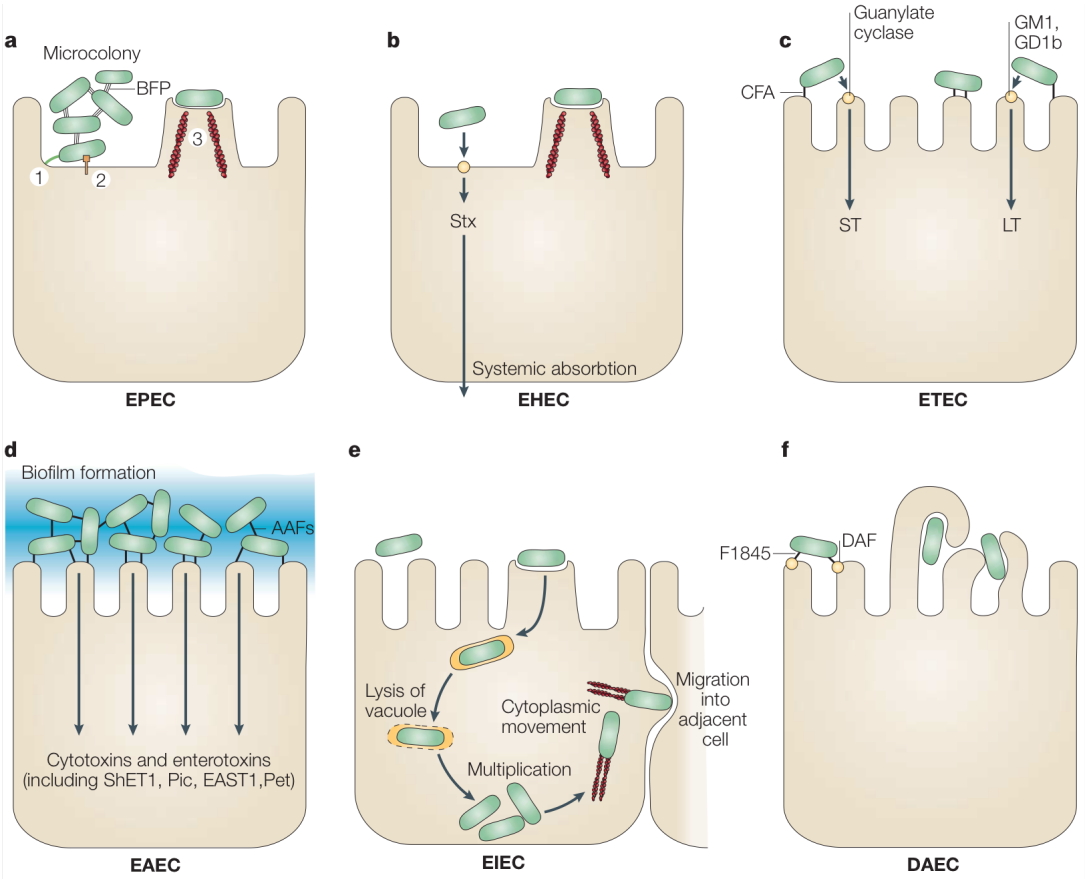

Figure 3. Traditional Diarrhoeagenic *E.coli* pathotypes. [19]
Illustration of the six pathotypes included in the diarrhoeagenic *E. coli.* (a) The Enteropathogenic *E. coli* (EPEC) encoding the bundle-forming pilus [BFP] (a.2) forms microcolonies (a.1) and it is included in the A/E pathogens (a.3) along with Enterohaemorrhagic *E. coli* (EHEC) shown in (b) and Enteroinvasive *E. coli* (EIEC) shown in (e) to form attaching and effacing lesions described by the rise of pedestal-like structures on which the bacteria rest and a functional T3SS is required for the A/E lesions. Diarrhoeagenic *E. coli* also include Enterotoxigenic *E. coli* (ETEC) shown in (c), Enteroaggregative *E. coli* (EAEC) shown in (d) and Diffusely adherent *E. coli* (DAEC) shown in (f), which are included in the pathotypes that are non-T3SS dependent.

Pathogenic strains are differentiated according to specific clinical disease caused, virulence factors and serotypic analysis, which is dependent on the O (somatic) and H (flagellar) antigens. In terms of virulence factors, pathotypes are also divided into T3SS dependent (EHEC, EPEC and EIEC) and non-T3SS dependent (ETEC, EAEC, STEAEC, DEAC and AIEC). A serotype with an emergent medical, as well as scientific, importance is

O157:H7 due to its ability to cause fatal outbreaks of foodborne disease worldwide. *E. coli* O157 is a member of EHEC which is regarded as a zoonotic pathogen with the main reservoir being cattle and other ruminants [20]. Transmission to humans is mediated through the consumption of contaminated food e.g. undercooked meat, milk, fruit and vegetables [21, 22]. Moreover, a human-to-human transmission is possible via the faecal-oral route due to the low infective dose (<100 colony-forming units) [23].

EHEC infections can lead to either non-bloody or bloody diarrhoea, haemorrhagic colitis or haemolytic uremic syndrome [4] with the latter being the most serious complication leading to acute renal failure in children. EHEC strains belong to the larger group of pathogenic clones known as Shiga toxin (Stx) producing *E.coli* (STEC). Most of the EHEC specific symptoms are directly linked to the production of Stx, also known as verocytotoxin. In EHEC, the different Stx variants are all encoded on a bacteriophage [19, 24]. The toxin is released in the colon and induces damages of the intestinal epithelial cells leading to bloody diarrhoea. Upon successful entry into the bloodstream the toxin is transported to the kidney where it destroys the renal endothelial cells leading to HUS.

Although O157:H7 is the most common and virulent serotype implicated worldwide in human disease, non-O157 EHEC serotypes (O26, O103, O111, O118 and O145) are also prevalent. Based on certain phenotypic differences, EHEC is divided into two divergent clones EHEC 1 (Figure 4.a) which includes O157:H7 and O55:H7 (atypical EPEC considered to be the ancestor of O157:H7) and EHEC 2, which includes mainly the non-O157 EHEC serotypes (Figure 4.b).

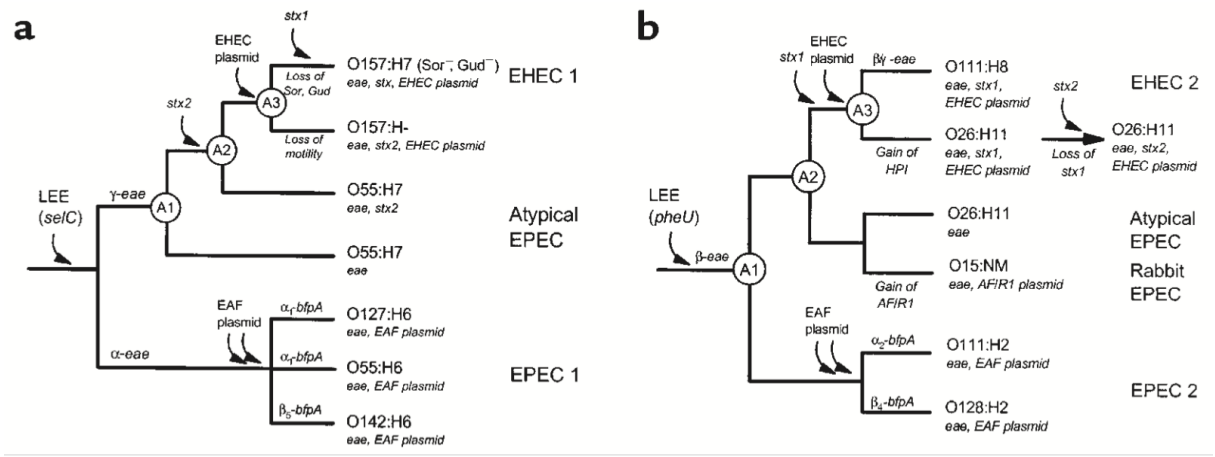

Figure 4. Evolutionary divergence of EPEC and EHEC pathotypes. [25]
Diagram showing evolutionary steps in the divergence of EPEC and EHEC pathotypes. The diagrams depict the presence of the LEE at two different loci; *selC* shown in (a) and *pheU* shown in (b). EHEC is divided into two divergent clones EHEC 1 (3.a) that includes O157:H7 and O55:H7 (atypical EPEC considered to be the ancestor of O157:H7) and EHEC 2 that includes mainly the non-O157 EHEC serotypes (3.b). EPEC strains are divided in lineage 1 (3.a) that are characterised by the expression of the flagellar antigen H6 and O serogroups include O55, O119, O125, O127 and O142. EPEC strains in lineage 2 express the H2 antigen and O serogroups O111, O114, O126 and O128 (3.b). EPEC strains are further divided into typical EPEC (tEPEC) harbouring the EAF plasmid, which encodes the bundle-forming pilus or atypical EPEC (aEPEC) lacking the EAF plasmid.

EPEC strains, frequently described as the cause of infantile diarrhoea in the developing world, are divided into two evolutionally distinct lineages (Figure 4). EPEC strains belonging in lineage 1 (Figure 4.a) are characterised by the expression of the flagellar antigen H6 and O serogroups include O55, O119, O125, O127 and O142. Those in lineage 2 express the H2 antigen and O serogroups include O111, O114, O126 and O128 (Figure 4.b). Additionally, EPEC strains are divided into typical EPEC (tEPEC) to describe strains harbouring the EAF plasmid, which encodes the bundle-forming pilus or atypical EPEC (aEPEC) lacking the EAF plasmid. Typical EPEC consists mainly of the serogroups O55, O86, O111, O119, O127 and O142 and atypical EPEC includes an even broader spectrum of O serogroups.

1.3 Attaching and Effacing Pathogens

Following bacterial colonisation of the gut mucosa, the so-called attaching / effacing (A/E) lesions are formed on the apical surfaces of enterocytes (Figure 5). These characteristic lesions describe the effacement of microvilli and the rise of pedestal-like structures on which the bacteria rest (Figure 1). The ability to form these lesions is dependent on the LEE (locus of enterocyte effacement) pathogenicity island, which encodes a type III secretion system (T3SS), effector proteins (Tir, Map, EspF, EspG, EspH and EspZ), gene regulators, intimin, chaperones and translocators (Figure 5) [26]. The A/E pathogen family includes EHEC, EPEC and the mouse-specific pathogen *Citrobacter rodentium* all of which share the LEE pathogenicity island and various effector proteins [27].

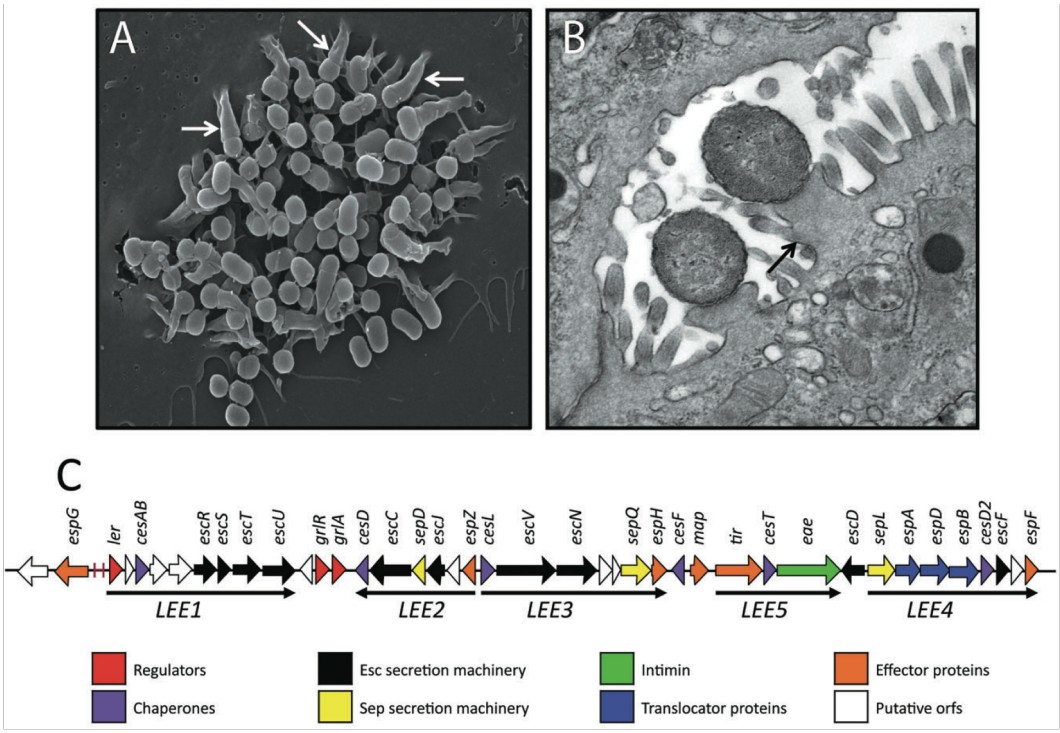

Figure 5. Attaching / Effacing (A/E) lesions in EPEC. [28]
The effacement of microvilli and the rise of pedestal-like structures on which the bacteria rest shown in A. (Scanning Electron Micrograph) and B. (Transmission Electron Micrograph). The genome organisation of LEE (locus of enterocyte effacement) pathogenicity island depicted in C.

The outer membrane adhesin, was the first gene product shown to be essential for this intimate attachement of bacteria [29]. Intimin is encoded by the *eae* gene located within the LEE and following secretion, the adhesin is inserted into the bacterial outer membrane [30]. The A/E pathogens also maintain a gene coding for an intimin-specific receptor. Tir or transmembrane intimin receptor is a LEE-encoded effector translocated via the T3SS into the host cell and targeted to the plasma membrane to interact with intimin and hence, allow the intimate bacterial attachment with the host cell [31, 32]. In addition to Tir, intimin can also interact with nucleolin, a host cell protein shown to be up-regulated in the presence of Stx [33].

Various studies have shown that different EPEC and EHEC strains encode distinct intimin and Tir types. To date, 27 intimin and 8 Tir types have been reported. Differences in the antigenicity of intimins is related to host tissue tropism. For example, the intimin expressed by EHEC O157:H7 has shown tropism towards the human and cattle follicle-associated epithelium [34, 35]. The one expressed by EPEC O127:H7 shows more specificity to the epithelium lining the small intestine and less specificity towards the large intestine, whereas the intimin from EHEC O103:H- shows low adherence levels in both small and large intestine [36, 37].

1.4 Type III secretion system

Gram-negative pathogens are able to interfere with biochemical pathways of their target cells via a complex multiprotein apparatus known as type III secretion system (T3SS), which is used to export effector proteins by directly delivering them into the host cell cytosol, a process known as translocation [38, 39]. Although, at the molecular level the T3SS between enteric pathogens slightly varies, the general consensus comprises of a cytosolic ATPase, the inner and outer membrane rings connected by the periplasmic channel, the projection channel required for protein export and the extracellular needle-like structure or injectisome. Approximately 20 genes encode the structural components of the T3SS.

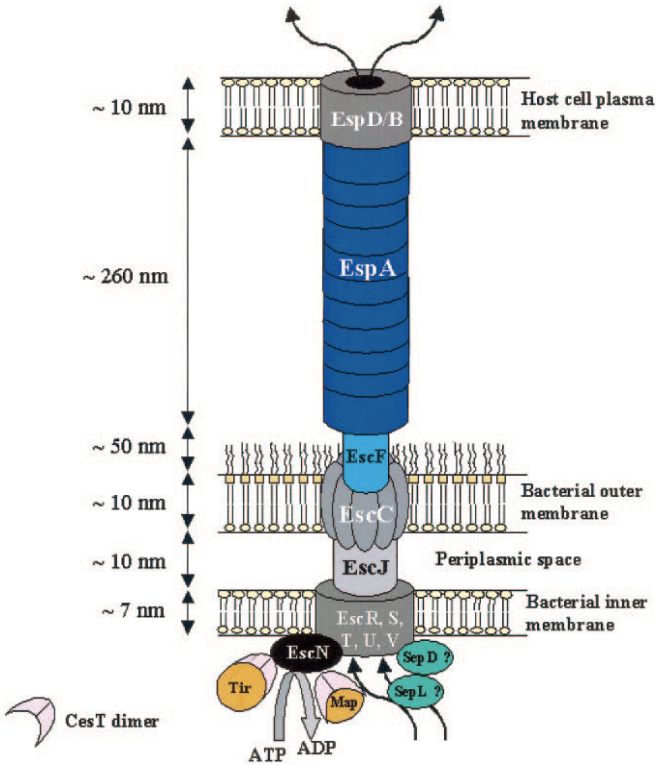

Figure 6. The type III secretion apparatus of EHEC / EPEC. [26]
The illustration depicts the type III secretion apparatus of EHEC and EPEC, which is encoded by genes located on the LEE pathogenicity island. It is comprised of the cytosolic ATPase, the inner (EscR, S, T, U, V) and outer (EscC) membrane rings connected by the periplasmic channel (EscJ), the projection channel (EscF) required for protein export and the extracellular needle-like structure or injectisome (EspA). The translocator proteins EspB and EspD form the membrane translocation pore that allows entry into the host cell cytoplasm.

In EHEC / EPEC the T3SS is comprised of protein rings which span the outer (EscC) and inner (EscR, S, T, U, V) membranes, EscJ which links the two membrane rings through a periplasmic channel and EscF that forms the projection channel required for protein secretion (Figure 6) [26]. In addition, a filamentous extension is generated by the polymerization of the translocator EspA [40]. Effector proteins travel through the EspA filament to reach a membrane translocation pore, formed by the translocator proteins EspB and EspD, which allow the entry into the cytoplasm [41].

The set of genes that encode the T3SS are found on plasmids or pathogenicity islands (PAI). In EHEC or EPEC the T3SS genes are located on the LEE PAI, *S.*Typhimurium has two PAIs called SPI-1 and SPI-2 that harbour the genes encoding for the T3SS and *S. flexneri* contains the T3SS genes within a plasmid. It is thought that horizontal gene transfer events have resulted in the acquisition of the T3SS to many gram-negative bacteria [42]. Despite the fact that all these enteric pathogens share a similar T3SS at the molecular level, there are significant differences in their interactions with host cells and this is mainly due to the diversity in effector repertoires.

There are seven distinct families of T3SS and the *S.* Typhimurium SPI-1 encoded T3SS along with the *S. flexneri* T3SS are the main examples of the second family. The T3SS in EHEC, EPEC and *S.* Typhimurium SPI-2 encoded T3SS are included in the third family [38]. This could be directly related to their pathogenesis where EHEC / EPEC remain extracellular and *Salmonella* or *Shigella* have an intracellular life cycle.

Their entry into epithelial cells but also their intracellular fate differs. For example *Salmonellae* utilize their SPI-1 T3SS to enter through the apical surface and remain enclosed within the SCV where the SPI-2 T3SS maintains survival and replication within the infected host. In contrast, *Shigellae* employ their T3SS to invade the epithelium and then

rapidly lyse the vacuole to enter the cytoplasm for replication and actin-based lateral spread into neighbouring cells [18, 43, 44]. However, EHEC / EPEC utilise their T3SS while being extracellular to translocate effector proteins and further establish an infective niche.

1.5 T3SS Effector Proteins

The translocation of T3SS effector proteins initiates the "biochemical cross-talk" between bacterial pathogens and their target cells [45]. This results in the subversion of various host cell processes, including the function of Rho GTPases, actin dynamics, phagocytosis, apoptosis and inflammatory signalling. In EHEC, the LEE codes for six effector proteins (Map, Tir, EspG, EspF, EspH and EspZ) [26] and at least 62 (including 12 pseudogenes) effector genes are estimated to exist around the chromosome [27, 46]. The diversity of effector protein repertoire within the A/E pathogens has been shown by various genome projects. The EPEC strain E2348/69 encodes 21 effectors and the incomplete genome sequences of EPEC strains E22 and E110019 encode at least 40 and 24 effectors respectively. In addition, the mouse specific A/E pathogen, *C. rodentium* encodes 30 effectors. A total of 21 effector proteins, also known as core effectors, are conserved among EHEC, EPEC and *C. rodentium* [46].

The non-LEE encoded effectors were described when the complete genome sequencing of EHEC O157:H7 has led to the identification of specific loci, named exchangeable effector loci (EELs) which contain most of the genes whose products are predicted or already known to be effectors [47]. The EELs were further divided into three groups; the pathogenicity islands (LEE and SpLE3), the lamboid prophages that contain most of the effector proteins and non-phage EELs. Examples of non-LEE encoded effectors include NleH whose gene is located on lamboid prophage Sp9 and acts as an inhibitor of apoptosis and subverts NFκB [48]; EspJ which is involved in phagocytosis and its gene is found on prophage Sp14 [49]; NleE whose gene is located on SpLE3 pathogenicity island is

known to block the nuclear translocation of p65 subunit of NF-κB leading to the manipulation of the host inflammatory pathway [50].

1.5.1 Interacting with host cells

The initial step towards an established infection, bacterial pathogens adhere or invade host cells through an intimate interaction. The cytoskeleton of the host cell is directly affected from these interactions and it is targeted mainly due to its important role in maintaining a normal cell physiology like cell architecture and selective epithelial permeability, transport and phagocytosis. Enteric bacterial pathogens like EPEC, EHEC, *C. rodentium, S.* Typhimurium and *S. flexneri* whose virulence is dependent to a great extent on the T3SS, inject numerous effector proteins to subvert the host cell cytoskeleton.

In EPEC, EHEC or *C. rodentium* the LEE-encoded effector Tir, which is inserted into the host cell plasma membrane acts as the receptor for the bacterial outer membrane protein, intimin (Figure 7) [31]. This interaction leads to the activation of cellular proteins N-WASP and the Arp2/3 complex leading to actin polymerisation which is responsible for the pedestal formation beneath the attached bacteria [51, 52]. In EPEC infections, the recruitment of N-WASP requires an interaction of Tir and the adaptor protein Nck [53]. This interaction is initiated by the phosphorylation of Tir at tyrosine 474 (Y474p) [54, 55]. On the contrary, EHEC promotes a different process of actin polymerisation due to its Tir lacking a tyrosine 474 equivalent (Figure 7). The T3SS effector protein, TccP (Tir-cytoskeleton coupling protein), also known as EspFu interacts with the proteins IRSp53 and IRTKS, which also bind Tir and thus, providing an indirect link of TccP/EspFu with Tir [56, 57]. This promotes an interaction of TccP/EspFu with N-WASP leading to its activation by

preventing its autoinhibition fold and hence, initiating an Nck-independent actin polymerisation pathway [58].

In contrast to EPEC and EHEC, *Salmonella* and *Shigella* subvert the cytoskeleton by targeting signalling pathways that lead to actin membrane ruffles, which enclose the infecting bacterium and allow the intiation of its intracellular life cycle. In *Salmonella,* the T3SS located on SPI-1 pathogenicity island is used for invasion into the intestinal epithelial cells. The SPI-1 encoded effectors, which are initially translocated into the infected cell to promote the internalisation of Salmonella include SipA [59] and SipC [60] that stabilise actin, SopE or SopE2 that induce membrane ruffles and lamellipodia through Rho-GTPase activation [61], SptP that counteracts the action of SopE and the phosphatidylinositol phosphatase SopB that also modulates invasion by indirect activation of Cdc42 Rho-GTPase [62-64]. Interestingly, SipA stimulates the early activation of caspase-3, which in turn cleaves the effector at a specific recognition motif that leads to two independent functional SipA domains [65]. In *S.* Typhimurium, this process appears to be common for many T3SS effector proteins (e.g. SopA, SopB, SopD, SopE, SptP and SifA) but potential caspase-3 recognition sequences are also predicted to exist in effector proteins from other enteric bacteria (Section 1.7 includes related information on the EspO family of effectors).

Inside the SCV (Salmonella-containing vacuole), the bacteria utilise the T3SS harboured in SPI-2 for intracellular survival and replication. The SPI-2 encoded effector, SifA promotes formation of the Salmonella-induced filaments (Sifs), which protrude from the SCV and elongate along the microtubules [66, 67] (Figure 7). This is suggested to be a Salmonella-specific mechanism used to fascilitate the interaction of SCV with other vesicles and further maintain the integrity of the vacuole [67, 68].

However, Shigella enters the intestinal epithelial cells through the basolateral side of the intestinal epithelium (Figure 7). The pathogen moves through M cells by transcytosis and upon release, Shigella is taken by macrophages where it can replicate and cause cell death [69]. When macrophages die, the bacteria are released in the submucosa and access the basolateral site of the epithelium. Host cell adhesion of Shigella is mediated by the interaction of the T3SS translocator proteins with two receptors. The translocator IpaB binds CD44 and the complex IpaBCD binds integrin α5β1, which result in lipid rafts accumulating at the site of bacterial entry [70, 71].

Similar to Salmonella, Shigella also induces actin membrane ruffles that enclose the bacteria and promote invasion. The process of internalisation followed by escape from phagolysosome is mediated by the action of T3SS effectors like the bacterial Rho GTPases IpaC [72], IpgB1 and IpgB2 [73-75], IpaA that promotes actin depolymerisation [75], the EPEC/EHEC EspG homolog, VirA that destabilises microtubules [76] and the IpaB [77] and IpaH(7.8) [78] that allow the phagosomal escape. Additionally, the inositol 4-phosphatase IpgD dephosphorylates phosphatidylinositol-4,5-biphosphate and this results in membrane and actin remodelling [79].

After lysis of the phagosome, Shigella establishes its replicative niche within the cytosol and further spreads laterally to neighbouring cells through actin-based motility. The recruitment of the T3SS effector VirG (also known as IcsA or intracellular spread A) at one pole of the bacterial cell allows directed motility within the cytoplasm of the infected cell [15, 80]. VirG attracts and further activates the actin polymerisation proteins, N-WASP and ARP 2/3 [81-83]. However, VirG is also targeted by the autophagy protein 5 (ATG5) and its integrity as well as inhibition of autophagy is maintained by the effector IcsB [84]. Additionally, the intracellular movement and lateral spread of Shigella requires VirA to degrade α-tubulin and further destabilise the microtubule network [85].

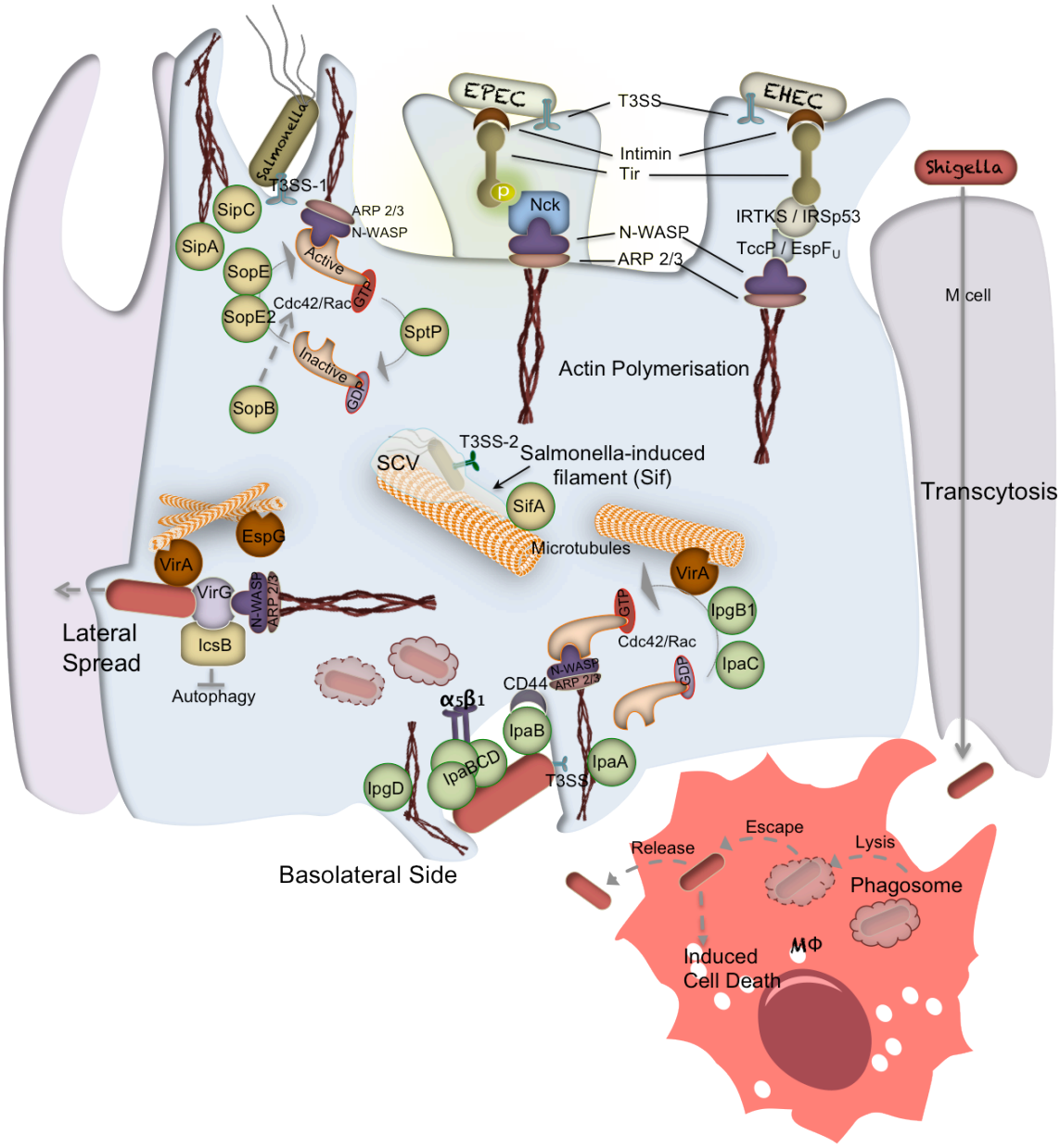

Figure 7. Bacterial interactions with host cell (Designed by author)
EPEC / EHEC T3SS effector Tir binds intimin to initiate actin polymerisation leading to pedestal formation. In EPEC phosphorylation of Tir initiates the interaction with Nck adaptor that recruits N-WASP and ARP 2/3, whereas EHEC Tir recruits the IRTKS/IRSp53 proteins, which interact with the T3SS effector TccP/EspFu that activates N-WASP. Salmonella SPI-1 T3SS effectors SopE, SopE2, SopB, SptP, SipA and SipC are all essential for internalisation. The integrity of the Salmonella-containing vacuole (SCV) is fascilitated by the SPI-2 T3SS effector SifA. Shigella translocators IpaB and the complex IpaBCD are required for host cell receptor binding. The effectors IpgB, VirA, IpaA and IpgD mediate Shigella invasion. The Shigella effector VirG is protected by IcsB that inhibits autophagy and allows VirG to recruit N-WASP and ARP 2/3 for actin-based movement. The Shigella VirA, which is the EPEC/EHEC EspG homolog disrupts the microtubule network and promotes intracellular movement and lateral spread of Shigella. Illustration designed by the author for this study.

In addition, T3SS effectors that are known to disrupt the Rho GTPase signalling and therefore, modulate the actin dynamics are also found in EPEC or EHEC [86] (Figure 8). The Rho family of small G proteins involved in the regulation of crucial cellular functions include Cdc42, Rac1 and RhoA, which induce filopodia, lamellipodia/ruffles and stress fibers respectively [87]. Bacterial effector proteins involved in the Rho GTPase signalling were grouped in the WxxxE family based on a conserved motif of two amino acids Trp and Glu separated by three variable amino acids [74]. The family comprises members from EPEC/EHEC e.g. Map, EspM, EspT, from Shigella spp e.g. IpgB1, IpgB2, IpaC and VirA and from Salmonella spp e.g. SopE, SopE2, SopB, SptP and SifA [63, 72, 74, 76, 86].

The T3SS effectors can function as guanine exchange factors (GEFs), which control the switch from the inactive GDP-bound to the active GTP-bound state, or GTPase-activating proteins (GAPs), which control the hydrolysis of GTP to revert back to the inactive state [88, 89]. Map and EspM function as GEFs on Cdc42 and RhoA respectively and EspT activates both Rac1 and Cdc42 [90-92]. Subversion of actin dynamics was also shown with the T3SS effector EspH which affects filopodia and pedestal formation by inactivating the mammalian only Rho GEFs, suggesting an EspH-dependent clearance of eukaryotic GEFs allowing the bacterial GEFs / WxxxE effectors to modulate the Rho GTPase signalling [93, 94]. Interestingly, a large number of the WxxxE repertoire is involved in the disruption of tight junctions and intestinal barrier [86]. Examples from EPEC or EHEC include Map and EspF from the WxxxE family (but also EspI) and the Salmonella SopB, SopE, SopE2 and SipA may additionally disrupt the tight junctions (Figure 8) [26, 95, 96].

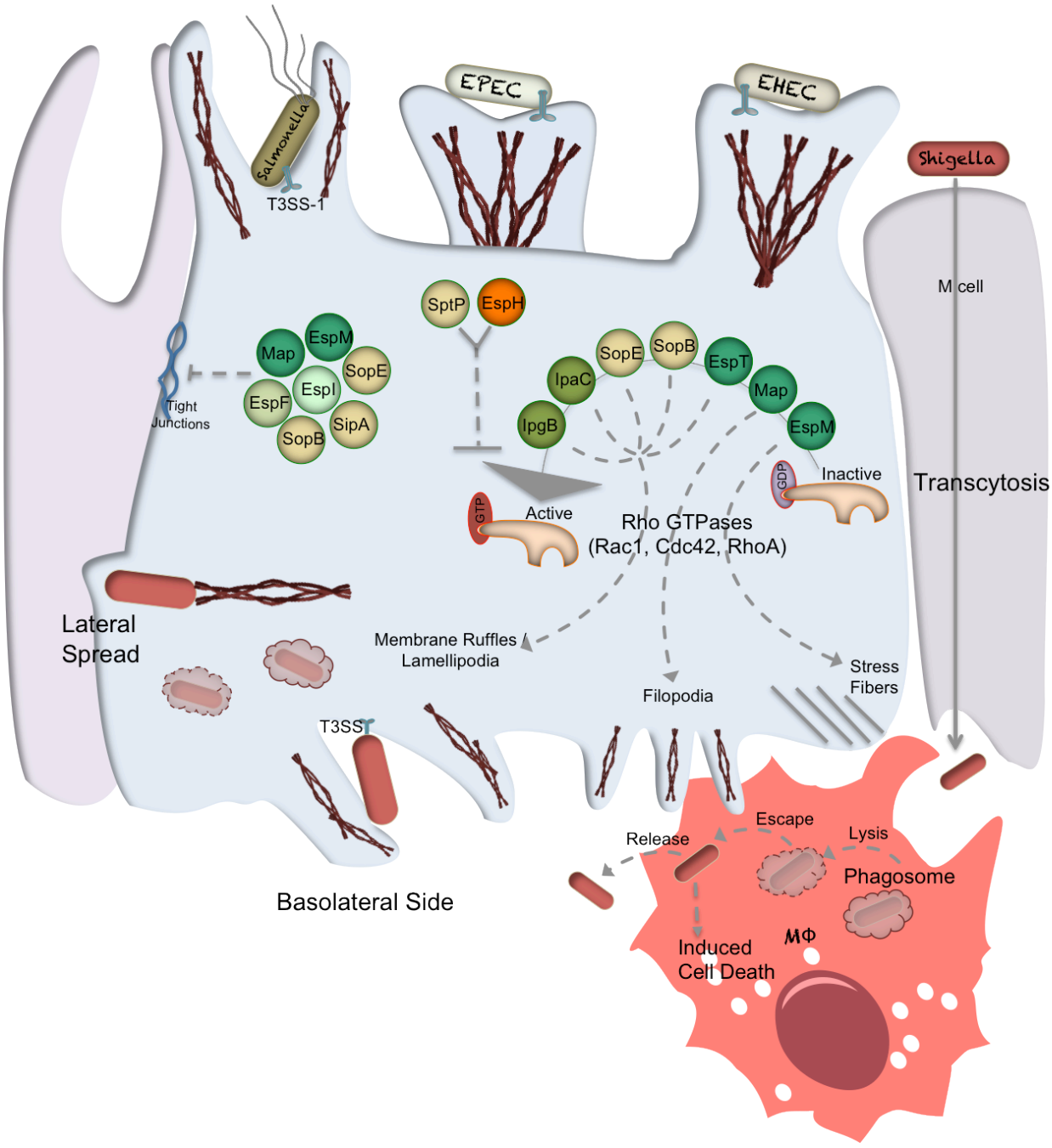

Figure 8. Modulating the actin dynamics (Designed by author)
Examples of T3SS effectors in EPEC / EHEC (Map, EspT, EspM and EspH), Salmonella (SopE, SopB and SptP) and Shigella spp. (IpgB and IpaC) that subvert the small G-protein signalling by direct activation or deactivation of the Rho GTPase family members Rac1 that induces membrane ruffles or lamellipodia, Cdc42 that promotes filopodia formation and RhoA that induces stress fibers. In addition to other effectors, many of the Rho GTPase signalling modulators may also dirsupt the tight junctions or intestinal barrier function. Illustration was designed by the author for this study.

1.5.2 Pass-through host cell defence

Apart from the intimate interactions with the intestinal epithelila cells, the T3SS is also necessary for avoiding the immune system. When bacterial pathogens enter the intestinal epithelium, the host cell pattern recognition is triggered via pattern recognition receptors (PRRs) and the innate or adaptive host cell immune response is activated. The PRRs include the Toll-like receptor family (TLR) and the Nod-like receptor family, which can specifically sense the pathogen-associated molecular patterns (PAMPs). These are pathogen-related motifs that involve the bacterial flagella and lipopolysaccharides. Once the PAMPs are recognised, the PRRs can activate the immune signalling responses leading to the phosphorylation and degradation of the inhibitory IκB proteins allowing the release of the bound dimeric transcription factor NF-κB [97, 98]. This is followed by the translocation of NF-κB to the nucleus and hence, initiation of transcription that is specific to inflammatory response (Figure 9).

Successful colonization leading to an established EHEC / EPEC infection requires amongst other factors, the bacterial manipulation of the host immune response and inhibition of phagocytosis. The NF-κB nuclear translocation is blocked by the effector proteins NleE and NleB (Figure 9), which inhibit the IκB degradation [50, 99]. The metalloproteases NleC and NleD can prohibit inflammatory responses by either targeting NF-κB or the mitogen activated protein kinases c-Jun N-terminal Kinase (JNK) and p38 respectively [100, 101]. In addition, previous work on the NleH effectors has shown both an upregulation of inflammatory responses but also an attenuation of NF-κB activation [102, 103]. NleH1 blocks the nuclear translocation of the RPS3 subunit of NF-κB whereas NleH2 induces expression of RPS3 coding genes [103-105]. The balance of pro- and anti-inflammatory responses is further maintained by the action of the multifunctional effector

EspT, which in addition to its role in actin polymerisation it can also induce the expression of pro-inflammatory genes through Erk, JNK and NF-κB pathways [106].

Similar to EHEC / EPEC, examples of T3SS effectors involved in the manipulation of immune responses also exist in other enteric pathogens such as *Shigella* and *Salmonella*. The *Shigella* effector OspF and the *Salmonella* homologue, SpvC block MAP kinase phosphorylation and down-regulate the expression of a subset of NF-κB-dependent genes [107-109]. OspZ, the NleE homologue from Shigella, shares the same NF-κB inhibitory activity [50]. The EHEC / EPEC NleH effectors are homologous to the Shigella OspG, which inhibits degradation of IκB and therefore, blocks activation of NF-κB [102, 110]. The $IpaH_{9.8}$ from Shigella and the SspH1 from Salmonella act as E3 ubiquitin ligases and affect the inflammatory MAPK signalling [111, 112]. Additionally, the Shigella effectors OspB and OspF were shown to cause particular chromatin remodelling that dampens the levels of IL-8 production [113]. Furthermore, the activity of SspH1 in Salmonella is balanced by the SPI-2 T3SS effector SseL, which acts as a deubiquitinase [114]. In *Salmonella*, the T3SS located on SPI-2 is also required for the systemic spread of the infection via infected phagocytes that is regulated by the SPI-2 T3SS effector, SrfH/SseI [115].

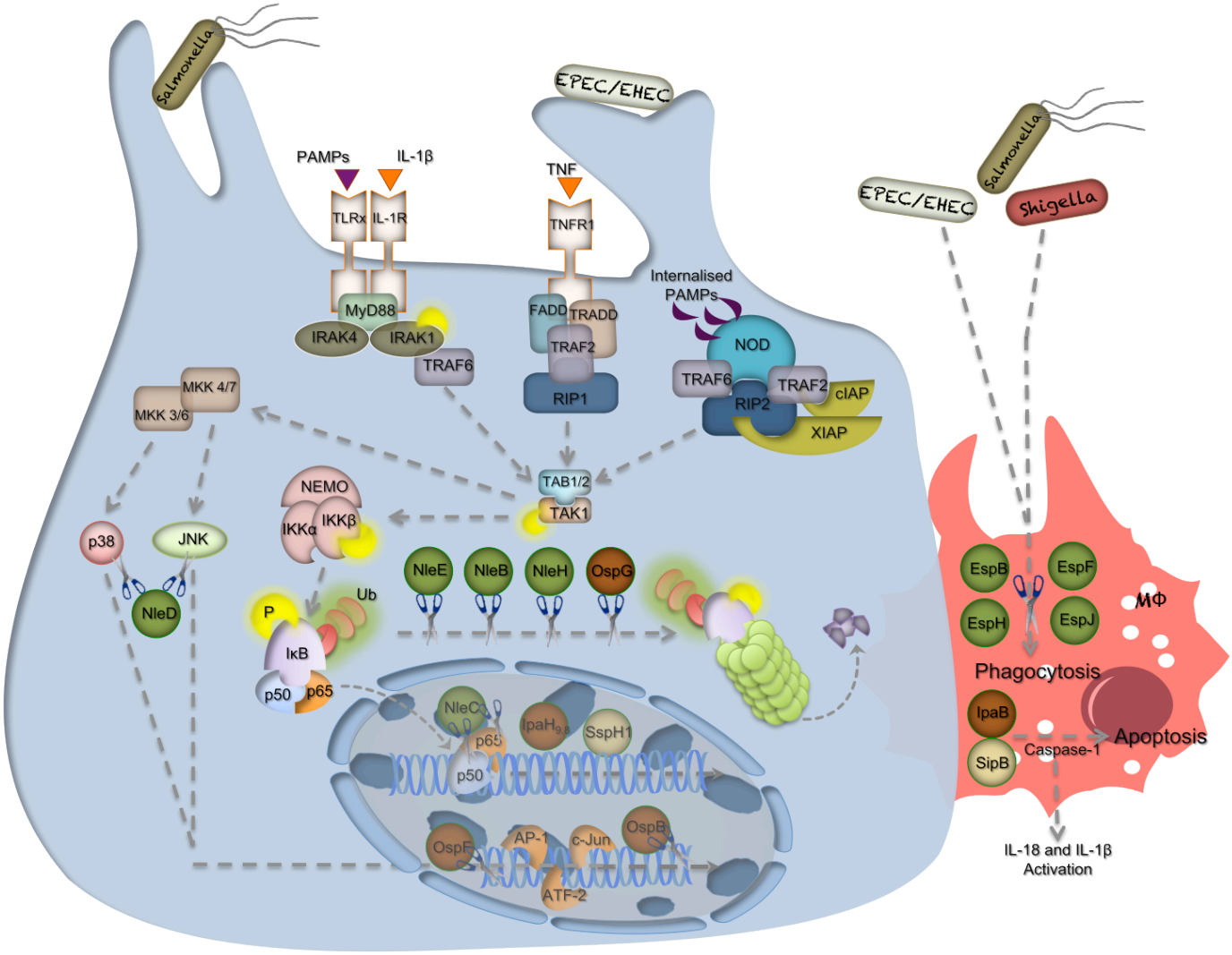

Figure 9. Manipulation of host cell defence (Designed by author)
Receptors sense bacterial infection and activate the downstream inflammatory signalling pathways. EPEC or EHEC effectors NleE, NleB, NleH and Shigella effector OspG inhibit the degradation of IκB and hence, suppress the nuclear translocation of NF-κB dimers p50 and p63. EPEC / EHEC effector, NleD targets JNK and p38 to suppress activation of AP-1, ATF-2 and c-Jun transcription factors. NleC (EPEC / EHEC), $IpaH_{9.8}$, OspF and OspB (Shigella) and SspH1 (Salmonella) are targeted to the nucleus and affect cytokine transcription levels. Host cell defence is also avoided through direct inhibition of immune cells; EPEC / EHEC effectors EspB, EspF, EspJ and EspH suppress phagocytosis and IpaB from Shigella or SipB from Salmonella induce cell death in macrophages through activation of the inflammatory caspase-1, which results in the activation and release of the proinflammatory cytokines IL-18 and IL-1β. Illustration was designed by the author for this study.

EHEC / EPEC have also evolved mechanisms to inhibit phagocytosis and therefore, maintain their extracellular life cycle. Internalisation of both unopsonised (cis-phagocytosis) and opsonised (trans-phagocytosis) bacteria, is inhibited by the effector EspF (Figure 9), which inhibits PI3K activation [116]. EspB can interact with several members of the myosin superfamily and hence, inhibit cis-phagocytosis whereas EspJ has been shown to inhibit trans-phagocytosis [117, 118]. Additionally, the effector EspH, which was previously shown to inactivate the Rho GTPase signalling, can also inhibit both cis- and trans- phagocytosis [94].

Both *Salmonella* and *Shigella* utilise mechanisms that allow survival within the phagosome and therefore, maintain their intracellular cycle. For example, *Salmonella* can survive within the macrophages by suppressing the phagocytic process in a SPI-2 T3SS fashion [119, 120]. In *Shigella,* the T3SS effector VirG that is essential for the intracellular actin-based motility, may also induce autophagy. This is suppressed by the action of another T3SS effector, IcsB that protects VirG from the cellular autophagy protein 5 (ATG5) and therefore, promote intracellular survival (Figure 7) [84]. In addition, the *S.*Typhimurium SipB translocated by the SPI-1 T3SS is known to induce a rapid onset of apoptosis through binding and activating the pro-apoptotic caspase-1 (Figure 9) [114, 121]. This apoptotic mechanism is also shared by the effector IpaB, the SipB homologue in Shigella [122, 123]. Activation of caspase-1 results in the cleavage of pro-IL-1β and pro-IL-18 that generates their active forms and their subsequent release from the dying macrophage [124, 125].

1.5.3 Fighting for survival

An established infective niche within the host is further maintained by balancing pro- and anti- apoptotic effectors to modulate apoptosis. Also known as programmed cell death, it describes the tightly regulated form of cell death that is mediated by specialised proteases named caspases, which regulate all three pathways (Discussed in detail later). It has been shown that apoptotic pathways are initiated in EHEC / EPEC infection and they can be triggered by either bacterial surface properties or the translocation of effector proteins [126, 127]. Known effector proteins involved in the induction of apoptosis include the effectors, EspF and Cycle inhibitory factor (Cif) (Figure 10). EspF is targeted to the mitochondria to interfere with the mitochondrial membrane potential, which induces the release of cytochrome c and cleavage of caspases -9 and -3 [128]. Cif has been shown to function as a bacterial cyclomodulin subverting the eukaryotic cell cycle resulting in apoptosis [129].

The action of pro-apoptotic effectors in EHEC / EPEC is balanced with the NleH family effectors, which block apoptosis via an interaction with the anti-apoptotic protein, Bax Inhibitor-1 [48]. The effector NleD also has an anti-apoptotic function by inactivating JNK, which results in the suppression of the transcription factor AP-1 involved in the regulation of apoptosis, proliferation and inflammation [101]. In addition, the EPEC or EHEC EspO family of effectors that includes OspE from Shigella and SopO from Salmonella bind integrin linked kinase (ILK) to promote the cell attachment to the submucosa and hence, maintain cell survival [130] (Figure 10). Similarly, the effector EspZ binds CD98, a host protein involved in integrin mediated cell adhesion and survival [131].

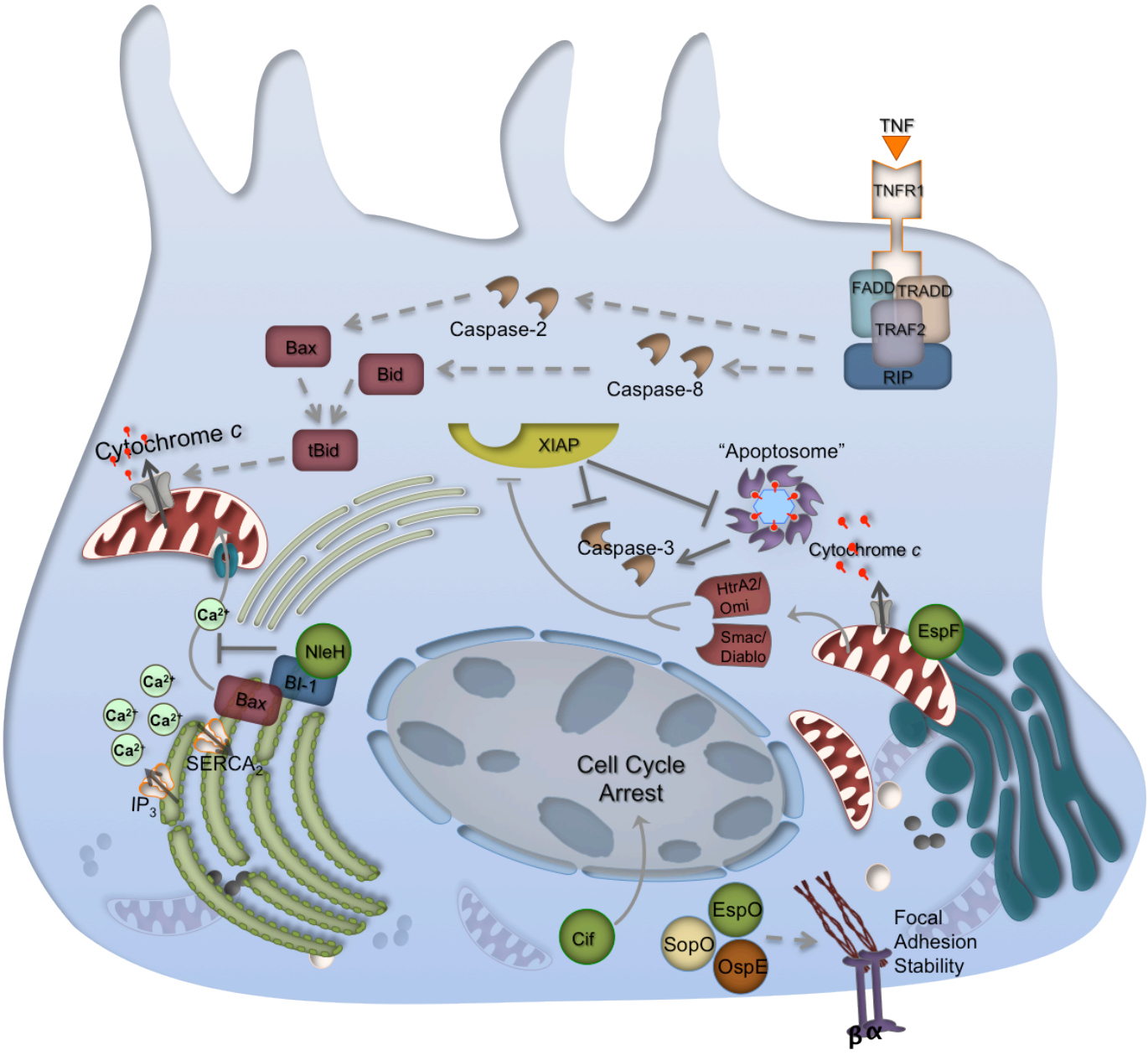

Figure 10. Balancing apoptosis (Designed by author)
Activation of apoptotic pathways by EPEC or EHEC effectors EspF (disruption of mitochondrial membrane potential) and Cif (cell cycle arrest) is balanced by the anti-apoptotic effector NleH that binds Bax-inhibitor 1 (BI-1). The EspO family of effectors that includes EspO from EPEC/EHEC, OspE from Shigella and SopO from Salmonella maintain cell survival through enhanced cell attachment. Illustration was designed by the author for this study.

As previously mentioned both Salmonella and Shigella are able to induce caspase-1 dependent apoptosis in macrophages [132, 133]. Salmonella was shown to induce apoptotic death in either SPI-1 or SPI-2 manner [134]. The SPI-1 T3SS effector SipB is involved in the caspase-1 dependent cell death, which is an early onset of apoptosis during the course of infection but interestingly, it can also induce a delayed apoptotic event that is caspase-1 independent [121, 135-137]. After prolonged infection, Salmonella may additionally utilise the SPI-2 T3SS to induce apoptosis in a caspase-1 dependent fashion in macrophages or via caspase-3 activation in epithelial cells [138-140]. The Salmonella SipB homolog in Shigella is IpaB and shares the same apoptotic function that mediates cell death through caspase-1 activation in macrophages [123, 141].

These apoptotic events are balanced by the SPI-1 T3SS effector SopB from Salmonella and its homolog IpgD from Shigella, which activate the phosphatidylinositol 3-kinase (PI3K)/Akt pathway [142, 143]. Akt is an anti-apoptotic protein that inhibits the release of cytochrome-c from mitochondria and therefore, prevents the activation of caspases [144]. Furthermore, the Shigella induced apoptosis in epithelial cells is inhibited by genes regulated by MxiE, the transcriptional activator of genes encoding a second wave of effectors that are secreted via the T3SS machinery intracellularly [145-147]. Intriguingly, the transcription of *ospE* (the *espO* homologue in Shigella) is under the control of MxiE [148].

1.6 *Citrobacter rodentium*: *In-vivo* model of infection

Citrobacter rodentium was firstly found in the mid-1960s from sporadic murine diarrhoeal outbreaks [149-151]. At the time, it was designated as an atypical *Citrobacter freundii* strain as the causative agent of one of these outbreaks and classified as atypical murine pathogenic *E. coli* (MPEC) for another [149, 150]. However, it was later shown that in all cases diarrhoea was accompanied by epithelial cell hyperproliferation or hyperplasia in the descending colon and in addition, their DNA relatedness has led to the classification of all *C. freundii* and MPEC isolates as *C. rodentium* species [152, 153].

The infectious disease is now known as transmissible murine colonic hyperplasia (TMCH) and describes pathological changes such as thickening of the colon, intestinal epithelial crypt elongation and goblet cell loss [153, 154]. Colonic tissue extracted from infected mice has shown intimate attachment of the bacteria to the epithelial cell surface with localised destruction of the brush-border microvilli, reminiscent of the A/E lesions in EPEC and EHEC infections [153]. As previously discussed, the A/E lesion formation is essential for pathogenicity and the genes responsible for induction of these lesions are harboured in the LEE pathogenicity island (*Reviewed in Section 1.3*). Therefore, due to its natural virulence in mice and the inability of EPEC / EHEC to infect mice, *C. rodentium* acts as an ideal *in-vivo* animal model for infection.

The roles of both LEE and non-LEE effectors and virulence genes in TMCH have been studied extensively in *C. rodentium*. Absence of the T3SS intimin receptor, Tir has shown attenuated *C. rodentium* colonization and virulence in mice [155, 156]. Map, which is known to interfere with the mitochondrial function, disrupt the intestinal barrier and

induce formation of filopodia shows no significant changes in colonization and disease when absent [157, 158]. Infection with an EspF (involved in mitochondrial membrane permeabilisation and disruption of the intestinal barrier) mutant indicated a moderate attenuation, whereas EspG (involved in microtubule network disruption) is not essential for pathogenesis *in-vivo* [158]. In addition, non-LEE effectors, which are not required for A/E lesion formation, still exhibit a significant role in infection as shown in competitive studies of *C. rodentium* mixed infections of wild-type and mutant strains. EspI/NleA mutant is rapidly outcompeted by the wt strain and mice infected with an EspJ mutant took longer to clear [49, 157].

1.7 Programmed Cell Death: Apoptosis

1.7.1 Cell Death: An Overview

Cell death was firstly identified in 1858 but knowledge within the field has mainly increased only in the past 40 years [159]. Historically, different terms of the cell death concept have been introduced to describe the three major morphologically distinct pathways of cell death (Figure 11); by the genetic mechanism named apoptosis or Type I programmed cell death; by lysosomes, which mainly describe the Type II programmed cell death or autophagy but also involved in necrosis and apoptosis; and by physicochemical stress e.g. heat shock or free radicals leading to necrosis [159]. Although, cell death may occur through a variety of biochemically distinct pathways, they are all interconnected to provide a fundamental cellular response that plays an important role in animal development and tissue homeostasis [159, 160].

Within the last 20 years, the mechanisms underlying cell death have been limited to the programmed or tightly regulated form of cell death as opposed to the more unordered or accidental form [159]. Ischemic cell death or oncosis, which describes the failure of ionic pumps in the plasma membrane, is considered to be the only accidental form of cell death [159, 161]. Although, necrosis has been improperly coined as a term to describe accidental cell death, it is now considered as a regulated process that includes the secondary changes resulting from any cell death mechanism [160, 161]. The main feature of accidental cell death is swelling, which led to the name oncosis (derived from the Greek onkos, meaning swelling) [159]. Oncosis leads to necrosis with cellular swelling, membrane blebbing and karyolysis (dissolution of the cell nucleus) as opposed to apoptosis, which leads to necrosis

with cell shrinkage, chromatin condensation (pyknosis) and karyorhexis (nuclear fragmentation) [159-161].

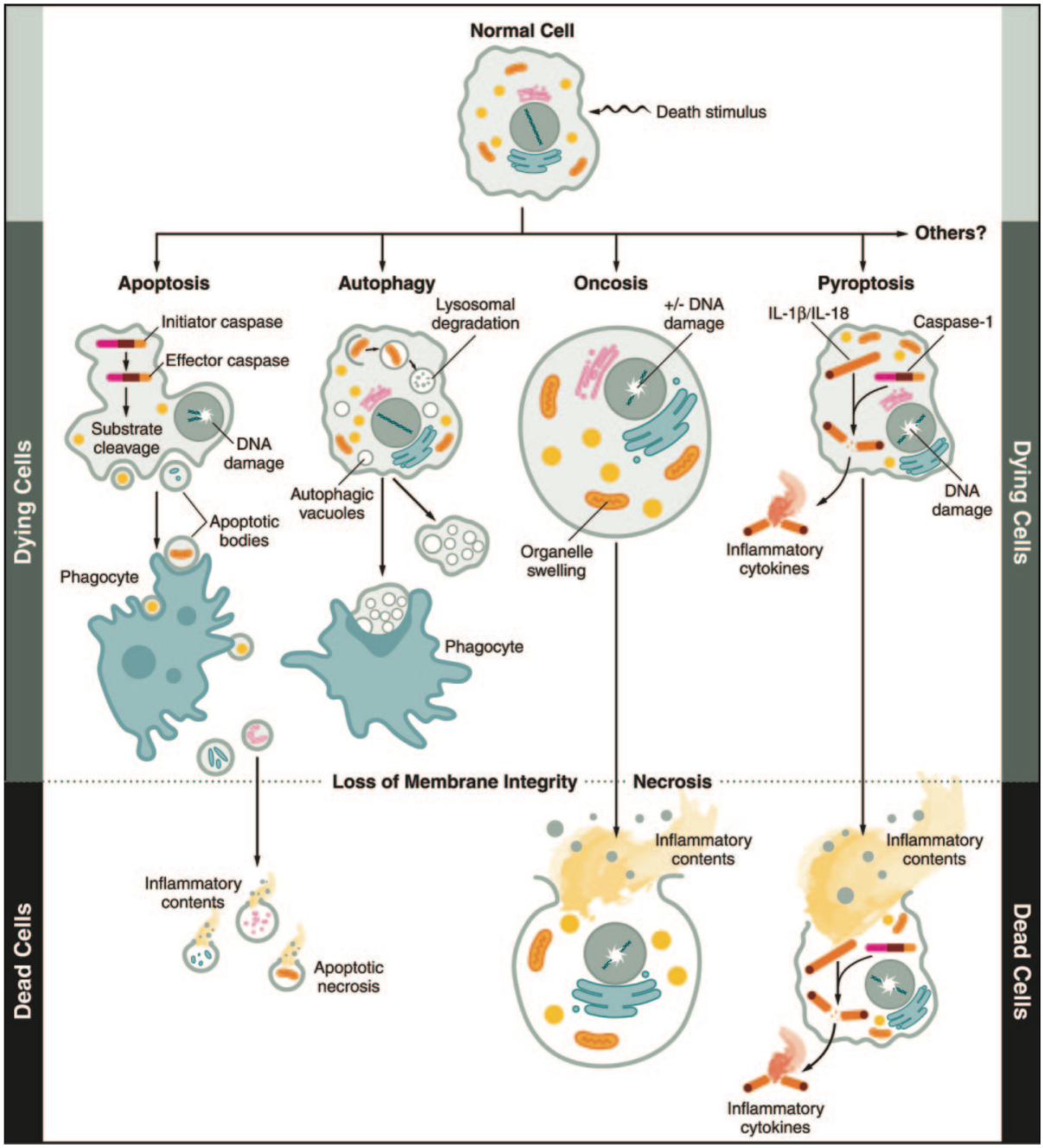

Figure 11. An overview of the major pathways of cell death. [162]

1.7.2 Programmed Cell Death

Programmed cell death Type I or apoptosis is the best-characterised type of regulated cell suicide and describes the typical morphological features of apoptotic cells, which eventually break down into apoptotic bodies and removed by phagocytes [163-165]. Apoptosis in Greek is used to denote "falling off" to describe leaves falling off a tree. The scientific term apoptosis describes the regulated physiological process of removing individual components of an organism without damaging the organism. Three tightly controlled pathways are known to result in apoptosis, which involve biochemical events leading to the activation of proteases known as caspases (cysteine-dependent aspartate-specific proteases). Autophagy or programmed cell death Type II describes the degradation of cellular components by autophagic vacuoles and is featured by partial chromatin condensation and vacuolisation. Autophagosomes are the primary vesicles to engulf cytoplasmic material, which then fuse with lysosomes to proceed with the degradation. Cells undergoing autophagy are then phagocytised by neighbouring cells.

However, apart from apoptosis and autophagy, other types of programmed cell death have been characterised and the specific mechanism determining cell fate depends mainly upon the initiating stimulus [163]. Pyroptosis is another form of regulated cell death, which was firstly seen in Salmonella and Shigella infections (Figure 11) [162, 163]. The name is derived from the Greek "pyro" meaning fire or fever and "ptosis" meaning falling off and pyroptosis is used to denote proinflammatory cell death. Similarly to apoptosis, one of the caspases, known as caspase-1 was shown to mediate pyroptosis but not apoptosis. Additionally, pyronecrosis is another form of regulated cell death, which was firstly seen in Shigella infections [166]. The term was coined to describe a form of necrotic cell death that may lead to the activation of caspases through initiation of a cathepsin-dependent apoptotic

mechanism. Cathepsins are proteases, which are localised within lysosomes under physiologic conditions and released in response to certain stress signals to induce normal apoptotic cell death [167].

A mechanism previously seen to show features of both apoptosis and necrosis was named necroptosis [168, 169]. Although, similar apoptotic stimuli induce necroptosis, the main mediator is a kinase with death-domain, known as RIP1, which is activated upon Fas ligand-induced and tumor necrosis factor-α (TNF-α) induced necroptosis. Various inhibitors specific to this mechanism have been identified and they were all classified in the family of necrostatins according to their ability to inhibit the kinase activity of RIP1 [170]. Additionally, necrosis can be induced in response to DNA damage, which leads to the activation of the DNA repair protein, poly(ADP-ribose) polymerase (PARP) [171, 172]. The cells respond with an increased energy consumption to support the activation of PARP and this leads to depletion of ATP, which triggers cell death [173].

1.7.3 Apoptosis: Pathways determining Cell Suicide

This tightly regulated form of cell death whose role is very crucial in various human diseases like cancer, autoimmune diseases and neurodegenerative diseases has led to an increased interest to identify the genes involved in the initiation, execution and regulation of apoptosis. The conserved family of caspases is central for a successful apoptotic cell response and maintains an irreversible biochemical cascade leading to cell suicide [174]. Caspases were firstly identified in a developmental processes study in *Caenorhabditis elegans* model and homologues were then shown to exist in all mammals. The main feature of caspases includes their proteolytic activity, which leads to the cleavage of proteins at aspartic acid residues. According to their role in apoptosis, caspases were further categorized into initiators (caspase-2, -8, -9 and -10), executioners (caspase-3, -6 and -7) and inflammatory caspases (caspase-1, -4 and -5) [175]. In addition, caspases-11, -12, -13 and -14 have been identified but their role has not been fully characterized [165].

Although, for many years it was thought that only two main pathways were involved in apoptosis, there is now evidence that a third pathway also exists. Named according to the specific apoptotic stimuli inducing each pathway, they are known as the intrinsic, extrinsic and perforin / granzyme pathways [165]. However, they are all interconnected and converge on the same downstream execution pathway (Figure 12). This shared pathway involves the cleavage and hence, activation of caspase-3, the main executioner of apoptosis, which leads to DNA fragmentation, degradation of numerous proteins, formation of apoptotic bodies, ligands for phagocytic cell receptors and ends with the uptake by phagocytic cells.

1.7.3.1 Intrinsic Pathway

The intrinsic pathway leading to apoptosis is initiated by numerous non-receptor mediated stimuli, which activate mitochondrial-initiated events. Such stimuli can either act in a positive manner i.e. toxins, radiation, hypoxia or viral infections or negatively in the absence of certain cytokines, hormones and growth factors involved in the suppression of apoptosis [165]. In both types, the mitochondrial permeability transition (MPT) pore opens to change the mitochondrial transmembrane potential leading to the release of pro-apoptotic proteins in the cytosol (Figure 12).

Early events include the release of cytochrome c, Smac/DIABLO and HtrA2/Omi to activate the caspase-dependent pathway [164, 176]. In the cytosol, cytochrome c directly interacts with Apaf-1 and pro-caspase-9 to form a trimeric complex known as the apoptosome [177]. This conformation activates caspase-9, which in turn cleaves and activates caspase-3. In contrast, Smac/DIABLO and HtrA2/Omi act by suppressing the regulation of caspases via direct inactivation of the inhibitors of apoptosis (IAPs) [178]. One such inhibitor, X-linked IAP or XIAP is able to block the proteolytic activity of caspases through direct binding and either Smac or HtrA2 can inhibit its action [176]. As a late event, pro-apoptotic proteins like the apoptosis-inducing factor (AIF), caspase-activated DNase (CAD) and endonuclease G are released from the mitochondria [171]. This event essentially leads to chromatin condensation and DNA fragmentation either in a caspase –dependent (CAD) or –independent (AIF and endonuclease G) manner.

These apoptotic events are tightly regulated by a total of 25 proteins included in the Bcl-2 family, which is further controlled by the tumor suppressor protein p53 [179]. Bcl-2 family members are divided in two groups, the anti-apoptotic (Bcl -2, -x, -XL, -XS, -w, BAG) and the pro-apoptotic (Bcl-10, Bax, Bak, Bid, Bad, Bim, Bik, Blk) proteins [179-181]. Whether a cell commits suicide or aborts the death program is determined by the

action of Bcl-2 proteins. Although, information regarding individual Bcl-2 members exists, further elucidation is required for an in-depth understanding of the crucial steps leading to the execution phase of apoptosis.

1.7.3.2 Extrinsic Pathway

The extrinsic pathway is governed by extracellular death signals induced by interactions with transmembrane receptors included in the tumor necrosis factor (TNF) receptor family [182]. They all share similar extracellular and cytoplasmic domains, which are required for successful initiation of the intracellular signalling pathways of apoptosis (Figure 12). Although, the known members of the family with their ligands include FasR/FasL, TNFR1/TNF-a, DR3/Apo3L, DR4/Apo2L and DR5/Apo2L, only the specific mechanisms followed by Fas and TNF-a are currently fully understood [182, 183].

In both mechanisms, the cytoplasmic adapter protein FADD is recruited to transmit the intracellular signals via association with pro-caspase-8. The resulting complex known as DISC (death-inducing signalling complex) promotes the auto-activation of caspase-8, which in turn triggers the execution phase. The only known negative mechanism to regulate the extrinsic pathway involves the protein c-FLIP, which can bind both FADD and caspase-8 to inhibit the DISC formation.

1.7.3.3 Perforin / Granzyme Pathway

The Fas mechanism of the extrinsic pathway leading to apoptosis is a form of T-cell mediated cytotoxicity, which is mediated by cytotoxic T lymphocytes (CTLs) to kill tumor and virally infected cells [165, 182]. In addition to Fas, CTLs can also mediate another pathway that involves the transmembrane pore-forming protein known as perforin (Figure 12). Granules containing proteases are then secreted through the perforin-formed pore and into the cytosol of the target cell.

The proteases granzyme A and B are crucial in CTL-induced apoptosis which involves both caspase dependent and independent downstream pathways (Figure 12). Granzyme B can directly activate caspases -3 and -10 but can also cleave and in this case suppress the action of ICAD (Inhibitor of Caspase Activated DNAse). Additionally, granzyme B has been implicated in the release of cytochrome c through cleavage of Bid, a pro-apoptotic Bcl-2 family member. Activation of Bid is an example of "cross-talk" between all three main pathways of apoptosis. On the contrary, granzyme A induces a caspase independent pathway through activation of the DNAse NM23-H1 leading to DNA degradation.

1.7.3.4 Execution Pathway

Once the cell has been irreversibly committed to suicide, the shared execution pathway is initiated. The main executioner is caspase-3 but caspases -6 and -7 are also involved in this phase of apoptosis [165]. Activation of such executioner caspases leads to chromatin condensation, nuclear fragmentation and cytoskeletal protein degradation, which all contribute to the morphological changes of apoptotic cells [164]. The cytoskeletal re-organisation is followed by the decomposition of the cell into membrane-enclosed fragments, known as apoptotic bodies. Recognition by phagocytic cells is facilitated by the externalisation of phosphatidylserine on the surface of apoptotic cells.

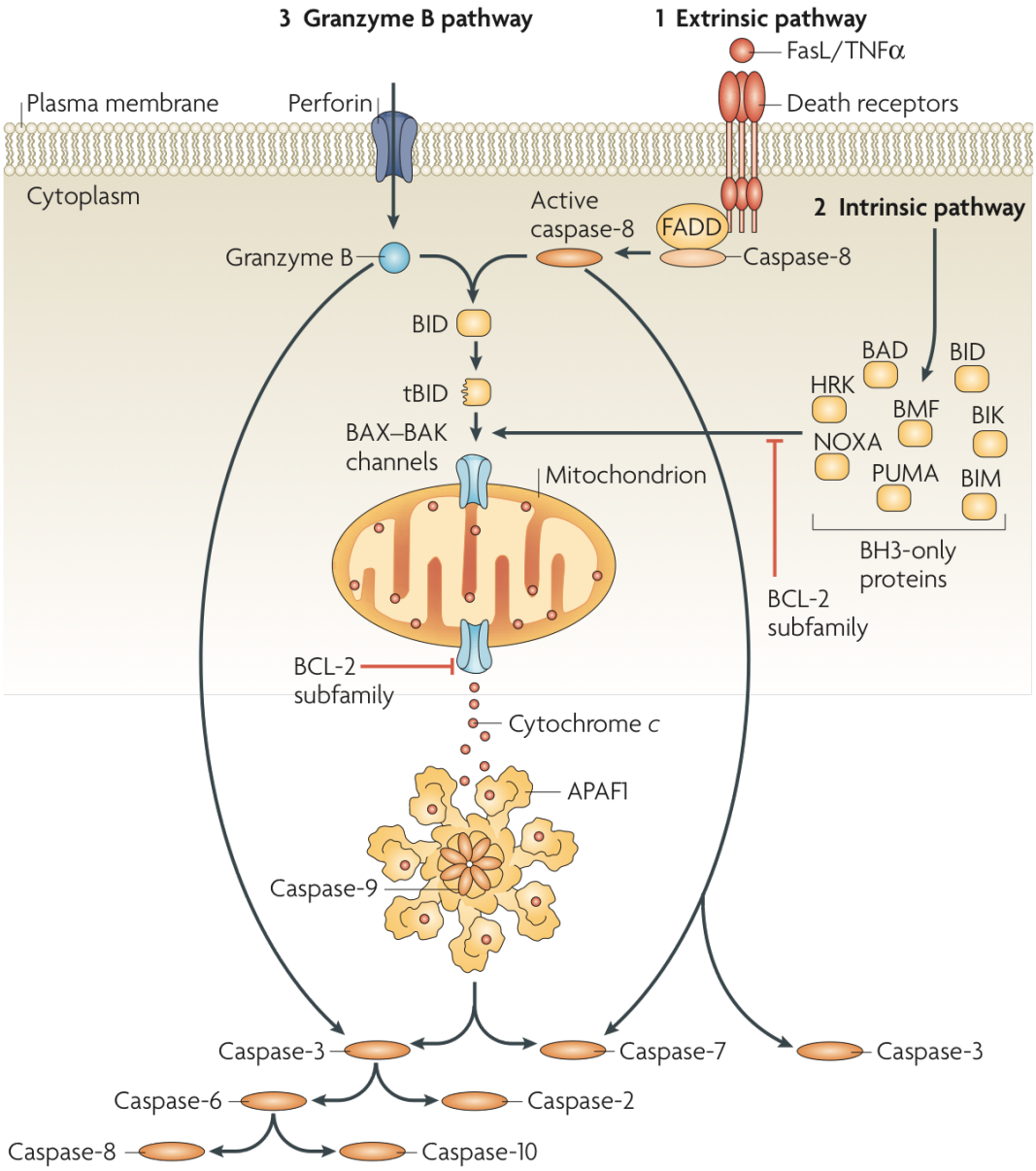

Figure 12. Programmed Cell Death Pathways. (Reviewed in [164])

1.7.4 Calcium-induced Apoptosis

Survival through changing environments is maintained by the cellular communication governed by calcium (Ca^{2+}) and phosphate ions. Amazingly, Ca^{2+} is one of the simplest ions known and yet controls everything in the life of Homo sapiens; from birth to death [184, 185]. Movement, heart beat, information processing by the brain and storage of memories are only a few of the activities regulated by Ca^{2+} as an intracellular messenger. It further coordinates cellular development and differentiation into specialised types, controls their activity and triggers their death.

Concentrations of Ca^{2+} within the cytosol determine cell fate. In high concentrations cells will disintegrate following either the necrotic or apoptotic cell death pathways [186]. In normal Ca^{2+} signalling, the ER and mitochondria communicate via constant shuttling of the ion to maintain higher levels in the ER lumen where Ca^{2+} resides and less in the mitochondria [187]. When this homeostatic cross talk between the two organelles changes, Ca^{2+} acts as an orchestrator of apoptosis [188]. The ER Ca^{2+} stores are depleted, leading in an overloading of mitochondrial Ca^{2+} and the combination of these has the consequence of either trigger stress signals that activate genes associated with cell death or initiate the downstream programmed events of mitochondria-induced apoptosis.

The Ca^{2+} concentrations within the cell cytosol are altered either via an external or internal source. It can enter the cell through plasma membrane spun Ca^{2+} channels, pumps or exchangers when neighbouring cells activate signalling [189]. Intracellularly the main source of Ca^{2+} is the ER but many other organelles also require the ionic messenger for normal functioning. Although, different types of transporters associated with various

organelles have been identified to date, in many cell types the ER localised transporters are those directly implicated in the induction or amplification of apoptotic signals [189, 190].

The sarcoendoplasmic reticulum Ca^{2+} ATPase (SERCA) pumps import Ca^{2+} ions from the cytoplasm and ER release of Ca^{2+} is regulated by inositol triphosphate (IP_3) and ryanodine receptors [190]. When these ER-specific regulators are impaired, Ca^{2+} homeostasis is altered leading to cell death (Figure 13). Additionally, members of the Bcl-2 family, derived from both the pro- and anti- apoptotic groups are involved in the regulation of ER Ca^{2+} load since the balance between the anti-apoptotic Bcl-2 (decreases ER Ca^{2+} load) and the pro-apoptotic proteins Bax and Bak (increase mitochondria Ca^{2+} load) is directly proportional to Ca^{2+} homeostasis [191, 192].

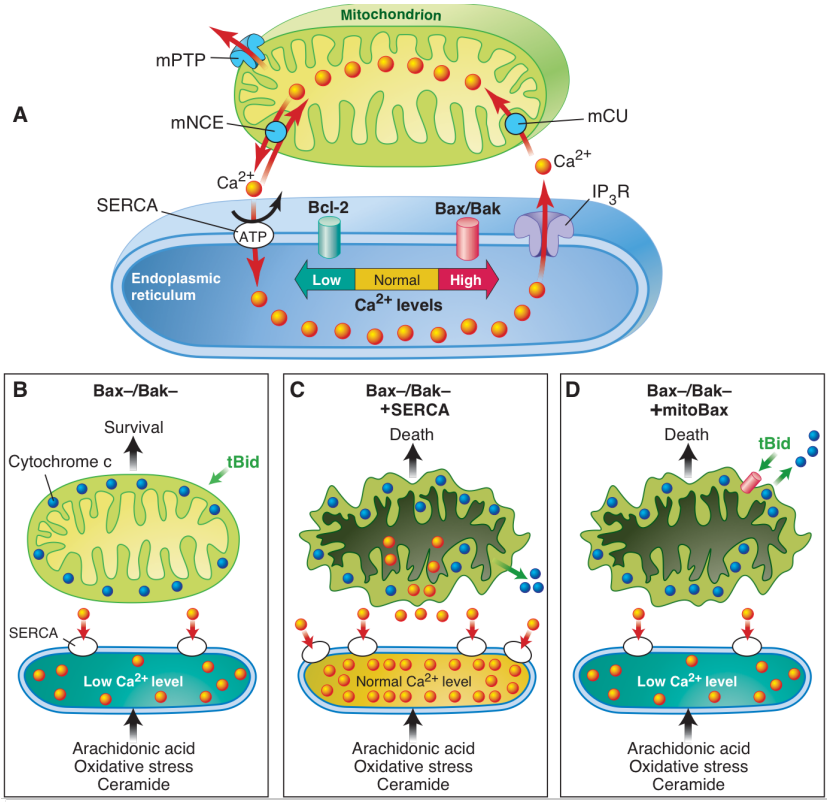

Figure 13. Calcium homeostasis in programmed cell death. [193]

1.7.5 The Apoptotic Regulator HAX-1

HS-1-associated-protein-X-1 (Hax-1) was discovered more than a decade ago in a yeast two-hybrid screen and since then its binding partner repertoire has been on a constant increase [194, 195]. Due to its numerous interactions, Hax-1 is involved in many cellular pathways [196]. However, growing evidence highlights its role in apoptosis as the main function (Figure 14). It has been implicated in diseases that involve diminished progression of apoptosis e.g. cancer and severe congenital neutropenia and considered a ubiquitously expressed protein interacting with multiple anti-apoptotic proteins [195, 196].

The intracellular stability of XIAP is dependent on a direct interaction with Hax-1, which prevents proteosomal degradation of XIAP and thus, promotes its anti-apoptotic function (Figure 14) [197]. Overexpression of Hax-1 also results in resistance to pro-apoptotic events signaled by granzyme B and caspase-3 as well as inhibition of caspase-9 [198-200]. Although, its intracellular localization has taken an atypical distribution pattern the consensus HeLa cell localization includes the mitochondria, ER and nuclear membrane [196]. This depicts an intracellular distribution of Hax-1 that involves organelles regulating different pathways of programmed cell death. Indeed, apart from the intrinsic and granzyme pathways, Hax-1 also regulates apoptosis through modulation of Ca^{2+} homeostasis [195].

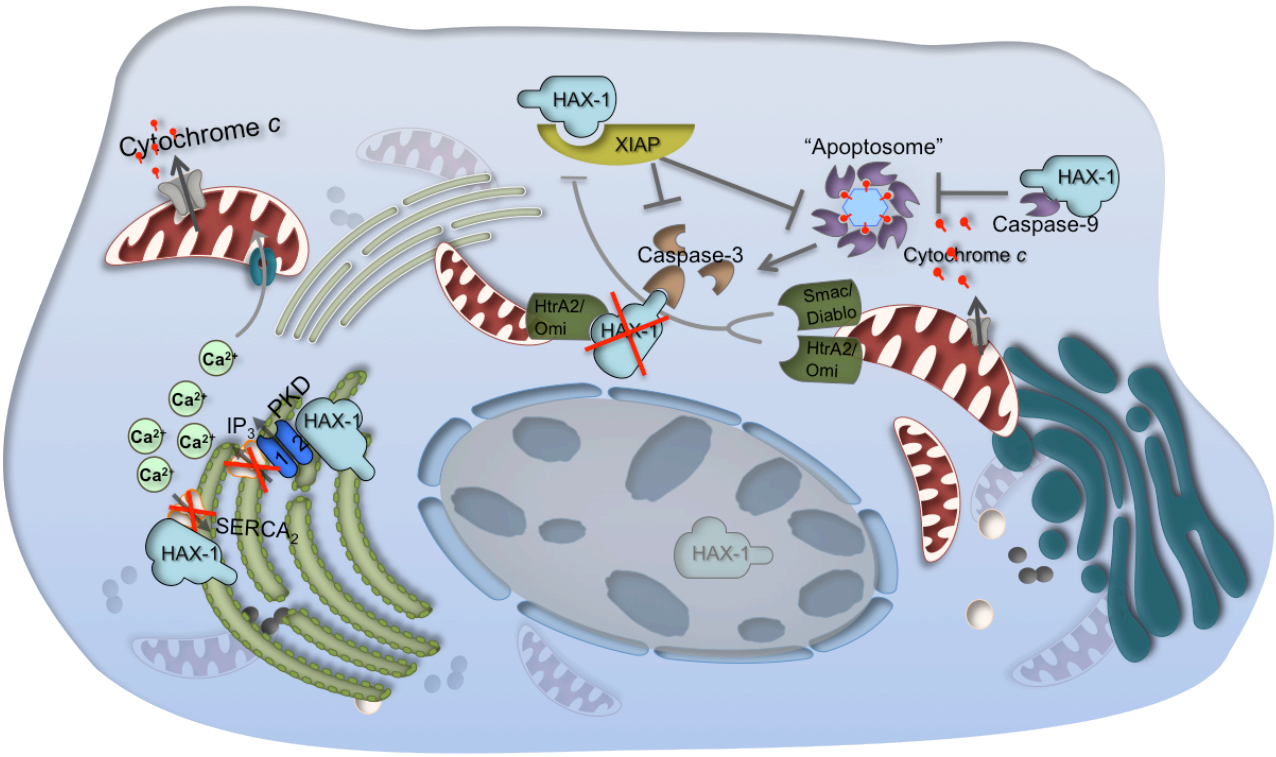

Figure 14. Hax-1 regulates apoptosis (Designed by author)
Hax-1 protects one of the main inhibitors of apoptosis (XIAP) from degradation. The interaction of caspase-9 with Hax-1 inhibits the apoptosome formation and the main executioner of apoptosis, caspase-3. Inhibition of apoptosis induced by ER stress is maintained by the interaction of Hax-1 with the ER Ca^{2+} importer pump $SERCA_2$ and the ER Ca^{2+} efflux channel PKD2. During apoptosis, Hax-1 degradation is fascilitated by direct caspase-3 and HtrA2/Omi cleavage. The role of the Hax-1 nuclear localisation has not been identified yet. Illustration was designed by the author for this study.

Hax-1 participation in Ca^{2+} homeostasis was firstly coined through its interaction with the ER localised polycystic kidney disease type II, PKD2 or TRPP2 [201]. In a dimeric complex, PKD1 and PKD2 form cationic channels that permit a two-way direction Ca^{2+} flux [202]. The PKD2 channels were shown to inhibit apoptosis by permitting less ER Ca^{2+} export to the cytosol and mitochondria in association with the ER Ca^{2+} efflux channels, inositol triphosphate receptors (IP3Rs) [203, 204]. It was later shown that Hax-1 related contribution to Ca^{2+} homeostasis also involves an interaction with the SERCA2 pumps, which play a crucial role in the regulation of Ca^{2+} levels by maintaining the interplay

between the ER and mitochondria [205]. Previous work has shown that Hax-1 C-terminus binds the nucleotide-binding domain of SERCA2 to prevent specific conformational rearrangements normally occurring via ATP hydrolysis. Evidence suggests that overexpression of Hax-1 results in down-regulation of SERCA2, which leads to inhibition of apoptosis through diminished ER Ca^{2+} content allowing normal mitochondrial Ca^{2+} load [205]. This Hax-1 inhibitory mechanism is consistent with the action of Bcl-2, another anti-apoptotic regulator known to promote cell survival by reducing ER Ca^{2+} efflux [192].

Regulation of Hax-1 expression levels is maintained by the pro-apoptotic Omi/HtrA2 and caspase-3 which were both shown to cleave and hence, deactivate Hax-1 during apoptosis [199, 206]. Furthermore, evidence suggests that *hax-1* transcription is regulated by NF-κB [207]. Importantly, many viruses (e.g. human immunodefficiency, Epstein-Barr and classical swine fever viruses) target Hax-1, which might be explained by its significantly emerging role as an anti-apoptotic regulator [208-212].

1.8 EspO : A "LifeGuard" In Enteric Bacteria

The genome of EHEC O157:H7 contains two *espO* genes (*espO1-1* and *espO1-2*), which share 58% amino acid identity (Figure 15.D) [213]. Additionally, *espO* genes were identified in the non-O157 strains, O111:H-, O103:H2 and O26:H11 (*See* Chapter 3). The two EspO proteins are encoded by the genes ECs1567 and ECs1821 of EHEC O157:H7 strain Sakai, which are located in two different EELs within lamboid prohpages Sp6 and Sp9 respectively (Figure 15) [213]. Although, EPEC strain E2348/69 is naturally *espO* negative, the EPEC clone O55:H7, which is considered a progenitor of EHEC O157:H7, contains one *espO*.

EspO orthologs exist singly in the A/E mouse pathogen *C. rodentium* and *Salmonella* strains. EspO in *C. rodentium*, which is located in close proximity to the inflammatory related T3SS effector EspT, shares a 58% amino acid identity with EHEC EspO1 (Figure 15.C). The Salmonella orthologs, appear to be closely related with EHEC EspO. The *S.* Typhi CT18 paralog that lacks the C-terminal 18 amino acids shares a 55% amino acid identity with EHEC EspO1 whereas SopO in *S.* Typhimurium SL1344 shares a 68% protein identity (Figure 15.D). On the contrary, the EspO ortholog OspE, which is highly conserved in Shigella strains, is distantly related to EHEC EspO1. Sequence alignment of EHEC EspO1 and OspE1 (*S. flexneri*) revealed 30% protein identity (Figure 15.D).

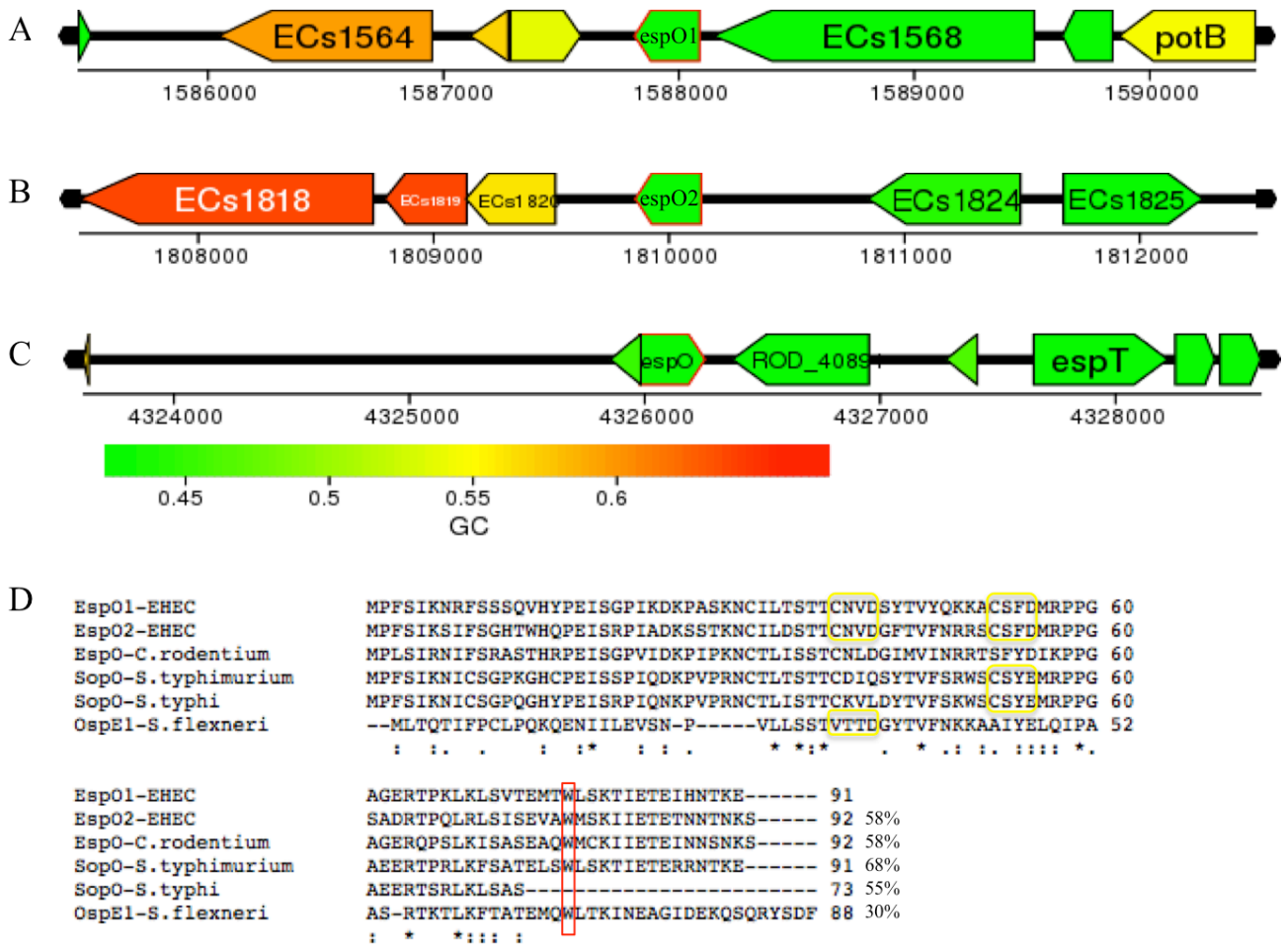

Figure 15. EspO Genome Organisation and Alignment
Genome organisation of EHEC O157:H7 strain Sakai EspO1 (A) and EspO2 (B) and EspO from *C. rodentium* (C). Amino acid alignment of EspO orthologs (D). Homology shown as %age of aa identity compared to EspO1 (EHEC). The red box encloses the tryptophan residue (W) required for the EspO-ILK interaction and it is highly conserved among orthologs. The yellow boxes enclose tetrapeptides which are predicted to be potential caspase-3 recognition sites.

Although, both EspO proteins are translocated via the T3SS, their exact role in EHEC / EPEC infection still remains to be elucidated. Srikanth *et al.* has recently shown that SipA, a *S.* Typhimurium SPI-1 T3SS effector protein is processed by caspase-3 at a specific tetrapeptide recognition site (DEVD) resulting in two functional domains of the protein [65]. This caspase-3 motif is common within T3SS effectors in *S.* Typhimurium but it also appears to be a shared mechanism between enteric pathogens since potential caspase-3

cleavage sites were predicted to exist in T3SS effector proteins from *S. flexneri* and EPEC. Using an online server that predicts caspase cleavage sites (CASVM, http://www.casbase.org), we identified potential caspase-3 motifs, which are predicted to exist in the EspO family of effectors (Yellow boxes in Figure 15.D). In EHEC EspO1 and EspO2 the tetrapepdite sites CNVD (position 42) and CSFD (position 55) were predicted. SopO from both *S.* Typhimurium and *S.* Typhi was also predicted to have at position 55 a potential caspase-3 cleavage site (CSYE) and OspE from *S. flexneri* has a potential site at position 34 (VTTD). However, these potential cleavage motifs still need to be confirmed whether they are functionally active.

Recently, Kim *et al*. reported that OspE and its orthologs bind integrin-linked kinase (ILK), which in turn, enhances the stability of the integrin-containing adhesion sites and blocks cell detachment [130]. This strategy keeps infected cells strongly adhered to the underlying extracellular matrix allowing the bacteria to establish and maintain their infective niche. This interaction was abolished when W68, which is conserved amongst the EspO orthologs, is substituted with alanine (W68A) (Figure 15.D). Ectopic expression of OspE facilitated focal adhesion formation, which reinforced cell adhesion. Consistently, HeLa cells infected with *Shigella* Δ*ospE* induced significantly greater cell detachment compared to infection with the parental wild type strain or the mutant complemented with the wild type *ospE* gene, whereas OspEW68A failed to complement the mutant. In addition, EspO2 only was also shown to localise in the cytoplasm, where it mediates the stress fibers induced by the RhoA GEF activity of EspM2 via a direct interaction [214]. This further enables EspO2 to stabilise the formation of focal adhesions.

In this project we identified Hax-1 as a novel protein partner of the family and we further investigated the role of EspO in apoptosis to elucidate a cytoprotective role in cell death induced by multiple pro-apoptotic compounds. Furthermore, Hax-1 depletion of HeLa

cells by siRNA techniques showed that the anti-apoptotic activity of the EspO orthologs is Hax-1 dependent. Taken together with previous findings, the results suggest an important contribution of the EspO orthologs in cell survival, which involves both cell attachment and inhibition of programmed cell death.

1.9 Aims

The aim of the project is to elucidate the exact role of the T3SS EspO family of effectors in EHEC, *Shigella*, *Salmonella* spp. and in *C. rodentium in-vivo* model of infection. The research interests lie mainly within the areas of novel protein partner identification, intracellular localisation and function of the EspO family (Figure 16).

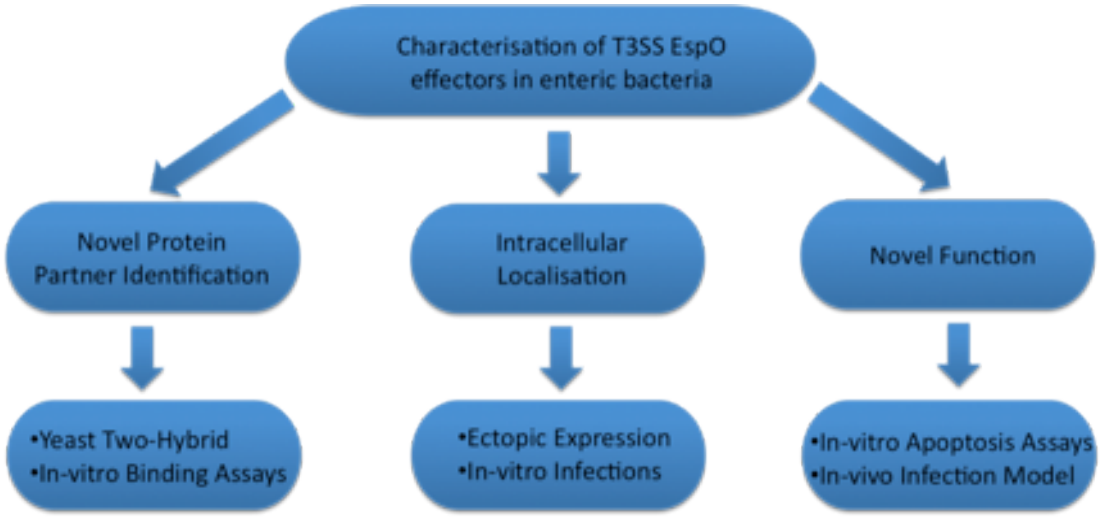

Figure 16. Research Strategy

2 Chapter 2 : Materials and Methods

2.1 Bacterial strains and growth conditions

Bacterial strains used in this project are listed in Table 4. Strains were maintained on Luria–Bertani (LB) broth or agar supplemented with ampicillin (100 μg/ml), chloramphenicol (25 μg/ml) or kanamycin (50 μg/ml), when necessary.

2.2 Molecular Biology techniques

2.2.1 Cloning

Plasmids and primers used in this study are listed in Table 5 and 6 respectively. Standard molecular biology techniques were used for all constructs. Inserts were amplified using the KOD Hot Start DNA Polymerase using the appropriate reactions for PCR (Table 1).

Reagent	Amount (μl)
dH_2O	34
10x Buffer	5
$MgSO_4$	3
dNTPs	5
Forward Primer (100pmol/μl)	0.5
Reverse Primer (100pmol/μl)	0.5
Genomic DNA	1
KOD DNA polymerase	1

Table 1. PCR Reactions for KOD Hot Start DNA Polymerase

The cycling conditions for the PCR were used according to the amount of the starting template, the size of the primers and the size of the target sequence. The cycling conditions for primers with a size of 20-25 bp used to amplify a target size of 1000 bp from a template with high number of copies, were 95°C for 2 mins to activate the polymerase, 95°C for 2 sec. to denature, 55°C for 10 sec. to anneal, 70°C for 20 s/kbp to extend and the cycles were repeated 30 times. The PCR product was purified to remove dNTPs, primers and enzymes using the PCR purification kit (Qiagen) and checked on an agarose gel (1% agarose and 5% SYBR Safe Invitrogen).

The vector and PCR product were digested with the appropriate restriction enzymes in a 50 µl reaction mix (Table 2). The reaction mix was incubated at the appropriate temperature required for the enzymes to work optimally and allowed for 1-2 hours.

Reagent	Low Copy Plasmid	High Copy Plasmid	PCR Product
dH_2O	0	13	13
Vector/PCR product	42.5	29.5	29.5
10x Buffer	5	5	5
BSA	0.5	0.5	0.5
Restriction Enzyme 1	1	1	1
Restriction Enzyme 2	1	1	1

Table 2. Restriction digest of vector and PCR product
Restriction enzymes, BSA and the appropriate buffer for each enzyme were purchased from NEB Biolabs. Amount for each reagent is shown in µl.

Alkaline phosphatase was added to prevent the vector from ligating to itself. 1 µl of alkaline phosphatase (NEB) was added to the restriction digest following digestion and incubated at 37ºC for 15 minutes. Digested products were run on agarose gel and then excised for purification with the Gel extraction kit (Qiagen). The purified digested PCR product was then ligated with the purified digested vector using 2 µl 10x T4 ligase buffer

(NEB), 1 µl of T4 ligase and the appropriate amount of insert and vector calculated for 3:1 ratio according to the formula Insert Mass (ng) = 3 x (Insert Length / Vector Length) x Vector Mass (ng). The ligation mix was incubated in 16 ºC overnight or 1 hour at room temperature. The ligation mix was then transformed in chemically competent Top10 *E. coli* bacteria as explained below (*See Bacterial Transformations*). The transformations were incubated on selective plates at 37ºC over night and screened by colony PCR using the Red Taq Ready Mix PCR Reaction (Sigma). Positive clones were grown in 5 mL LB broth with the appropriate antibiotic at 37ºC, 250 rpm over night and centrifuged at 4000 rpm for 15 min to collect the pellet for purification.

Minipreps were performed with the appropriate Qiagen kit. The pellet was resuspended in 350 µl of buffer P1 (25mM Tris-pH8.0, 50mM glucose, 10mM EDTA, 5mg/ml lysoszyme, 200ug/ml RNAse A) and 250 µl buffer P2 (0.2M NaOH, 1% SDS) was added for lysis. 250 µl of buffer P3 (K^+acetate pH 4.8) was added for neutralisation and precipitated samples were centrifuged at 13000 x g for 10 mins to collect the supernatant (SN). The SN was transferred in a spinning column to collect the DNA by centrifugation at 13000 x g for 1 min. The samples were washed with 900 µl of 70% ethanol and columns were centrifuged at 13000 x g for 1 min. Centrifugation was repeated to completely remove residual ethanol and then 50 µl of sterile MilliQ H_2O was added. The columns were allowed to stand for 1 min and then centrifuged for 1 min to collect the purified DNA. The concentration of DNA was determined by spectrophotometry (NanoDrop) and samples were sent for sequencing to ensure successful cloning.

2.2.2 Bacterial Mutations

EHEC EDL933 single and double *espO* mutant strains were constructed using the one-step PCR λ-red-mediated mutation protocol [215]. Disruption of *espO1* was performed with a chloramphenicol resistance containing cassette generated with primers c1 and c2 (Table 6) using pKD3 as a template. For *espO2*, a kanamycin resistance containing cassette was generated with primers k1 and k2 using pSB315 as a template. The PCR product of each resistance cassette contained 50 bp of the appropriate *espO* gene and was transformed into strains harbouring pKD46 (λ-Red recombinase expression plasmid). Mutants were selected on LB plates containing the appropriate antibiotic and further confirmed by PCR.

2.2.3 Site-Directed Mutagenesis

The QuickChangeII Site-Directed Mutagenesis kit (Stratagene) was used for single amino acid changes or point mutations. Two complimentary oligonucleotides containing the desired mutation were synthesised and the appropriate PCR reactions were prepared (Table 3)

Reagent	Amount (µl)
10x Reaction buffer	5
dNTP mix	1
Double-stranded DNA template	1
Forward primer (100pmol/µl)	0.5
Reverse primer (100pmol/µl)	0.5
dH_2O	41
PfuUltra HF DNA Polymerase	1

Table 3. Site-Directed Mutagenesis PCR Reaction

The appropriate cycle parameters for the PCR were adjusted according to the type of mutation desired (e.g. 12 cycles for point mutations) and the length of the plasmid used in the reaction. The PCR product is treated with Dpn I endonuclease to digest the parental DNA template and therefore, select for the vector DNA containing the mutation. The resulting mutated vector was then transformed into chemically competent Top10 *E. coli* bacteria and minipreps were performed on positive clones to extract plasmid for further confirmation of the desired mutation by sequencing.

2.3 Bacterial Transformations

Chemically competent cells were prepared for heat shock transformation by growing cells until an OD_{600} of 0.5, and after a centrifugation at 5000 rpm for 10 min at 4°C the cells were resuspended in 25 mL of cold 50 mM $CaCl_2$. Following, 30 min incubation on ice the cells were further centrifuged and resuspended in 2.5 mL of cold $CaCl_2$. The cells were further incubated for 1hr on ice.

Transformation by heat shock was done by adding 10 ng of DNA in 100 µl of competent top10 *E. coli* bacteria or 200 µl of EHEC EDL933 or EPEC E2348/69 lab strain competent bacteria and incubated for 30 min on ice. Heat shock was performed by incubating 2 min at 42°C followed by 10 min on ice. 900 µl of SOC medium was added and bacteria were allowed to recover for 1 hr in 37 °C. An overnight incubation on selective media allowed the selection of positive clones.

Electrocompetent cells were prepared by growing cells as above and then incubating for 15 min at 4°C. After an initial centrifugation at 4000 rpm at 4°C for 15 min, the cells

were washed with 50ml of cold H_2O 15% glycerol. This step was repeated and the pellet was resuspended in 1mL of cold H_2O 15% glycerol. Finally, the cells were spun once more in order to increase concentration by resuspending in a final volume of 100 µl in cold H_2O 15% glycerol. 10 ng of concentrated PCR product was electroporated into the 100 µl of electrocompetent cells. 700 ml of SOC medium was added and bacteria were grown for 1h30 at 37°C. Selection of positive clones was done by plating on selective media and further confirming by colony PCR.

2.4 Yeast transformations

S. cerevisiae wild type yeast strain AH109 was grown overnight at 30°C in YPDA broth (1% w/v Bacto yeast extract, 2% w/v Bacto peptone and adenine 80 mg/l) and then centrifuged at 4000 rpm for 15 min. The pellet was washed twice with sterile H_2O and resuspended in the transformation mix containing 50% w/v PEG 3350, 36µl 1M LiAc, 50µl Herring sperm DNA (2 mg/ml), 34µl sterile H_2O and 1µg of the appropriate plasmid to be transformed [216, 217]. The mixture was incubated at 30°C for 30 min and then heat shock was applied by incubating at 42°C for 20 min. Sample was centrifuged at 13000 x g for 15 sec. and resuspended in 1mL sterile H_2O. 100µl of each sample was plated onto appropriate selective plates.

2.5 Yeast two-hybrid screening

A yeast two-hybrid (Y2H) screen was performed using EHEC EDL933 EspO1 as a bait with the Matchmaker Pretransformed Normalised HeLa cDNA library (Clontech)

according to the manufacturer's instructions. In a Y2H assay the bait protein (EspO1) is fused to the Gal4 DNA-binding domain (DNA-BD) and the prey proteins (HeLa cDNA library) are fused to the Gal4 activation domain (AD). If the bait protein interacts with a prey protein, the DNA-BD and AD are brought into close proximity to initiate transcription of reporter genes, which are under the control of Gal4 upstream activating sequence (UAS). These include genes encoding essential amino acids e.g. histidine (*HIS3*) and adenine (*ADE2*) but also enzymes like α-galactosidase (*MEL1*) and β-galactosidase (*LacZ*) that turn yeast colonies blue when the chromagenic substrate X-α-Gal is present in the medium.

The yeast strain AH109 was transformed with the bait construct pGBKT7-EspO1 using the LiAc method described above and mated with the yeast strain Y187 pretransformed with the pGADT7 Rec plasmid carrying the HeLa cDNA library. The mating happens overnight when the two yeast strains are incubated in appropriate broth medium (YPDA) at 30°C and slow shaking (50 rpm). Positive clones were selected by plating on quadruple dropout media (QDO) or high-stringency SD / DO media (0.67% Yeast nitrogen base without amino acids, 2% agar and 10x Dropout Solution lacking Trp, Leu, His and Ade). Tryptophan and leucine act as a selection for the bait pGBKT7 and prey pGADT7 vectors respectively whereas histidine and adenine are two of the reporter genes that select for positive protein interaction. Clones were also plated onto low stringency or double dropout (DDO) SD media (SD/-Leu/-Trp) as a selection of only diploids with both prey and bait plasmids. Colonies were re-streaked on QDO to ensure expression of reporter genes and therefore, positive interaction. The pGADT7 cDNA inserts from all remaining colonies were amplified using the AD-LD primers (Clontech). The PCR products were then sequenced and identified using Blastn and Blastx.

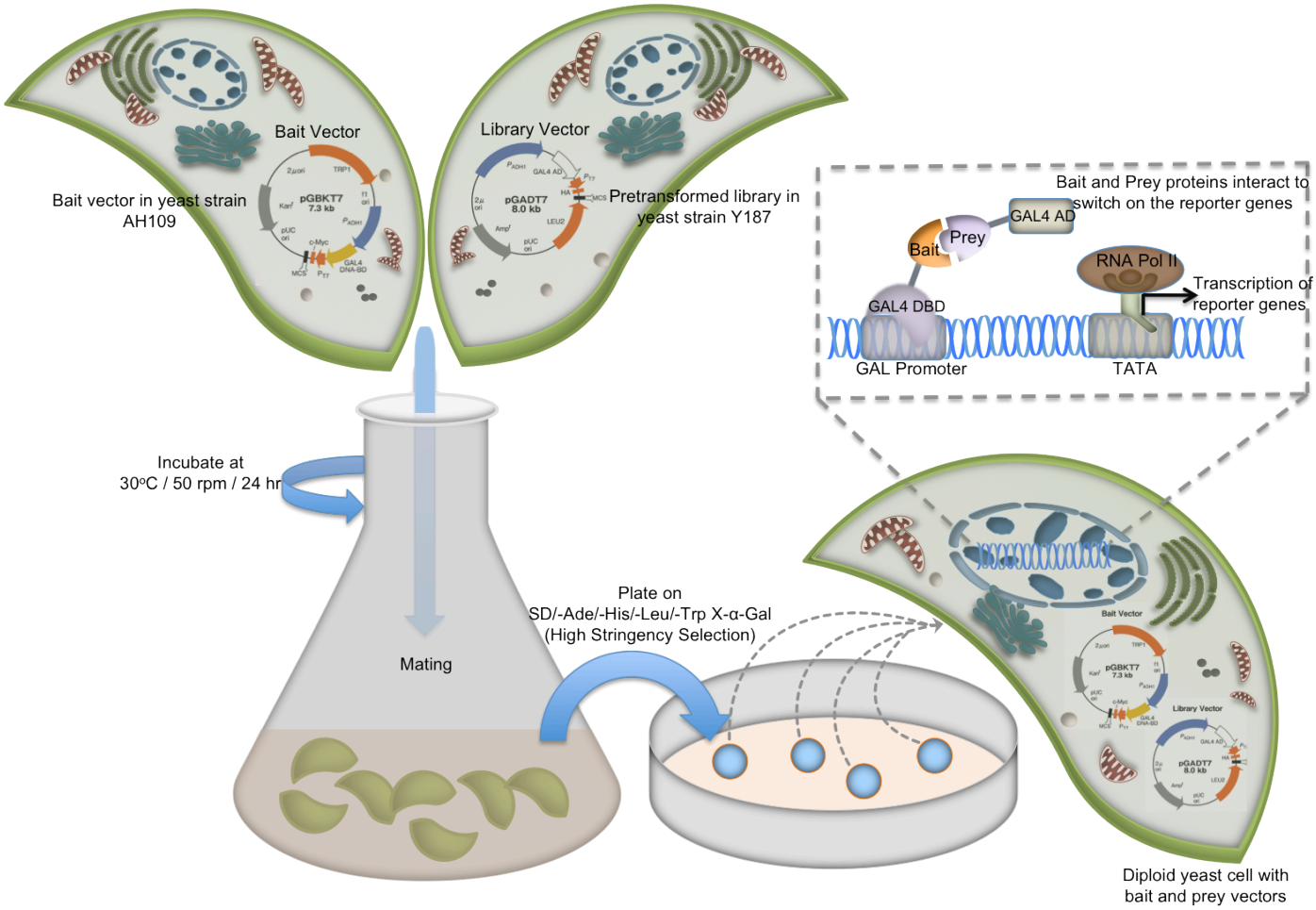

Figure 17. Yeast Two-Hybrid Assay (Designed by author)
Illustration of a yeast two-hybrid (Y2H) assay. The bait vector pGBKT7 expressing EspO1 fused to Gal4 DNA-binding domain (GAL4 DBD) is transformed in yeast strain AH109. The yeast strain Y187, pretransformed with the HeLa cDNA library, is incubated with AH109 to allow mating to occur overnight at 30°C and slow shaking at 50 rpm. The overnight culture is plated onto high stringency medium or quadruple dropout media (QDO) to select for diploid yeast cells containing both bait and prey vectors and a positive protein interaction. If there is a successful interaction between the bait and a prey protein, the Gal4 activation domain (GAL4 AD), which is fused to the prey protein is brought into close proximity with the GAL4 DBD to initiate transcription of the reporter genes and hence, allow blue colonies to grow on QDO. The illustration was designed by the author for this study.

2.6 Cell lines and growth conditions

HeLa ATCC were grown in flasks containing DMEM (1 g/l glucose) supplemented with 2mM Glutamax and 10% FCS at 37^{o}C in 5% CO_2. Adherent cells were washed with sterile PBS and brought into suspension with trypsin/EDTA at 37^{o}C for 10 mins. Equal amount of fresh serum containing medium was added to neutralise the trypsin and 250 µl of cell suspension were mixed with an equal volume of Trypan Blue to obtain a dilution factor of 2. 10 µl of the mixture were used to fill the chambers of the haemocytometer to count the cells with a light microscope at x20 mignification. The number of viable (bright cells) and non-viable (stained blue) were counted and the concentration of cells was calculated [concentration of viable cells per ml = (Total viable cells / Number of squares) x Dilution Factor (2) x Correction Factor (10^4)]. The remaining suspension was centrifuged at 1000 x g for 3 mins and cell pellet was resuspended in fresh serum containing DMEM. Cells were seeded 24h or 48h prior to transfection or infection onto 24-well plates containing glass coverslips at a density of $5x10^4$ per well unless stated otherwise.

2.7 Transfections

Transfections were performed with FuGENE6 (Roche) or GeneJuice (Novagen) at 1:3 ratio (reagent:DNA) in Opti-MEM (Invitrogen) as recommended by the manufacturers. In the case of co-transfection, cells were transfected with equal amounts of the two plasmids.

The cells were incubated with the transfection:DNA mix for 24 hours in a 5% CO_2 incubator at 37^{o}C and then washed in PBS and fixed in 3 % PFA.

2.8 Infection of HeLa cells

EHEC was grown o/n in LB with the appropriate antibiotics when necessary. Bacterial growth was diluted in 1:500 DMEM with antibiotics and bacteria were statically incubated o/n at 37^{o}C, 5% CO_2. Expression was induced for 30 min with 0.1mM IPTG when required. HeLa growth medium was replaced with 0.5 mL warm DMEM without FCS for 30 mins prior to infection and cells were infected approximately at 1 x 10^9 cfu. Infected plates were centrifuged for 5 min at 1000 rpm to increase bacterial attachment and incubated at 37^{o}C, 5% CO_2 for 5h. After 2h 30 min of incubation, HeLa cells were washed three times with PBS to remove non-adherent bacteria and warm DMEM added for the remaining incubation.

Overnight EPEC cultures were prepared in LB with the appropriate antibiotic. On the day of infection, the bacteria were primed by diluting the o/n culture 1:50 in DMEM 1g/l glucose. Priming was allowed for 3h at 37^{o}C, 5% CO_2 under static conditions. Bacterial cultures were induced with 0.1mM IPTG for 30 min prior to infections. HeLa cells were washed with PBS and 0.5 mL of the primed overnight culture was added in the wells. Infections were allowed to proceed for 1h before adding 300 μg/ml gentamicin to kill extracellular bacteria and incubation continued for a further 1-2hs. All cells were washed with PBS and fixed with 3% PFA at RT for 15 min.

2.9 Scanning Electron Microscope

Tissue samples from mouse *in-vitro* cultures (mIVOC) were fixed in 2.5% glutaraldehyde in phosphate buffer (PBS). After fixation tissues were incubated in PBS for 1h30 and then fixed with secondary fixative 1% osmium tetroxide (OsO4) in PBS for 30 mins. Samples were washed with PBS followed by distilled water prior to ethanol dehydration; a sequential 10 min treatment of samples with increasing concentration of aqueous ethanol solutions. Tissue samples were dried using Emitech K850 Critical Point drier according to manufacturer's instructions and mounted on aluminium stubs for gold/palladium mix coating using Emitech Sc7620. Samples were examined using Jeol JSM-6390 Scanning Electron Microscope.

2.10 Immunofluorescence staining

After PFA fixation, cells were washed with PBS and remaining PFA was neutralised with ammonium chloride. Cells were then permeabilised with 0.1% Triton X-100 in PBS for 4 mins at RT, washed twice in PBS, and blocked in 3% BSA-PBS for 20 mins. Coverslips were incubated with the appropriate primary antibody diluted in blocking agent for 45 min at RT [mouse α- Myc (1:500 - Sigma), mouse α- Hax (1:50 - BD), rabbit α- cleaved Caspase 3 (1:100 – BD), mouse α- Cytochrome -*c* (1:100 - Merck), rabbit α- O157 (1:500) for EHEC and rabbit α- O127 (1:500) for EPEC]. The cells were washed three times with PBS for 15 mins and stained with appropriate secondary antibodies Donkey α- mouse^{FITC}, α- rabbit^{FITC}, α- rabbit^{Cy5} at 1:200 (Jackson Immunoresearch) or DAPI for DNA staining (1:500). When necessary a directly conjugated α- myc^{FITC} (1:200 – Sigma) was added for a third antibody incubation. Coverslips were washed three times in PBS, once in distilled H_2O and mounted

on glass slides using ProLong Gold reagent (Invitrogen). Immunoflourescent staining was visualised with a Zeiss AxioImager fluorescence microscope (M1 and Z1) by Carl Zeiss. Images were analyzed with the AxioVision Release 4.8 and Fiji softwares.

2.11 Microscopy and Imaging

Immunoflourescent staining was visualised with a Zeiss AxioImager fluorescence microscope (M1 or Z1) by Carl Zeiss. Images were analyzed with the AxioVision Release 4.8 software and the open source image processing Fiji / Image J package (http://fiji.sc/Fiji). Appropriate deconvolution algorithms were used to optimise the point spread function (PSF), which is the point source of light that passes through a lens and describes the diffraction of light in an optical system. A useful PSF results from acquiring and processing multiple z-stacks (i.e. multiple images of different focus). For best results, z-stacks for all images were acquired above and below the object of interest (20-30 z-stacks). The appropriate z-step interval can be set to automatic and calculated by the Zeiss AxioImager software but can be also calculated manually using the Abbe-Rayleigh diffraction limit equation: z-step interval (nm) = (emission wavelength x refractive index of the mounting medium) / (numerical aperture of the objective^2). The z-step interval was ~ 250nm for all images. For deblurring / deconvolution the "Regularized Inverse Filter" algorithm which is a 3D deblurring method from Z-stacks with Nyquist oversampling (Nyquist sampling theorem is used in the process of converting a signal into numeric sequence). The processed images were exported from the AxioVision or Fiji softwares in appropriate file formats (i.e. .jpg or .png). The Fiji software was used to calculate scale bars for IF images. The JACoP,

Coloc2 and Colocalisation Threshold plugins were used in Fiji to quantify colocalisation and perform the statistical anylisis.

2.12 Western Blots

Cells were lysed with RIPA buffer [150mM sodium chloride, 1.0% NP-40, 0.5% sodium deoxycholate, 0.1% SDS, 50mM Tris – pH 8.0, with complete, mini, EDTA-free protease inhibitor cocktail (Roche) and phosphatase inhibitors (2mM Na_3VO_4, 10mM NaF and 1mM PMSF)]. Protein concentration was determined using the BCA assay (ThermoScientific) according to the manufacturer's manual. Samples were denatured with Laemmli buffer and heated at 95 ^oC for 5 mins. Samples were separated by SDS-PAGE and gels were either stained with Coomassie Brilliant Blue R-250 or transferred to PVDF membrane. Membranes were blocked in 5% milk or BSA – PBST for 1 hour and then incubated in primary antibody overnight at 4 ^oC under agitation (mouse α- Hax (1:500 - BD), mouse anti- α-Tubulin (1:2000 – Sigma) and mouse α- MBP (1:1000 – NEB) followed by HRP-conjugated secondary antibodies (1:2500 – Jackson Immunoresearch). HRP was detected with ECL+ Detection Kit and visualised with LAS-3000 Imaging System (Fuji).

2.13 Pull-Downs

EspO MBP fusion constructs in Top10 *E. coli* were grown to an OD of 0.5-0.6 at 37^oC or 30^oC in LB broth with the appropriate antibiotic and then induced with 0.3 mM IPTG for 2 or 3 hours. Cells were harvested, resuspended in Column Buffer (20 mM Tris-HCL, 200 mM NaCl and 1 mM EDTA) and sonicated for 5 min in short pulses of 15 sec. Insoluble

protein was removed by centrifugation at 9000 x g for 30 mins and soluble protein allowed to bind onto an amylose column. Bound protein was washed three times with 2ml of Column buffer with 1mM DTT before eluting with maltose and analysed by SDS-PAGE and Coomassie Brilliant Blue staining.

2mL of bacterial lysate (MBP:EspO or MBP:lacZ control) were added to 1mL cleared amylose beads. HEK293 cells grown at suspension were collected by centrifugation at $2x10^6$ cell density and lysed with 5 mL RIPA buffer [150mM sodium chloride, 1.0% NP-40, 0.5% sodium deoxycholate, 0.1% SDS, 50mM Tris – pH 8.0, with complete mini- protease and phosphatase inhibitors EDTA-free (Roche)]. 1mL of HEK293 cell lysate was added to appropriate samples. Samples were incubated on a rotating wheel overnight at 4 ^oC. Supernatant was removed by centrifugation and beads were washed 3x in column buffer. Bound proteins were eluted in 10mM maltose in column buffer on ice for 20 min and analysed by SDS-PAGE and western blot.

2.14 Apoptosis experiments

Apoptosis was induced in HeLa cells 24 hours after transfection with 1μM staurosporine (Sigma) for 3 hrs, 10μg/ml tunicamycin (Sigma) for 16-24hrs or 1μM thapsigargin (Sigma) for 4hrs. Cells were fixed with 3% PFA and stained with cleaved caspase-3 and condensed nuclei and/or TUNEL (Promega). TUNEL staining was performed according to the users manual; apoptotic nuclei were stained with the fluoroscein-12-dUTP supplied and healthy nuclei were stained with DAPI (1:500). 100 transfected cells per condition were counted for staurosporine and tunicamycin and 50 cells counted for thapsigargin; all of them assessed for markers of apoptosis.

2.15 Infection of mice with *C. rodentium*

C. rodentium wild-type (ICC169), *espO* mutant (prepared with one-step PCR λ-red-mediated mutation protocol) and mutant strain complemented with pACYC-*espO* or *espO*(W77A) were pelleted by centrifugation and resuspended in PBS. Specifc-pathogen-free 6- to 8- week-old C57BL/6 mice (Harlan, UK Ltd.) were inoculated by oral gavage at $2x10^9$ cfu in 200 μl PBS. All animals were housed in individual cages with sterile bedding and free access to sterilized food and water. Two independent experiments were performed using four mice per group. The viable counts of each inoculum were determined by plating dilutions on selective plates. Stool samples were collected daily up to 18 days post-inoculation. The viable count per gram of stool was determined by plating serial dilutions of stool samples onto selective media.

Hyperplasia was assessed 18 days post inoculation by collecting segments of the cecum, rinsed and fixed in 10% formalin. Fixed tissues were then processed, paraffin embedded, sectioned at 5 μm and stained with hematoxylin and eosin (H&E). The length of at least four well-oriented crypts was evaluated for each section and a non-parametric analysis of variance (ANOVA) was performed using GraphPad Prism Statistical Software. *P* values of ≤0.05 were considered significant.

Snap-frozen colonic tissues were sectioned with a cryostat to a thickness of 5 μm. The sections were then mounted on polysine slides and air dried over night before acetone fixation. The sections were air dried for 1 hour and re-hydrated in Tris-buffered saline (TBS) for 5 mins. Incubation with the appropriate antibodies (Ly6 for neutrophils and CD4 antibody for staining CD4+ T cells) at a dilution 1:50 followed for 1 hour. The sections were then washed in TBS and biotinylated anti-`rat immunoglobulin G was added at a dilution 1:200. 0.1% avidin-peroxidase (Sigma-Aldrich, Dorset, United Kingdom) was then

added at 1:200 and left for 30 min before further washing and treatment with diaminobenzadine substrate (Sigma-Aldrich) for 5 min. Sections were then counterstained with Mayer's hematoxylin (Sigma-Aldrich) for 30 s, dipped in acid alcohol, and washed in tap water for 5 min. Dehydration followed through an ethanol gradient of 70%, 90%, and 100% solutions (2 min each). Stained cell populations were counted in five randomly selected fields per section, and data were expressed as the number of Neutrophil or T cells per 250 μm^2 of lamina propria.

2.16 siRNA experiments

Cells were seeded at $5x10^3$ cells/well in 24-well plates with coverslips 24h prior to the introduction of siRNAs (Dharmacon). Cells were transfected with 20μM Hax-1 targeted siRNA according to the HiperFect user manual. Optimum knockdown of Hax-1 was seen after 72 hrs of incubation as confirmed by western blots analysis. The cells were then used for the apoptosis experiments as described above and 100 transfected cells were assessed for apoptosis per condition.

2.17 Statistical significance

Results from apoptosis experiments include three biological replicates (each biological consists of two technical replicates) and were analysed for statistical significance using the GraphPad Prism Statistical Software Version 6 (GraphPad Software Inc.,San Diego). Results are represented as means ± standard deviations analysed by a two-tailed unpaired *t*-test with equal SD.

2.18 Diagramatic illustrations

Illustrations prepared for this study were designed by the author using Adobe Illustrator and Microsoft Office Power Point.

Table 4. List of strains

ICC	Strains	Description	Source/Reference
	EDL933	EHEC O157:H7 *stx*-	ATCC 700927
	EDL933 Δ *espO1-1*	Single *espO1-1* deletion mutant in EHEC EDL933 (CmR)	This study
	EDL933 Δ *espO1-2*	Single *espO1-2* deletion mutant in EHEC EDL933 (KnR)	This study
	EDL933Δ*espO1-1*Δ*espO1-2*	Double *espO* deletion mutant in EHEC EDL933 (CmR, KnR)	This study
	EDL933Δ*espO1-1*Δ*espO1-2* pSA10:: *espO1-1*	Complemented double mutant overexpressing *espO1-1* with c-terminal HA-tag	This study
	E2348/69 wt	EPEC O127:H6 wild type	[218]
303	E2348/69 Δ*nleH1* Δ*nleH2*	EPEC O127:H6 double *nleH* mutant	[48]
	E2348/69Δ*nleH1*Δ*nleH2* pSA10::*espO1-1*	EPEC O127:H6 overexpressing *espO1-1* (untagged)	This study
	E2348/69Δ*nleH1*Δ*nleH2* pSA10::*espO1-1*$_{W77A}$	EPEC O127:H6 overexpressing *espO1* W77A (untagged)	This study
169	*C. rodentium* wt	Wild type strain	This study
	C. rodentium Δ *espO*	Single *espO* mutant	This study
	C. rodentium Δ *espO* pACYC::*espO*	Complemented mutant with full length *espO*	This study
	C. rodentium Δ *espO* pACYC::*espO*$_{W77A}$	Complemented mutant with Trp deletion mutant at position 72 of *espO* (equivalent of W77A in EspO1-EHEC and W68A in OspE – *S. flexnerie*)	
	AH109	S. cerevisiae HIS3, ADE2, lacZ, and MEL1 reporters for interaction, and TRP1 and LEU2 transformation markers	Clontech
	Y187	S. cerevisiae lacZ, and MEL1 reporters for interaction, and TRP1 and LEU2 transformation markers	Clontech

Table 5. List of plasmids

pICC	Name	Description	Reference
	pKD4	*oriRg, blaM*, KanR cassette flanked by FRT sites	[215]
	pKD3	*oriRg, blaM*, CmR cassette flanked by FRT sites	[215]
	pKD46	*ori101, repA 101* (ts), *araBp-gam-bet-exo, blaM*	[215]
	pRK5::myc	Mammalian expression vector with N-term Myc tag	Clontech
563	pRK5:: *gfp*	Full-length GFP	[48]
	pRK5::myc- *espO1-1*	Full length *espO1-1* (EHEC EDL933)	This study
	pRK5::myc- *espO1-2*	Full length *espO1-2* (EHEC EDL933)	This study
	pRK5::myc- *espO*	Full length *espO* (*C. rodentium* ICC168)	This study
	pRK5::myc- *sopO* (TYM)	Full length *ospE1* (*S.* Typhimurium)	This study
	pRK5::myc- *ospE1*	Full length *ospE1* (*S. flexnerie*)	This study
	pRK5::myc- *espO1-1* (W77A)	Trp deletion mutant at position 77 of *espO1-1* (EHEC)	This study
	pRK5::myc- *ospE1* (W68A)	Trp deletion mutant at position 68 of *ospE1* (*S. flexnerie*)	This study
	pRK5::myc- *sopO* (TY)	Full length *sopO* (*S.* Typhi)	This study
512	pRK5::myc- *nleH1*	Full length *nleH1* (EPEC E2348/69)	[48]
	pCDNA::Flag- *espO1-1*	Full length *espO1-1* (EHEC EDL933)	This study
	pCMV::myc- *hax-1*	Full length *hax-1* fused to myc tag.	[205]
	pGADT7-Rec	Y2H vector containing GAL4 DNA activation domain (GAL4-AD)	Clontech
	pGADT7-Rec::*hax-1*	Full length *hax-1* fused to GAL4-AD (Y2H)	This study
	pGBKT7	Y2H expression vector with GAL4 DNA binding domain (GAL4-BD)	Clontech
	pGBKT7::*espO1-1*	Full length *espO1-1* fused to Gal4 DNA-BD (Y2H)	This study
	pGBKT7::*espO1-2*	Full length *espO1-2* fused to Gal4 DNA-BD (Y2H)	This study
	pGBKT7::*espO*	Full length *espO* (*C. rodentium* ICC168)	This study
	pGBKT7::*sopO* (TYM)	Full length *ospE1* (*S.* Typhimurium)	This study
	pGBKT7::*sopO* (TY)	Full length *ospE1* (*S.* Typhi)	This study
	pGBKT7::*ospE1*	Full length *ospE1* (*S. flexnerie*)	This study
	pGBKT7::*espO1-1* (W77A)	Trp deletion mutant at position 77 of *espO1-1* (EHEC)	This study
	pGBKT7::*ospE1* (W68A)	Trp deletion mutant at position 68 of *ospE1* (*S. flexnerie*)	This study
	pGBKT7::*espO1-1* (1-45)	N-terminal deletion mutant of *espO1-1* (EHEC)	This study
	pGBKT7::*espO1-1* (45-91)	C-terminal deletion mutant of *espO1-1* (EHEC)	This study
	pGBKT7::*espO1-1* (1-73)	C-terminal 18 aa deletion mutant of *espO1-1* (EHEC)	This study
	pGBKT7::*espO1-1 -myc*	C-terminal tagged *espO1-1* (EHEC)	This study
	pSA10	pKK177-3 induced expression vector containing lacI gene	[219]
	pSA10:: *espO1-1*	Derivative of pSA10 expressing *espO1-1*	This study
	pSA10:: *espO1-1* (W77A)	Derivative of pSA10 expressing *espO1-1* (W77A)	This study
	pACYC184	*orip154*, CmR, TcR	NEB
	pMAL::MBP- *lacZ*	MBP tag expression vector	NEB
	pMAL::MBP- *espO1-1*	Full length *espO1-1* fused to MBP	This study
	pMAL::MBP- *espO1-2*	Full length *espO1-2* fused to MBP	This study

pCDNA3.1::HA-CREB3	Mammalian vector expressing ER marker CREB3	This study
pACYC184::*espO*	In-vivo *espO* mutant complementation (*C. rodentium*)	This study
pACYC184::*espO* (W77A)	In-vivo Trp deletion mutant at position 72 of *espO* mutant complementation (*C. rodentium*)	This study

Table 6. List of primers (RE sites underlined and Point mutations or insertions in bold)

No.	Name	Nucleotide Sequence (5'-3')
1	pSA10-EspO1-F	GCTGAATTCATGCCATTTTCAATCAAAAAC
2	pSA10-EspO1-HA-R	GCTCTGCAGCTATGATTTGTTTGTATTATTTG
3	pSA10-EspO1-R	GCTCTGCAGTTCTTTTGTGTTGTGTATC
4	pRK5-EspO1-F	TTGAATTCATGCCATTTTCAATCAAAAAC
5	pRK5-EspO1-R	CCAATGCACTGCAGTTAAGCGTAGTCTGGGACGTCGTATGGGTATTCTTTTGTGTTGTGTATC
6	pRK5-EspO2-F	TTGAATTCATGCCATTTTCAATAAAAAG
7	pRK5-EspO2-R	CCAATGCACTGCAGTTAAGCGTAGTCTGGGACGTCGTATGGGTATGATTTGTTTGTATTATTTG
8	pRK5-OspE1-F	GCTGGATCCGGAGCACTTACACAAACTATATTCCC
9	pRK5-OspE1-R	GCTGAATTCTCAGAAATCAGAATACCGTTGGCTTT
10	pRK5-SopO(TYM)-F	GCTGGATCCGGAGCACCATTTTCAATCAAAAAC
11	pRK5-SopO(TYM)-R	GCTGAATTCTCATTCTTTTGTGTTGC
12	pRK5-EspO(CR)-F	GCTGGATCCGGAGCACCATTGTCAATAAGAAATATAT
13	pRK5-EspO(CR)-R	GCTGAATTCTCAGGATTTATTTGAGTTATTAATCTCG
14	pRK5-SopO(TY)-F	GCTGGATCCGGAGCACCATTTTCAATCAAA
15	pRK5-SopO(TY)-R	GCTGAATTCTGATGCTGATAATTTTAGTCGTG
16	EspO1(W77A)-F	GTTACTGAGATGACA**GC**GCTATCTAAAACTATAG
17	EspO1(W77A)-R	CTATAGTTTTAGATAGC**GC**TGTCATCTCAGTAAC
18	OspE1(W68A)-F	GCTACAGAAATGCAA**GC**GTTGACAAAGATAAATG
19	OspE1(W68A)-R	CATTTATCTTTGTCAAC**GC**TTGCATTTCTGTAGC
20	pGBKT7-EspO1-F	TTGAATTCATGCCATTTTCAATCAAAAAC
21	pGBKT7-EspO1-R	CGCGGATCCCTATTCTTTTGTGTTGTGTATC
22	pGBKT7-EspO2-F	TTGAATTCATGCCATTTTCAATAAAAAG
23	pGBKT7-EspO2-R	CGCGGATCCCTATGATTTGTTTGTATTATTTG
24	pGBKT7-OspE1-F	GCTGAATTCCTTACACAAACTATATTCCCTTGTC
25	pGBKT7-OspE1-R	GCTGGATCCTCAGAAATCAGAATACCGTTG
26	pGBKT7-SopO(TYM)-F	GCTGAATTCCCATTTTCAATCAAAAAC
27	pGBKT7-SopO(TYM)-R	GCTGGATCCTCATTCTTTTGTGTTGC
28	pGBKT7-EspO(CR)-F	GCTGAATTCCCATTGTCAATAAGAAATATATTTTC
29	pGBKT7-EspO(CR)-R	GCTGGATCCTCAGGATTTATTTGAGTTATTAA
30	pGBKT7-EspO1(1-45)-F	GCTGAATTCCCATTTTCAATCAAAAACAGATTTTC
31	pGBKT7-EspO1(1-45)-R	GCTCTGCAGTGTATAGCTATCTACATTACATGTT
32	pGBKT7-EspO1(45-90)-F	GCTGAATTCGTGTACCAAAAAAAAGCCTGTA
33	pGBKT7-EspO1(45-90)-R	GCTCTGCAGCTATTCTTTTGTGTTGTGTATCT
34	EspOΔ18-F	CTCTCAGTTACT**TAG**GAGATGACATGG
35	EspOΔ18-R	CCATGTCATCTC**CTA**AGTAACTGAGAG
36	c-terminal myc pGBKT7-	GCAGAACAAAAACTTATTTCTGAAGAAGATCTGTTAGGGATCCGTCGACCTGCAGCG
37	c-terminal myc pGBKT7-	**CTA**ACAGATCTTCTTCAGAAATAAGTTTTTGTTCTGCTTCTTTTGTGTTGTGTATCT
38	pGADT7-Hax1-F	GCTGAATTCAGCCTCTTTGATCTCTTCCG
39	pGADT7-Hax1-R	GCTGAATTCCTACCGGGACCGGAACC
40	AD-LD F	CTATTCGATGATGAAGATACCCCACCAAA
41	AD-LD R	AGATGGTGCACGATGCACAGTT
42	pMAL-EspO1-F	GCTGAATTCCCATTTTCAATCAAAAACAGATTTTC
43	pMAL-EspO1-R	GCTGGATCCCTATTCTTTTGTGTTGTGTATC
c1	EspO1 del. F	CAACTTATAACGGAATAGCATAAAAACACTTTTCATGGAGCAAAGGAGAAAACATGTGTAGGCTGGAGCTGC
c2	EspO1 del. R	GTCAGGTGTTTCGGGTCTGTGGCTTTTTGTGTTCTCTGGTAAGTGGTTGCATATGAATATCCTCCTTAGTTCC
k1	EspO2 del. F	CTAAATACATTAAATTGCACTATAAGAGAAAGACATAATGTGAGGATAAAATGTGTAGGCTGGAGCTGCTTC
k2	EspO2 del. R	GTTAGGAAGTTATTCATGGCTAGTGTACCAACTCTTTTCTGGGCTAATAGCATATGAATATCCTCCTTAGTTCC
44	Ext.- EspO1-F	ATAAGCAAGATCCACTTATCAAAAGAGCATTA
45	Ext.- EspO1-R	ACTATCACTTATTTAAGTGATACT
46	Ext.- EspO2-F	AATACCCTGTCGTGCCCATTTTTCCATCGGACGCA
47	Ext.- EspO2-R	CGTTTTTCGTGTCTTTAAGTGAT

48	Cm-pKD3-R	TTTTGAGGCATTTCAGTCAGTTGC
49	Kn-pKD4-R	CATCGCCATGGGTCACGACGAGAT
50	pACYC184-EspO-F	gctggatcctagAAGAAGGAGATATACCATGCCATTGTCAATAAGAAA
51	pACYC184-EspO-R	gctgtcgacTCAGGATTTATTTGAGTTATTAATCTCGGTC
52	EspOcr(W77A)-F	GCCTCAGAAGCTCAGGCGATGTGCAAAATTATAG
53	EspOcr(W77A)-R	CTATAATTTTGCACATCGCCTGAGCTTCTGAGGC

2.19 References

1. Datsenko, K.A. and B.L. Wanner, *One-step inactivation of chromosomal genes in Escherichia coli K-12 using PCR products.* Proc Natl Acad Sci U S A, 2000. **97**(12): p. 6640-5.
2. Gietz, R.D. and R.H. Schiestl, *Quick and easy yeast transformation using the LiAc/SS carrier DNA/PEG method.* Nat Protoc, 2007. **2**(1): p. 35-7.
3. Gietz, R.D. and R.H. Schiestl, *Frozen competent yeast cells that can be transformed with high efficiency using the LiAc/SS carrier DNA/PEG method.* Nat Protoc, 2007. **2**(1): p. 1-4.
4. Levine, M.M., et al., *Escherichia coli strains that cause diarrhoea but do not produce heat-labile or heat-stable enterotoxins and are non-invasive.* Lancet, 1978. **1**(8074): p. 1119-22.
5. Hemrajani, C., et al., *NleH effectors interact with Bax inhibitor-1 to block apoptosis during enteropathogenic Escherichia coli infection.* Proc Natl Acad Sci U S A, 2010. **107**(7): p. 3129-34.
6. Schlosser-Silverman, E., et al., *Characterization of Escherichia coli DNA lesions generated within J774 macrophages.* J Bacteriol, 2000. **182**(18): p. 5225-30.

3 Chapter 3 : Novel Interacting Partners

3.1 Distribution of EspO in enteric bacteria

In order to find the prevalence of EspO in enteric bacteria and look at the relationships between EspO homologues, we performed EHEC EspO1 amino acid sequence searches against translated reference genomic sequences of the Enterobacteriaceae genera using TBLASTX of the NCBI database and the relationship between EspO homologs, orthologs and paralogs was determined with the TreeView (BioEdit) and visualised as an EspO phylogeny of the ClustalW2 (EMBL-EBI) multiple sequence alignments.

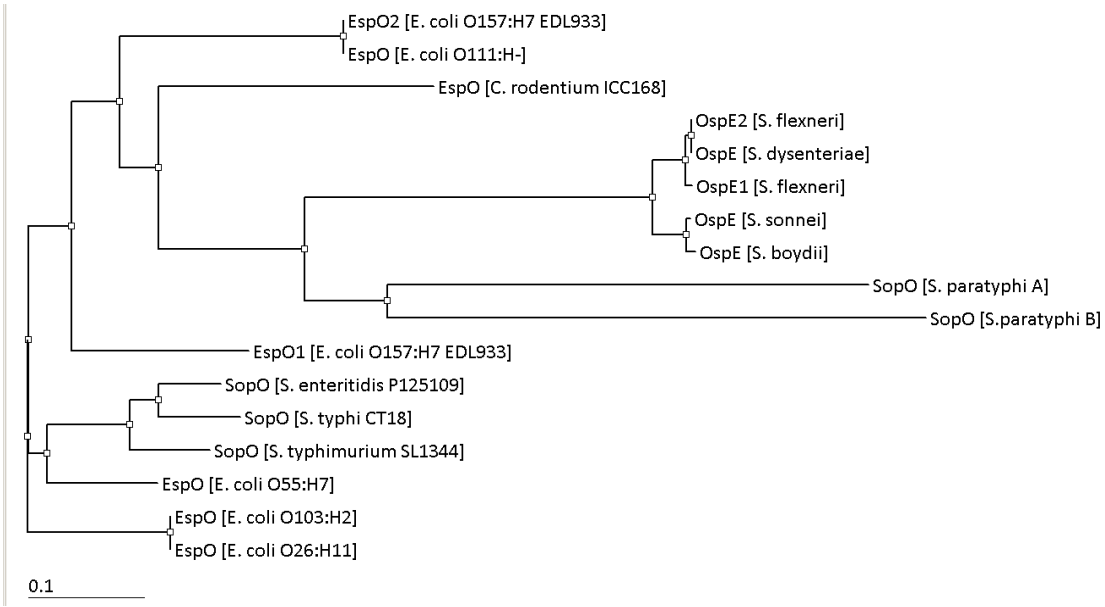

Figure 18. Phylogram of EspO family members conserved in enteric bacteria.
Phylogram showing the homologues of the EHEC or EPEC EspO in Shigella and Salmonella strains. The phylogram was created with TreeView, BioEdit.

Bioinformatic analysis identified EspO primarily in EHEC O157:H7 strains and non-O157 strains O111:H-, O103:H2 and O26:H11 (Figure 18). EspO orthologs exist singly in C. rodentium and Salmonella strains. As shown in the phylogram, the Salmonella orthologs, appear to be closely related with EHEC EspO. Only, SopO in *S.* Paratyphi A and B strains, which is a truncated form, seems to be more distant. On the contrary, the EspO ortholog OspE, which is highly conserved in Shigella strains, is distantly related to EHEC EspO1 (Figure 18).

As previously mentioned, the prototypical EPEC strain E2348/69 is naturally *espO* negative but the EPEC clone O55:H7, which is considered a progenitor of EHEC O157:H7, contains one *espO*. To further understand the prevalence of *espO* among EPEC strains, we performed a mini PCR screen on clinical EPEC isolates using two sets of primers designed to detect *espO1-1* and *espO1-2* from EHEC strain EDL933 and identified *espO* in 18/72 EPEC isolates (25%) of serogroups O55 (7/13 - 54%), O26 (2/5 – 40%), O111 (1/5 – 20%), O154 (1), O85 (1), O123 (1), O49 (1), O109 (1) and ONT (2) (Table 7). Of note is the fact that due to sequence variation the primers used for the screen might not amplify all the *espO* variants. As a positive control we used EPEC O111:H9 strain E110019 whose genome has been partially sequenced and revealed the presence of one *espO* gene. The *espO* screen and bioinformatic analysis indicate that EspO might have an important role in pathogenesis due to its relatively high abundance in enteric bacterial pathogens.

	Pathotype and serotype (no. of strains)	EspO1	EspO2
aEPEC			
	O55:H7 (1)	+	-
	O55:H7 (3)	-	+
	O26:H- (1)	-	+
	O26:H11 (1)	+	+
	O154:H9 (1)	+	-
	ONT:H- (1)	+	+
	O85:H- (1)	+	-
	O123:H-(2)	+	-
	O49:H- (1)	+	+
	ONT:H7 (1)	+	-
	O109:H9 (1)	+	+
tEPEC			
	O111:H- (1)	+	-
	O55:H- (2)	+	-
	O55:H6 (1)	-	+

Table 7. EspO distribution in EPEC isolates
PCR screen on clinical EPEC isolates using primers designed to detect *espO1-1* and *espO1-2* from EHEC strain EDL933. Positive *espO* strains are shown in the table. The strains are divided into atypical EPEC (aEPEC) that include strains lacking the EAF plasmid and typical EPEC (tEPEC) that describe strains harbouring the plasmid.

espO-negative strains are as follows: O104:H2 (2), O2:H49 (2), O26:H- (3), O45:H- (1), O111:H- (1), O153:H- (1), OR:H- (1), O13:H- (1), O8 (1), O103:H2 (1), O109:H2 (1), O128:H2 (1), O15:H- (1), O55:H- (2), O55:H6 (2), O55:H7 (2), O86:H34 (3), O111:H2 (3), O119:H2 (4), O119:H6 (4), O125:H6 (1), O127:H6 (1), O127:H40 (3), O128:H2 (4), O128ab:H2 (1), O142:H6 (3), O142:H34 (3).

3.2 Identifying novel EspO interacting partners

To identify protein partners interacting with EspO, a yeast two-hybrid screen was done with a Matchmaker Pretransformed Normalised Library from HeLa cells and EspO1 (EHEC) bait construct expressing the full-length protein. The 77 diploid clones, which survived after two re-streaks on high-stringency media (QDO) were further confirmed by colony PCR. The sizes of the PCR products were in the range of 900bp to 1500 bp (Figure 19).

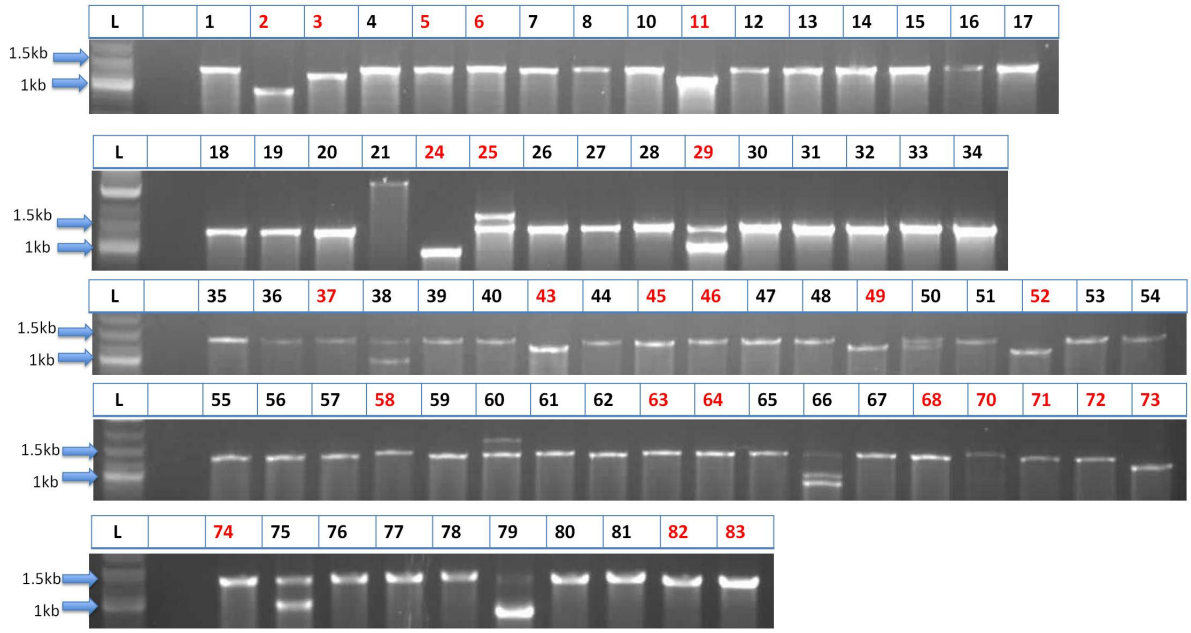

Figure 19. PCR confirmation of yeast clones.
Colony PCR performed on yeast clones grown on high stringency media (QDO). Clone numbers in red indicate the PCR products selected for sequencing.

The majority of the clones (53/77) yielded 1.5kb PCR product and six of these clones were further confirmed by sequencing. Blastn and blastx algorithms (PubMed) were used to analyse the sequencing results, which revealed that the 1.5kb PCR product is Hax-1 (HCLS associated protein X-1). The clones 25 and 29 (Table 8) appeared to have two plasmids and each PCR product yielded from these clones was separately gel purified and

sequenced. This is a normal yeast two-hybrid outcome since transformed yeast cells are able to accommodate more than one version of a related plasmid. All PCR products of size other than 1.5kb were also sequenced (17/77) (Table 8). Another interesting hit, which was detected more than once was the DnaJ homolog or Heat shock protein 40 (Hsp40) subfamily B.

Table 8. Sequencing results for 27 clones

Clone No.	Accession No.	Protein
2	NM_012328.1	Homo sapiens DnaJ (Hsp40) homolog, subfamily B, member 9
3	NM_015322.3	Homo sapiens fem-1 homolog b (C. elegans) (FEM1B)
5	NM_005494.2	Homo sapiens DnaJ (Hsp40) homolog, subfamily B, member 6
6	NM_006118.3	Homo sapiens HCLS1 associated protein X-1 (HAX1)
11	NM_006118.3	Homo sapiens HCLS1 associated protein X-1 (HAX1)
24	NM_002537.2	Homo sapiens ornithine decarboxylase antizyme 2 (OAZ2)
25A	NM_006118.3	Homo sapiens HCLS1 associated protein X-1 (HAX1)
25B	NM_000521.3	Homo sapiens hexosaminidase B (beta polypeptide) (HEXB)
29A	NM_001009186.1	Homo sapiens chaperonin containing TCP1, subunit 6A (zeta 1)
29B	NM_006118.3	Homo sapiens HCLS1 associated protein X-1 (HAX1)
37	NM_006118.3	Homo sapiens HCLS1 associated protein X-1 (HAX1)
43	NM_006145.1	Homo sapiens DnaJ (Hsp40) homolog, subfamily B, member 1
45	NM_006118.3	Homo sapiens HCLS1 associated protein X-1 (HAX1)
46	NM_006118.3	Homo sapiens HCLS1 associated protein X-1 (HAX1)
49	NM_005494.2	Homo sapiens DnaJ (Hsp40) homolog, subfamily B, member 6
52	NM_006118.3	Homo sapiens HCLS1 associated protein X-1 (HAX1)
58	NM_006118.3	Homo sapiens HCLS1 associated protein X-1 (HAX1)
63	NM_006118.3	Homo sapiens HCLS1 associated protein X-1 (HAX1)
64	NM_006118.3	Homo sapiens HCLS1 associated protein X-1 (HAX1)
68	NM_006118.3	Homo sapiens HCLS1 associated protein X-1 (HAX1)
70	NM_006118.3	Homo sapiens HCLS1 associated protein X-1 (HAX1)
71	NM_006118.3	Homo sapiens HCLS1 associated protein X-1 (HAX1)
72	NM_006118.3	Homo sapiens HCLS1 associated protein X-1 (HAX1)
73	NM_006118.3	Homo sapiens HCLS1 associated protein X-1 (HAX1)
74	NM_006118.3	Homo sapiens HCLS1 associated protein X-1 (HAX1)
82	NM_006118.3	Homo sapiens HCLS1 associated protein X-1 (HAX1)
83	NM_006118.3	Homo sapiens HCLS1 associated protein X-1 (HAX1)

3.3 EspO1:Hax-1 interaction confirmed by direct Y2H

To further confirm the interaction, the bait construct pGBKT7-EspO1 or pGBKT7-EspO2 and the Gal4/AD vector, pGADT7 expressing HAX-1 were co-transformed in yeast strain AH109 (Figure 20). True positive interactions were assessed by the ability of co-transformed AH109 to grow on high stringency media. To show that HAX-1 alone does not activate the reporters, AH109 containing the empty pGBKT7 vector with the pGADT7-Hax-1 construct was also grown on high stringency media. Also to confirm that EspO1 or EspO2 alone do not activate the reporters the pGBKT7 vectors expressing the effectors were co-transformed with the empty pGADT7 vector. The transformed yeast strains were allowed to grow for five days and as shown in Figure 20, a clear difference in growth was observed on high stringency media between strains expressing both proteins and those expressing only one.

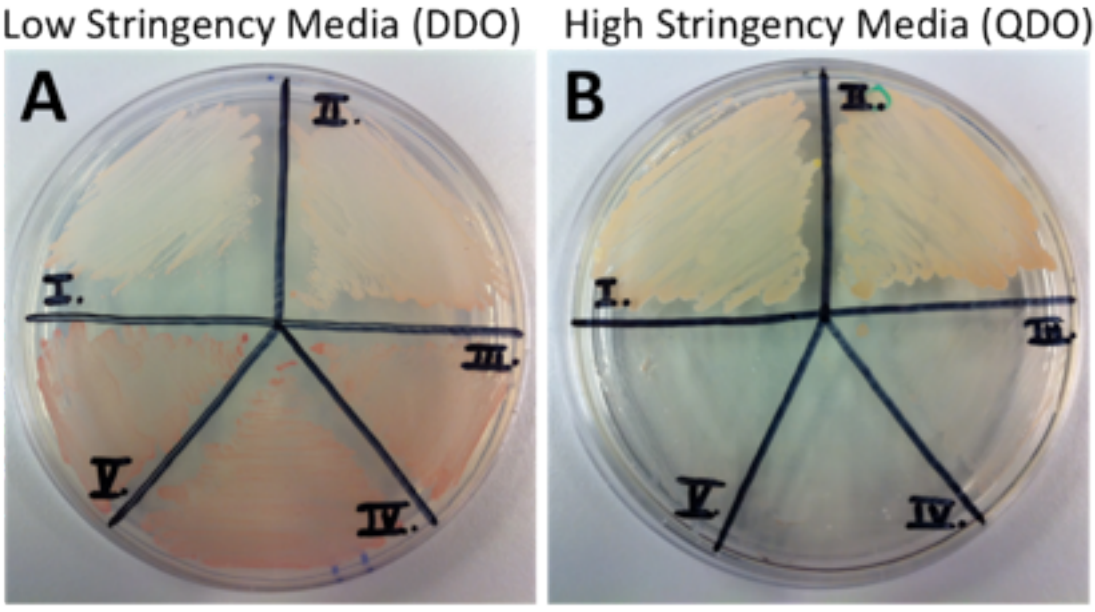

Figure 20. Direct Y2H confirmation of EspO1 with Hax-1
[I] pGBKT7-EspO1/pGADT7-HAX-1, **[47]** pGBKT7-EspO2/pGADT7-HAX-1, **[III]** pGBKT7-/pGADT7-HAX-1, **[IV]** pGBKT7-EspO1/pGADT7- , **[V]** pGBKT7-EspO2/pGADT7-.

3.4 EspO1:Hax-1 interaction confirmed by Pull-Downs

To further confirm the *in-vitro* EspO binding to Hax-1, the pMAL constructs (See Table 5) were used for an inducible expression and purification of EspO and then used for the pull-down assays. The pMAL system provides expression of the protein fused to MBP (maltose binding protein) and allows purification, which results from the binding of MBP to amylose. The expression profiles of EspO1 and EspO2 fused to MBP were sought in order to determine the solubility of the effector proteins and the optimum conditions required for increased yield. Growth at 30^{o}C, 200 rpm until an OD of 0.5-0.6 was reached and then induction with 0.3 mM IPTG for 2 hours showed that both proteins are adequately expressed and remain soluble. The purified EHEC EspO1 and EspO2 fused to MBP were run on a 10% SDS-PAGE gel for validation (Figure 21).

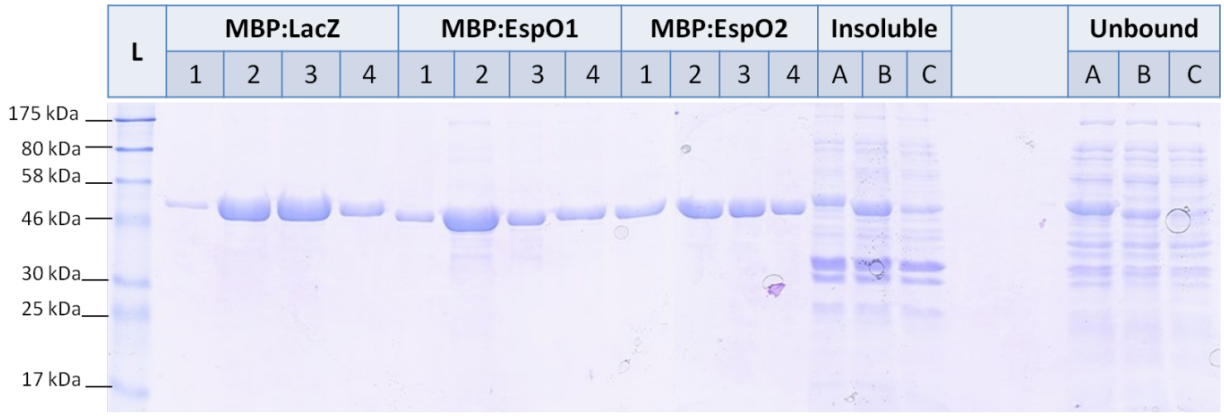

Figure 21. EspO purification
The pMAL plasmids expressing EspO1 and EspO2 fused to MBP and empty pMAL vector expressing MBP fused to LacZ were used. Four samples were collected for each purified protein. The insoluble material and the unbound fraction (amylose column flow through) are also included (A-MBP:LacZ control, B-MBP:EspO1 and C-MBP:EspO2). The MBP:EspO1 and MBP:EspO2 fusion proteins are 53 kDa.

For the pull-downs, we mixed amylose beads with whole HEK293 cell extracts with purified MBP-EspO1 or the negative control LacZ. The bound proteins were analysed by WB using MBP and Hax-1 antibodies, which showed that Hax-1 bound specifically to MBP-EspO1 but not to the negative control (Figure 22).

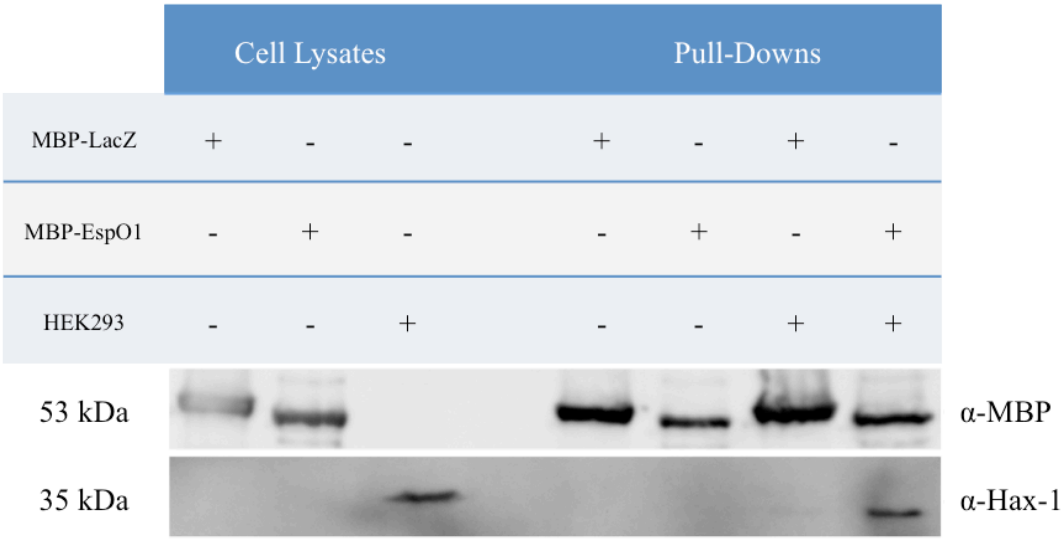

Figure 22. In-vitro binding assay of EspO1:Hax-1
Interaction of EspO1 (EHEC) with HAX-1 was confirmed with pull-down of endogenous HAX-1 from HEK293 cell lysates using Maltose Binding Protein (MBP):EspO fusions.

3.5 The EspO orthologs bind Hax-1

Using the direct Y2H we investigated whether the other members of the EspO family of effectors also bound Hax-1. We found that similarly to EspO1, EspO2 of EHEC, EspO of the EHEC/EPEC-like mouse pathogen *Citrobacter rodentium*, OspE of *Shigella* and SopO of *S.* Typhimurium, also bound Hax-1 (Figure 23). Importantly, sequence alignment of the orthologs revealed that EspO shares 30 and 70% sequence identity with OspE and SopO of *S.* Typhimurium, respectively, while the SopO of *S.* Typhi (a human-restricted pathogen causing a systemic infection) is truncated, missing the C-terminal 18 amino acids (*See* Introduction, Figure 15.D). The direct Y2H assay revealed that SopO of *S.* Typhi did not bind Hax-1 (Figure 23).

Consistently, deletion of the C-terminal 18 amino acids of EspO1 ($EspO1_{1\text{-}73}$), or addition of an HA tag to the C-terminus, abolished EspO:Hax-1 interaction (Figure 23), while the N-terminal 45 amino acids were dispensable (Figure 23). These results suggest that the C-terminus of EspO is essential for the interaction with Hax-1. As the interaction of the EspO orthologs with ILK is dependent on the conserved tryptophan (W68A in OspE and W77 in EspO), we tested the ability of $EspO1_{W77A}$ and $OspE_{W68A}$ to bind Hax-1. Importantly, using the direct Y2H assay we found that the conserved tryptophan residues play no role in the interaction between the EspO orthologs and Hax-1 (Figure 23). Additionally, we were unable to confirm the interaction of EspO orthologs with ILK, using the direct Y2H assay. In conclusion, these results show that the EspO orthologs can also interact with other host cell partner proteins, which might confer insights to a novel EspO function.

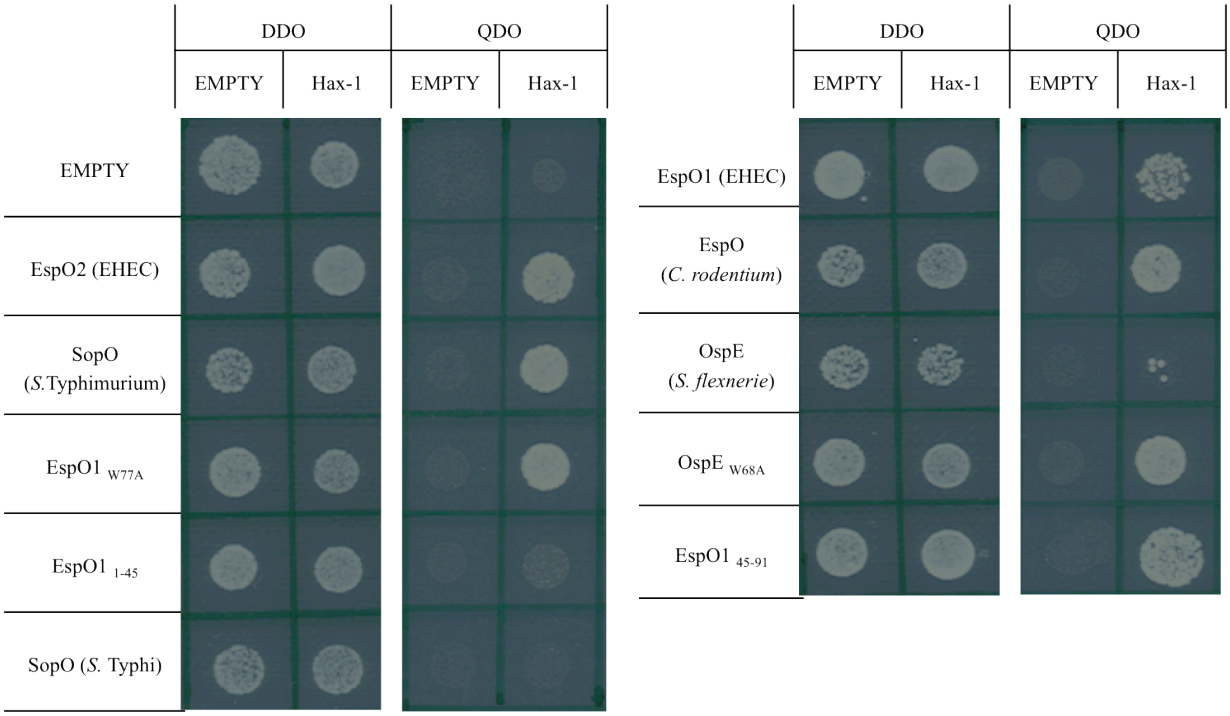

Figure 23. EspO orthologs interact with Hax-1
Hax-1 interacts with EspO orthologs from EHEC, *C. rodentium, S.* Typhimurium and *S. flexneri*. Mutation of the tryptophan residue ($EspO1_{W77A}$ or $OspE_{W68A}$), previously shown to be important for the ILK interaction, does not affect binding to Hax-1, which interacts only with the N-terminal 45aa of EspO. The EspO homologue in *S. typhi* missing the C-terminal 18 aa does not interact with either Hax-1.

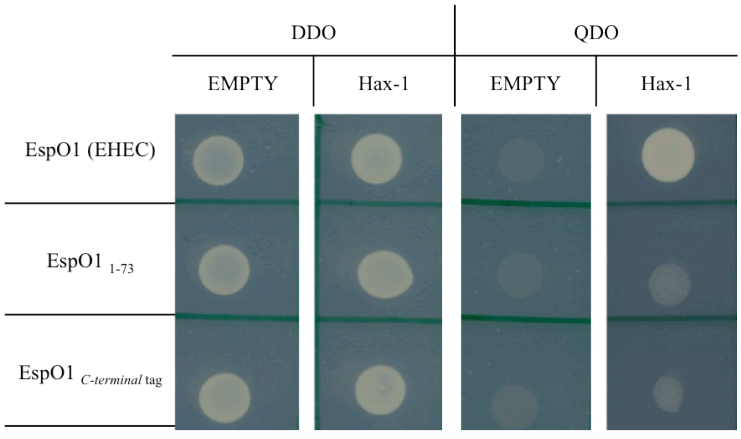

Figure 24. C-terminus of EspO1 required for Hax-1 interaction
Deletion of the C-terminal 18 amino acids of EspO1 ($EspO1_{1-73}$) or addition of a C-terminal tag, abolished the EspO:Hax-1 interaction.

3.6 EspO interaction with DnaJ homolog subfamily B

The Y2H screen also revealed members from the DnaJ homolog subfamily B. We further examined member 6 or DnaJB6 with direct Y2H. To further confirm the interaction, the bait construct pGBKT7-EspO1 or pGBKT7-EspO2 and the Gal4/AD vector, pGADT7 expressing DnaJB6 were co-transformed in yeast strain AH109 (Figure 25). As previously described, true positive interactions were assessed by the ability of co-transformed AH109 to grow on high stringency media. To show that DnaJB6 alone does not activate the reporters, AH109 containing the empty pGBKT7 vector with the pGADT7-DnaJB6 construct was also included. As shown in Figure 25, a clear difference in growth was observed on high stringency media between strains expressing both proteins and those expressing only one.

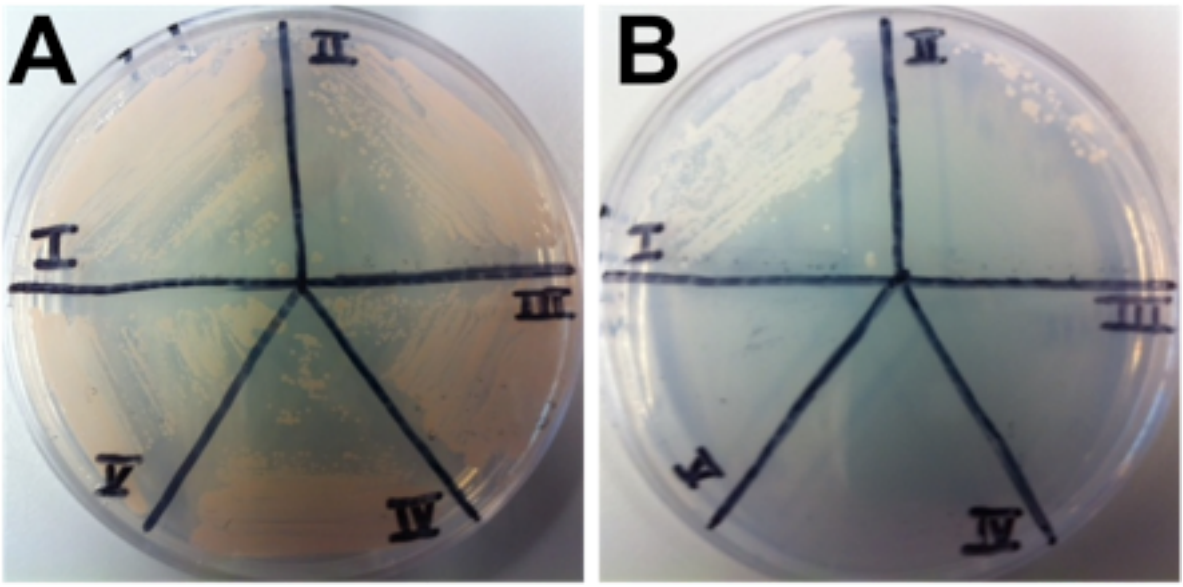

Figure 25. EspO interacts with DnaJB6
Yeast can only grow on high stringency media when there is a true positive interaction between either EspO1 or EspO2 with DnaJB6. **[I]** pGBKT7-EspO1/pGADT7-DnaJB6, **[47]** pGBKT7-EspO2/pGADT7- DnaJB6, **[III]** pGBKT7-/pGADT7- DnaJB6, **[IV]** pGBKT7-EspO1/pGADT7- , **[V]** pGBKT7-EspO2/pGADT7-.

The DnaJ or Heat shock protein 40 (Hsp40) family is a major class of molecular co-chaperones and its members are characterised by a highly conserved N-terminal amino acid sequence known as the 'J-domain' [220]. Although, distinct members are involved in a wide range of cellular processes, their main functions include protein folding and assembly of oligomeric complexes. Members of the human DnaJ family are classified in three subfamilies according to their conserved domains. Those included in subfamily A are closely related to the bacterial (*E.coli*) DnaJ and contain the N-terminal J-domain, a glycine or phenylalanine –rich domain and a cysteine-rich domain. Subfamily B members do not have the cysteine-rich domain and those in subfamily C lack both of these amino acid –rich regions but also their J-domain can be either N- or C- terminal. However, all of the DnaJ members require a functional J-domain, which is required to stimulate the ATPase-functioning Hsp70 chaperoning machineries and hence, activate processes like protein refolding.

Existing evidence suggests that members of the subfamilies A and B may act as chaperones independently of the Hsp70 machinery. Indeed, the EspO protein partner DnaJB6 or human homolog MRJ has been shown to suppress toxic protein aggregation [220]. Additionally, it is involved in other cellular processes like cell adhesion and motility through an interaction with the urokinase plasminogen activator surface receptor (uPAR or PLAUR) [221], the regulation of keratin turnover through interaction with keratin intermediate filaments (K8/K18) [222] and the regulation of cell cycle due to its up-regulation in the M-phase of mammalian cell cycle but also due to its nuclear translocation during interphase [223]. Furthermore, DnaJB6 / MRJ has been suggested to have a role in cancer due to an interaction with a metastasis suppressor protein, BRMS 1 [224].

Using the direct Y2H we found that similarly to Hax-1, DnaJB6 also interacts with EspO1, EspO2 of EHEC, EspO of the EHEC/EPEC-like mouse pathogen *Citrobacter rodentium*, OspE of *Shigella* and SopO of *S.* Typhimurium but not with SopO of *S.* Typhi, which lacks the C-terminal 18 amino acids (Figure 26). Consistently, DnaJB6 also binds only the C-terminal 45 amino acids of EspO1 (Figure 26). These results suggest that the C-terminus of EspO is essential for both the interaction with Hax-1 and DnaJB6. The direct Y2H assay also revealed that the conserved tryptophan residues (W68A in OspE and W77 in EspO), which were previously shown to be important for the ILK binding, play no role in the interaction between the EspO orthologs and DnaJB6 (Figure 26). In total the Y2H results show that, similar to many other T3SS effectors, the EspO orthologs can interact with multiple host cell partner proteins.

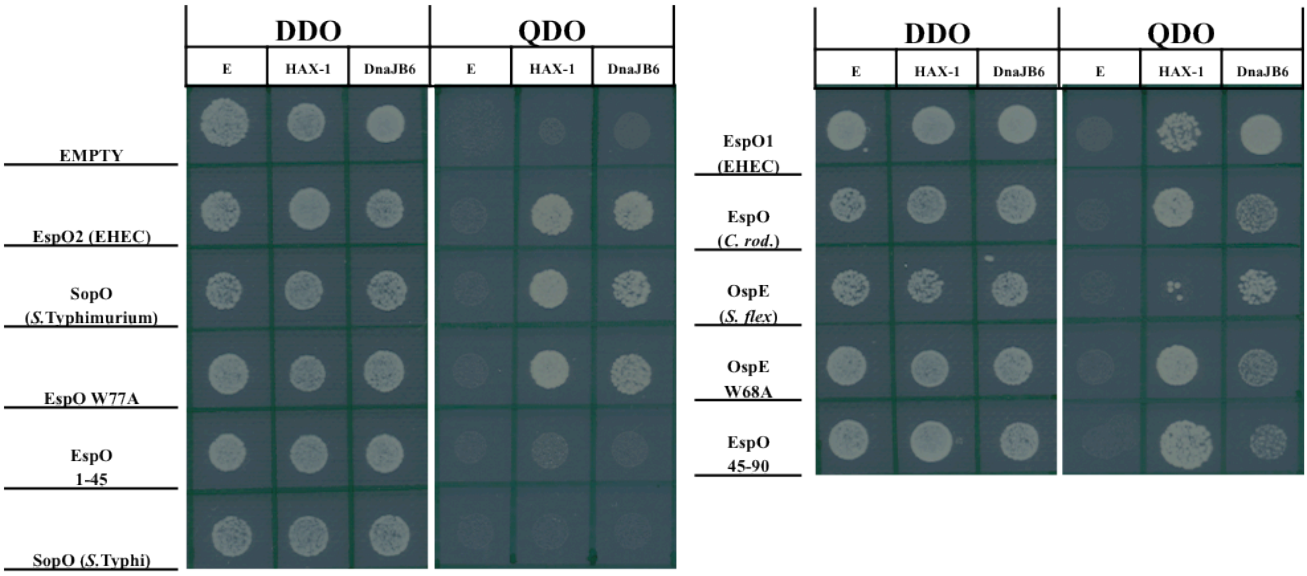

Figure 26. EspO orthologs bind DnaJB6
The interaction pattern of DnaJB6 is identical to Hax-1 and shows positive interaction with the EspO orthologs from EHEC (EspO1 and EspO2), *C. rodentium* (EspO), *S.* Typhimurium (SopO) and *S. flexneri* (OspE). Mutation of the tryptophan residue ($EspO1_{W77A}$ or $OspE_{W68A}$), previously shown to be important for the ILK interaction, does not affect binding to DnaJB6, which interacts only with the N-terminal 45aa of EspO. The EspO homologue in *S. typhi* missing the C-terminal 18 aa does not interact with either Hax-1 or DnaJB6.

4 Chapter 4 : Intracellular Localisation

4.1 Protein Structure Prediction

To gain further insights in the localisation and function of EspO, we analysed the prediction of the protein structure using bioinformatic softwares available online. The three-dimensional (3D) protein structure of EspO1 from EHEC, SopO from *S.* Typhimurium and OspE from *S. flexneri* were predicted by I-TASSER (http://zhanglab.ccmb.med.umich.edu /I-TASSER/). This is an online platform that accepts the amino acid sequence of the target protein and returns the model of the 3D structure based on sequence alignments or homology between the target protein and a representative set of all known structures and further retrieves information by scanning templates from other libraries including enzyme classification, gene ontology and ligand-binding sites [225, 226]. The models were analysed with the Chimera package (http://www.cgl.ucsf.edu/chimera) to present images of the ribbon and the resulting surface of each structure (Figure 27.A).

The N-terminal region of EspO1 contains a small alpha helix (position 5-6) and a second alpha helix is predicted between the 72nd and 86th amino acid (Figure 27.B). Interestingly, the tryptophan at position 77 (W77) previously shown to be important for the ILK binding lies within the alpha helix. As previously shown in this study, the direct Y2H experiments confirmed that the C-terminal 18 amino acids of EspO1 are also required for the interaction with both Hax-1 and DnaJB6. EspO1 and SopO share many structural properties due to their high levels of homology. As previously mentioned, the two orthologs

share 70% amino acid identity. Both sequences contain long amino acid chains, which are found within beta strands.

A. Models of 3D structures

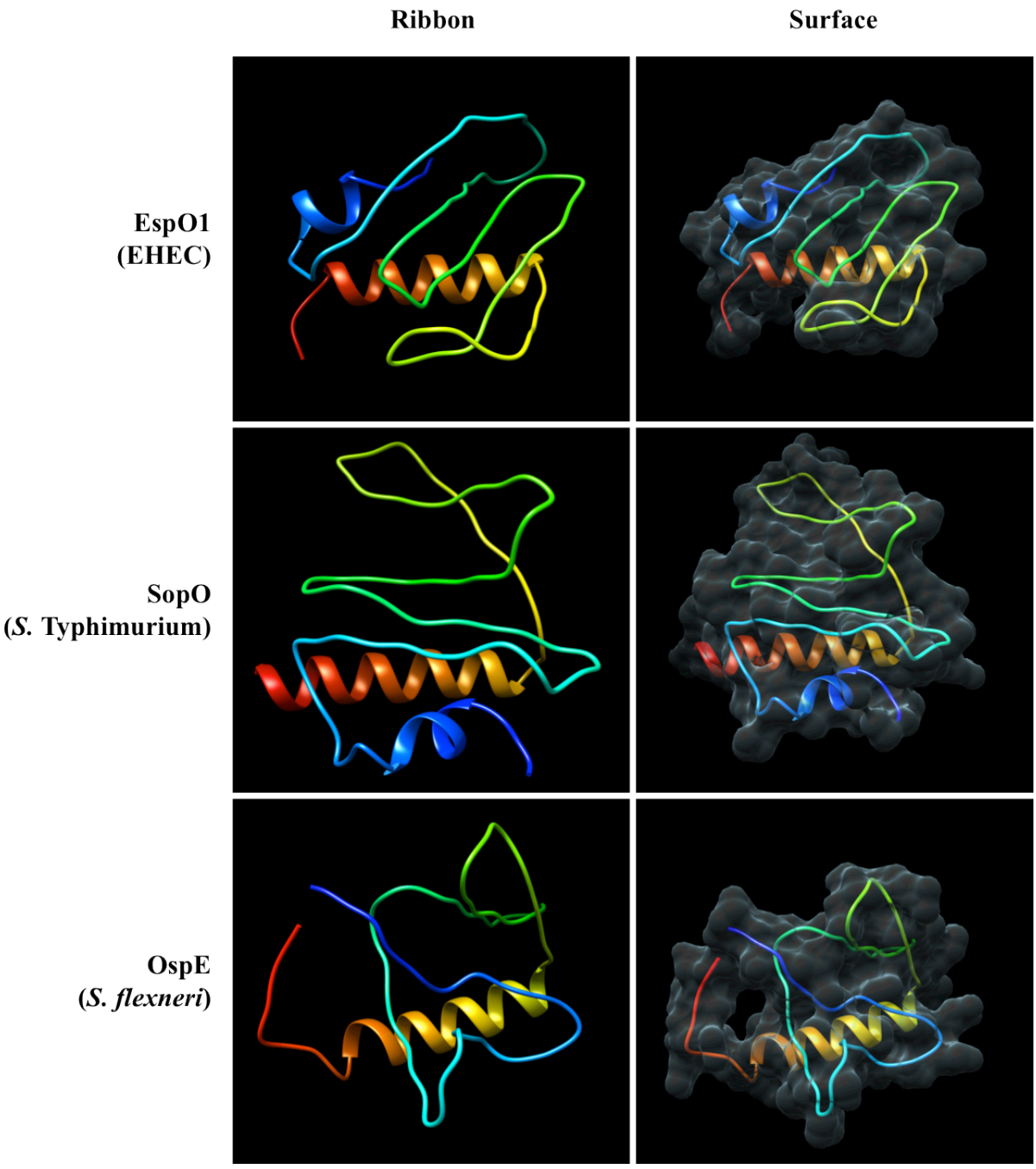

B. Secondary structure prediction

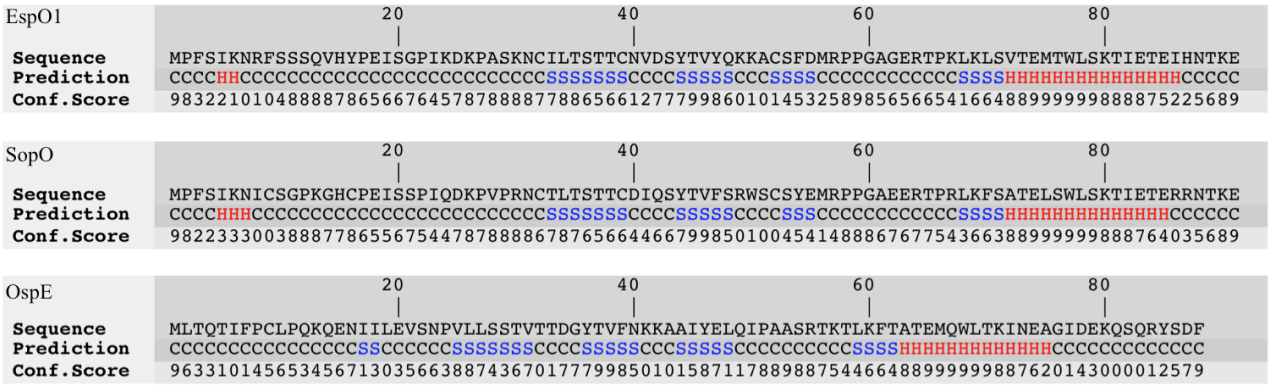

Figure 27. Models of EspO1, SopO and OspE
A. The 3D structures of EspO1 (EHEC), SopO (*S.* Typhimurium) and OspE (*S. flexneri*) modelled by I-TASSER and analysed with the Chimera package to show the ribbon from N-terminus (Blue) to C-terminus (Red) and the resulting surface of each predicted ribbon structure. B. The amino acid residues for each protein with the prediction of the secondary structure (coil-C, helix-H and strand-S) and the level of confidence shown on a scale of 0-10.

Similarly to EspO1, the N-terminal region of SopO, contains 3 amino acids that are found within an alpha helix and the C-terminal region is mainly comprised of an alpha helix with 14 amino acids (from 72 to 86). In contrast, the secondary structure prediction for OspE does not have the N-terminal alpha helix that exists in both EspO1 and SopO models (Figure 27.B). However, the protein folding modelled by I-TASSER predicts highly similar final models for the 3D structures of EspO1, SopO and OspE.

Additionally, the predicted structures were matched with structures of known biological function and localisation with TM-align, a software included in the I-TASSER platform for structural alignment. The ranking of the best matches is based on a scale from 0 to 1. EspO1 shows structural similarities with ferredoxin oxidoreductases (e.g. PDB 2x9oA with alignment score 0.527) and phosphatases (e.g. PDB 3fxoA1 with score 0.508). The

consnesus gene ontology (GO) terms predicted for EspO1 includes an oxidoreductase process for biological function (GO:0055114) with mitochondrial localisation (GO:0005739).

SopO shows structural similarities with nucleoporins (e.g. PDB 3ikoC with score 0.528), methyl coenzyme-M reductases (e.g. PDB 1hbuD with score 0.524) and bacteriophytochromes (e.g. PDB 4ehoA with score 0.502). The consesus GO terms for SopO describe the enzymatic release of energy from organic compounds (GO:0009061) with a nuclear membrane localisation (GO:0005643). Interestingly, OspE shows structural similarities with another Salmonella SPI-2 T3SS effector, PipB2 (PDB 2lezA with score 0.519) that binds kinesin light chain and it is involved in Sif formation and additionally localises on vesicles [227-229]. OspE also shares similarities with a yeast protein Ndc10 (PDB 3t79A with score 0.513), which is involved in mitosis.

4.2 Transfection of EspO in HeLa cells

To examine the sub-cellular localisation of EspO, HeLa cells were transfected with mammalian vectors expressing either *espO1* or *espO2* from EHEC, *espO* from *C. rodentium*, *sopO* from *S.* Typhimurium and *ospE* from *S. flexneri* all with an N-terminal myc tag. Ectopically expressed GFP was used as a control. Immunofluorescence staining of myc-EspO showed that intracellular EspO appears at the surface of a large vacuole (Figure 28). Moreover, transfection of EspO in HeLa cells induces reorganisation of the mitochondria labelled with Mitotracker compared to the GFP transfected cells. Mitochondria are pulled closer together forming a concentrated cluster surrounded by EspO (Figure 28). In contrast, OspE, the EspO ortholog from Shigella, appears as smaller tubular vacuoles, which co-localise with the mitochondria without any effect on their organisation.

In order to confirm the reorganisation observed with MitoTracker, the mitochondria were also labelled with the specific antibody anti Cytochrome C oxidase IV (COX IV), which is one of the enzymes localised to the inner mitochondrial membrane. In the presence of EspO1 (EHEC) or SopO (*S.* Typhimurium), the mitochondria show no reorganisation when compared to the untransfected control (Figure 29). However, the Shigella homologue OspE shows co-localisation with the mitochondria similarly to MitoTracker labelling (Figure 29). In the case of EspO1 the staining with COX-IV confirms that MitoTracker is a false positive whereas OspE shows co-localisation in both stainings confirming a possible role related to the mitochondria. As previously mentioned, the bioinformatic analysis of the 3D structures and motifs included in the EspO orthologs predicts an ability to act as bacterial electron carriers. This might further explain the false positive result observed with MitoTracker, which is a probe that enters the cell in its reduced form and becomes fluorescent when oxidised.

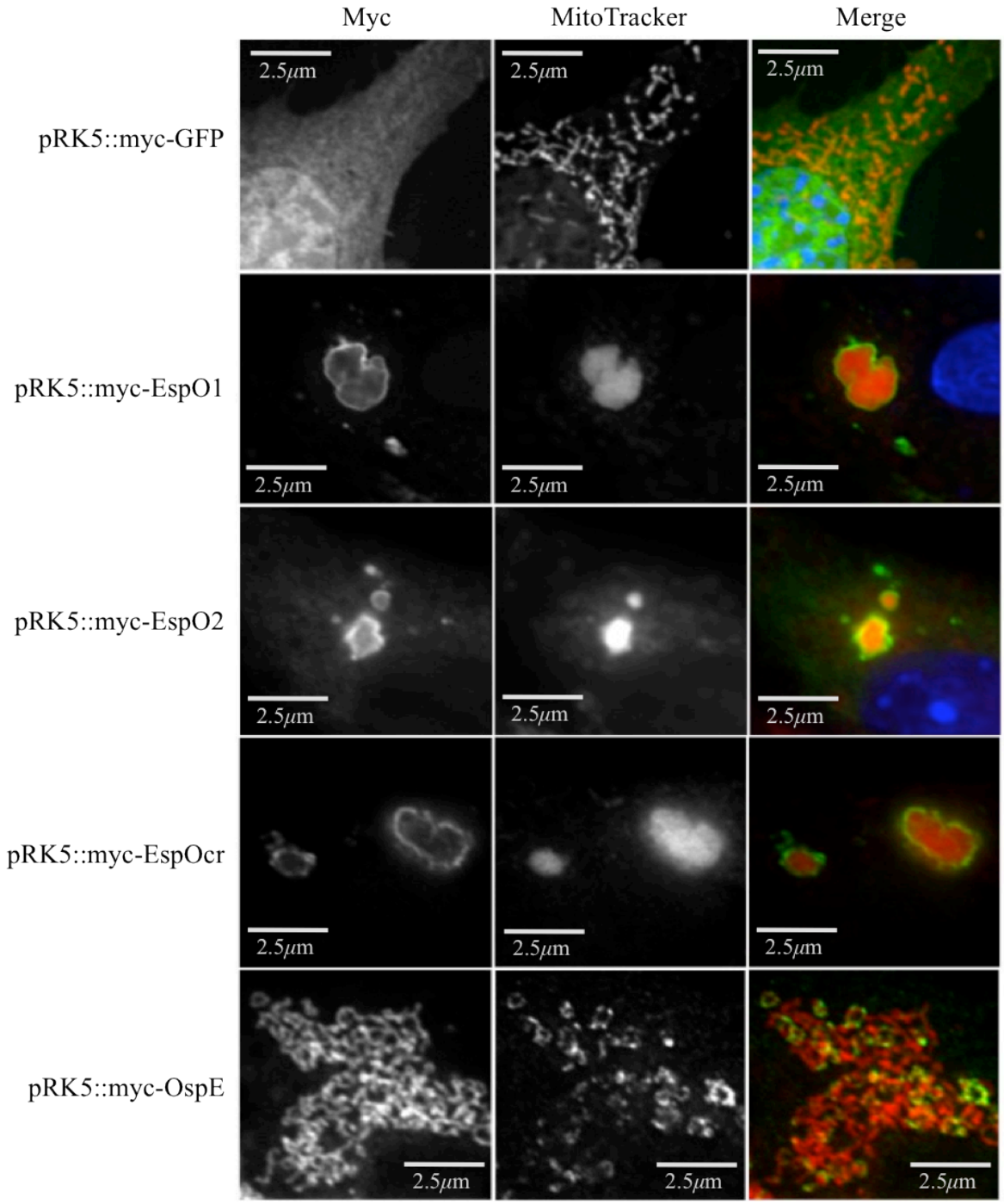

Figure 28. Intracellular localization of EspO (A)
Localisation of EspO1 and EspO2 (EHEC) or EspO (*C. rodentium*) in transfected HeLa cells appears at the surface of a large vacuole, which reorganises and further colocalises with mitochondria labelled with MitoTracker. In contrast, OspE only co-localises with the mitochondria. The effectors were detected with an anti-myc antibody (Green) and mitochondria were stained with MitoTracker Red CMXRos (red). A negative control pRK5 expressing GFP is also shown in the figure.

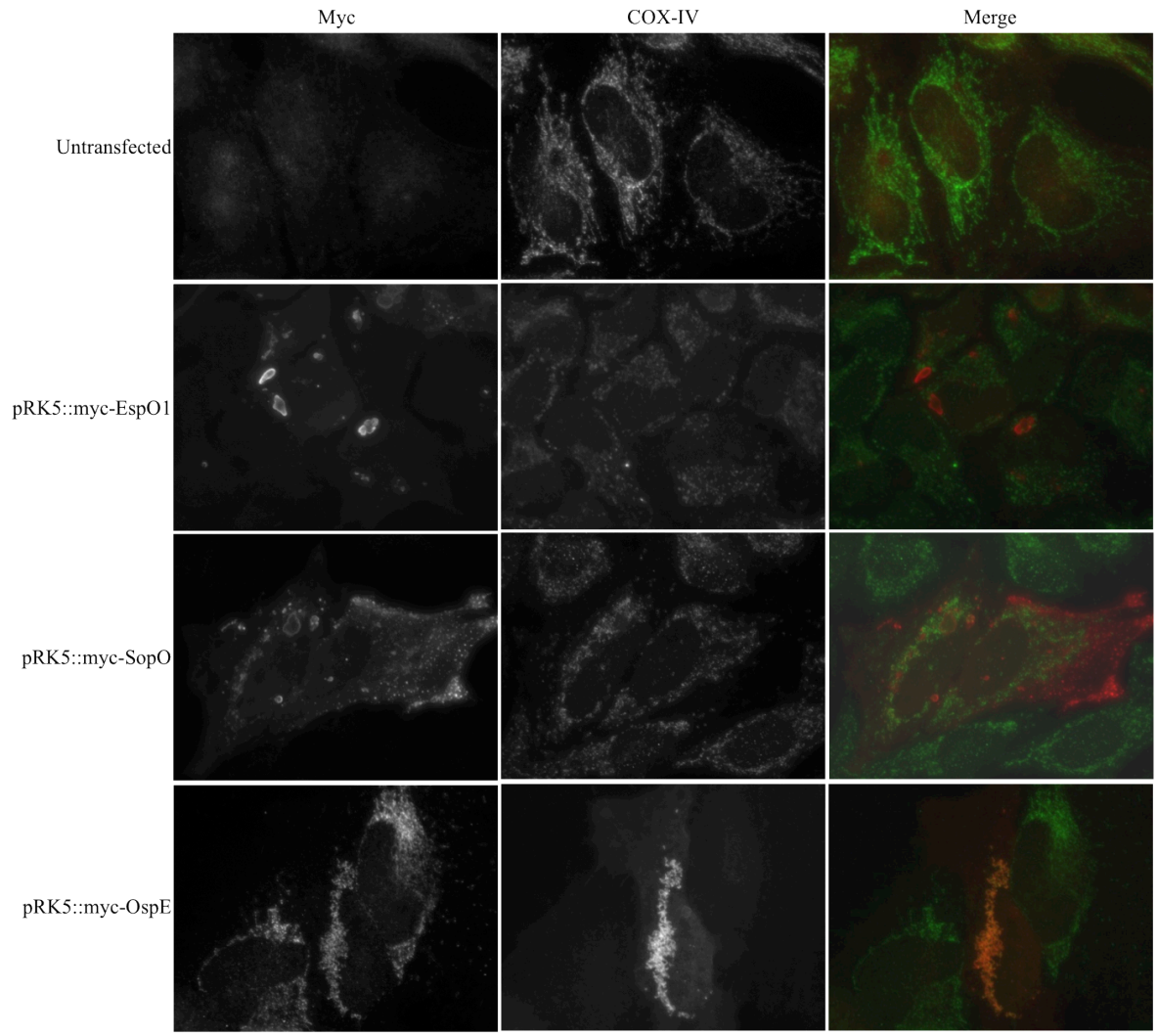

Figure 29. Intracellular Localisation of EspO (B)
The specific mitochondrial antibody COX-IV (Green) shows no co-localisation or re-organisation of the mitochondria in HeLa cells transfected with EspO1 (EHEC) or SopO (*S.* Typhimurium) and detected with anti-myc antibody (Red). Whereas OspE (*S. flexneri*), also stained with anti-myc antibody (Red) co-localises with the mitochondria.

To further characterise the composition of the EspO vacuole, specific markers of various cellular compartments were used. No co-localisation was observed with the early endosomes (Rab5), late endosomes (Rab7) or Golgi apparatus (GM130). In co-transfections of EspO1 with the endoplasmic reticulum (ER) marker CREB3, we observed re-organisation of the ER compared to the CREB3 only transfected cells (Figure 30). However, this result remains inconclusive due to lack of reproducibility with other ER specifc markers. The ER network labelled with the ER-GFP (CellLight, Invitrogen) remains unaffected in EspO1 transfections and the vacuole appears to reside above the ER network (Figure 31).

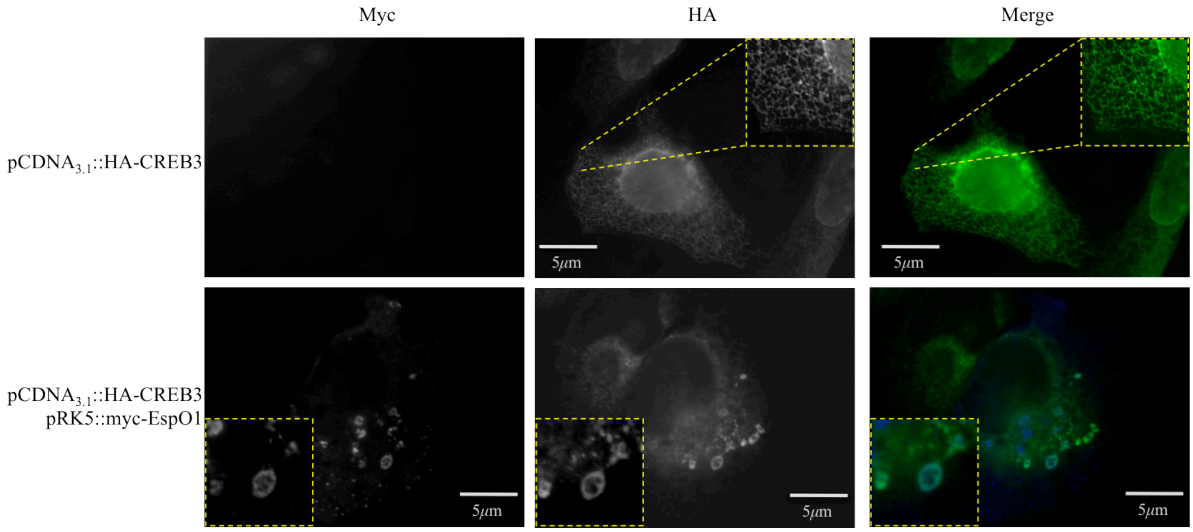

Figure 30. Intracellular Localisation of EspO (C)
The EspO vacuole stained with anti-myc antibody (Blue) re-organises the ER network stained with the ER specific marker CREB3 and labelled with anti-HA antibody (Green). The ER network is re-organised in the EspO1-CREB3 co-transfected cells compared to the CREB3 only tranfected cells. Scale bars indicate 5 µm.

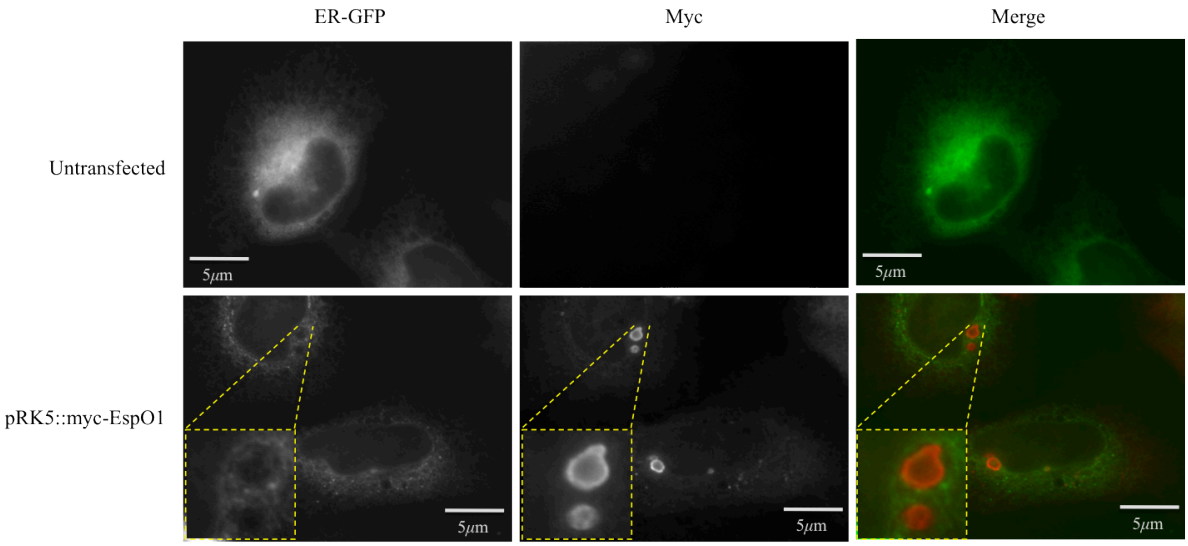

Figure 31. Intracellular Localisation of EspO (D)
Endoplasmic reticulum (ER) network stained with the CellLight ER-GFP, Invitrogen (Green) is not re-organised in pRK5-EspO1 HeLa cell transfections. The EspO vacuole stained with anti-myc antibody (Red) appears to reside above the ER network. Scale bars indicate 5 μm.

We also investigated whether the EspO phenotypes seen when transiently expressed with the mammalian vector pRK5 and tagged with an N-terminal myc epitope, are confirmed in a different construct background. For this, we transfected HeLa cells with pCDNA3.1 expressing Flag tagged EspO1. Although, the main phenotypes observed were the same as the pRK5 background, we additionally observed in 10% of the transfected cells a combined phenotype of vacuole formation and focal adhesion localisation (Figure 32). This might be a case of difference in expression levels between the two constructs allowing the formation of smaller vacuoles and hence, other minor phenotypes can be detected by immunofluorescence, which are otherwise masked by the large and brighter vacuolar concentration of EspO.

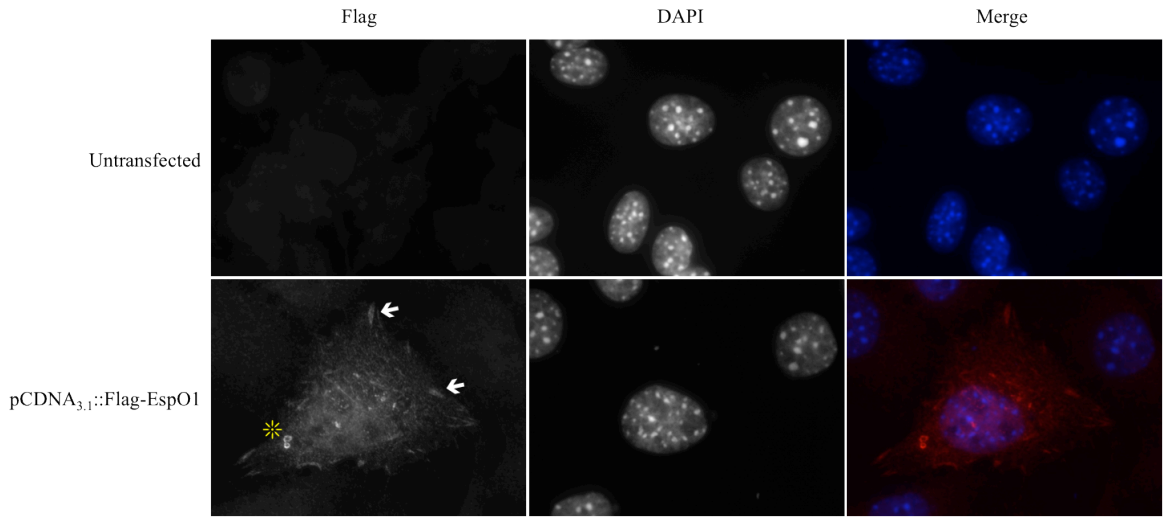

Figure 32. EspO1 localised at focal adhesions and vacuoles
Ectopic expression of EspO1 (EHEC) using N-terminal Flag tag localises on the surface of vacuoles and focal adhesion sites. EspO1 was detected with an anti flag antibody (Red) and DAPI was used to detect nuclei (Blue). Arrows show focal adhesion site localisation and star shows vacuoles.

In conclusion, the EspO vacuoles seen in transfected HeLa cells might be localised only within the cytoplasm. However, more experimental work is required to confirm our current understanding regarding the intracellular localisation.

4.3 EspO1 localisation in EHEC / EPEC infections

In order to localize EspO during infection, we generated a double EHEC *espO1*/*espO2* mutant. The mutant was complemented with an IPTG inducible plasmid encoding C-terminal HA-tagged EspO and the IPTG concentration was optimised to balance the inducible expression of *espO* with the effects on growth rate. We infected mouse illeal epithelium in an *ex-vivo* model and using scanning electron microscopy (SEM), we investigated whether the absence of *espO* affects the A/E lesion formation and cellular exfoliation. There was no difference in either A/E formation or cellular exfoliation between EHEC EDL933 and double *espO* mutant (Figure 33).

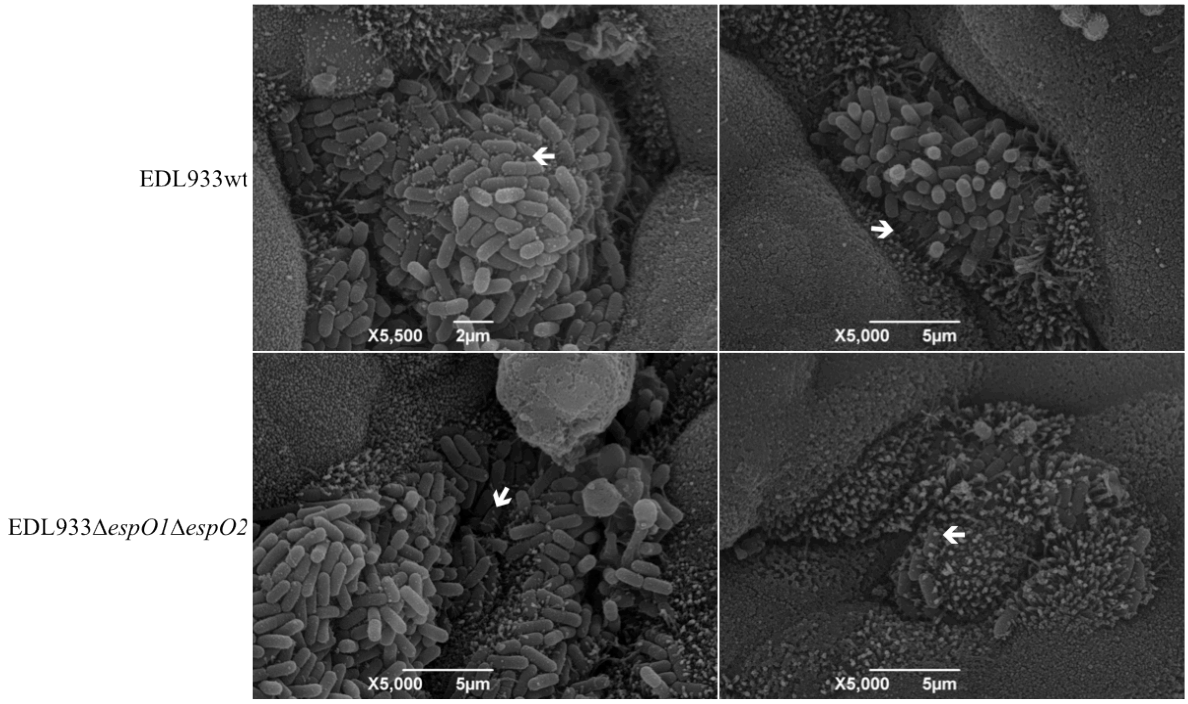

Figure 33. Scanning Electron Micrograph of EHEC infections
Deletion of *espO* in EHEC does not affect the A/E lesion formation compared to the EHEC EDL933 wild type strain. Arrows show pedestal formation.

Kim *et al*. [130] have shown that OspE localises at the sites of focal adhesion where it binds ILK to increase adherence of infected cells. Immunofluorescence staining showed that similarly to OspE, the tagged EspO1 localized at FA during EHEC infections (Figure 34). However, the direct Y2H showed that the C-terminus of EspO1 is important for Hax-1 binding (*See* Chapter 3), which means that the C-terminal tag interferes with this interaction. Additionally, the N-terminus of EspO1 contains the translocation signal, meaning that we were also unable to insert an N-terminal tag. Therefore, we could not determine any further information related to the localisation of EspO attributed to the Hax-1 interaction during infections.

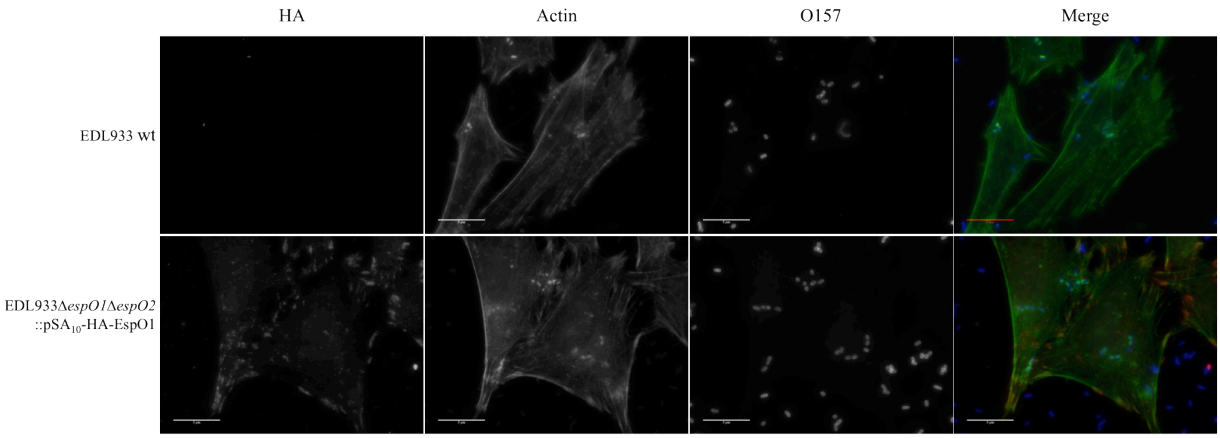

Figure 34. EspO1 localised at FA in EHEC infections
C-terminal HA-tagged EspO1 is localised at focal adhesion sites in the complemented double EspO EDL933 mutant. EspO1 was detected with an anti-HA antibody (Red), Actin with Phalloidin Green and an anti-O157 antibody (Blue) for EHEC bacteria. Scale bars indicate 5 µm.

4.4 EspO1 co-localises with Hax-1

Ectopic expression was used to study the intracellular localisation of EspO without interfering with the Hax-1 interaction. To investigate whether EspO affects the localisation of Hax-1 we transfected HeLa cells with eukaryotic expression vectors encoding N-terminal *myc*-tagged EspO1 and detected with an anti myc antibody. Endogenous levels of Hax-1 were detected with an anti Hax-1 antibody using immunofluorescence microscopy. This reveealed that endogenous Hax-1 appears to co-localize with EspO1 at the vacuoles. In untransfected HeLa cells endogenous Hax-1 is dispersed in the cytosol, which is reorganised into a vacuole in EspO transfected cells (Figure 35). Additionally, Hax-1 appears to translocate into the nucleus in EspO transfected cells. These results are consistent with the reported nuclear localization of endogenously and ectopically expressed Hax-1 in HeLa cells [201, 230].

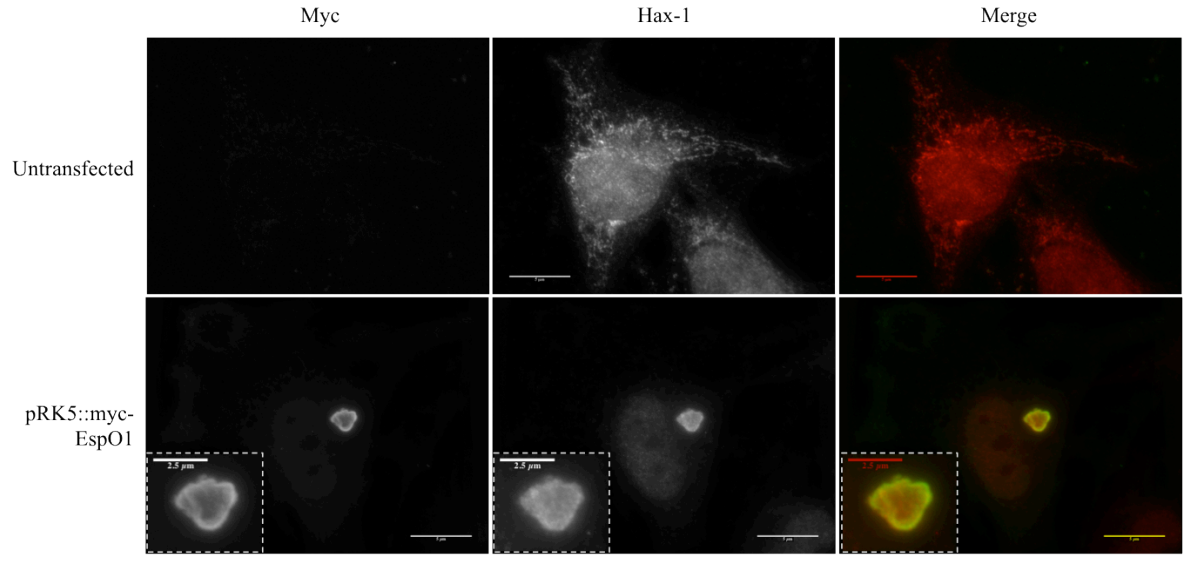

Figure 35. EspO1 co-localises with endogenous Hax-1
Endogenous Hax-1 is re-organised and co-localises with the large vacuole formed in ectopically expressed myc tagged EspO. EspO1 was detected with an anti myc antibody (Green) and endogenous Hax-1 was detected with anti Hax-1 antibody (Red). Scale bars indicate 5 µm in main images and scale bars for ROIs show 2.5 µm.

To confirm the visual estimate of colocalisation shown in Figure 35, we used a statistical approach to analyse the images and quantify co-localisation as a coincidence of intensity distributions. This approach is based on intensity correlation coefficients, which were calculated with ImageJ / Fiji, a freely-available online open source software package for image processing (http://fiji.sc/Fiji). The Pearson's coefficient (PC) was calculated to provide a quantitative indication of the linear relationship between the grey values of the two channels or images (Figure 36). The values from the two images were plotted against each other and displayed on a scatter plot which shows complete co-localisation between the two images (Figure 37). This is determined by the relationship of the pixel values from each channel, which is represented by the distribution of the dot cloud along the fitted line. PC provides this distribution and gives a measure of the quality of the relationship or correlation between the two channels. The PC values range from -1 to 1 where -1 means negative correlation, 0 indicates no correlation and 1 for complete positive correlation.

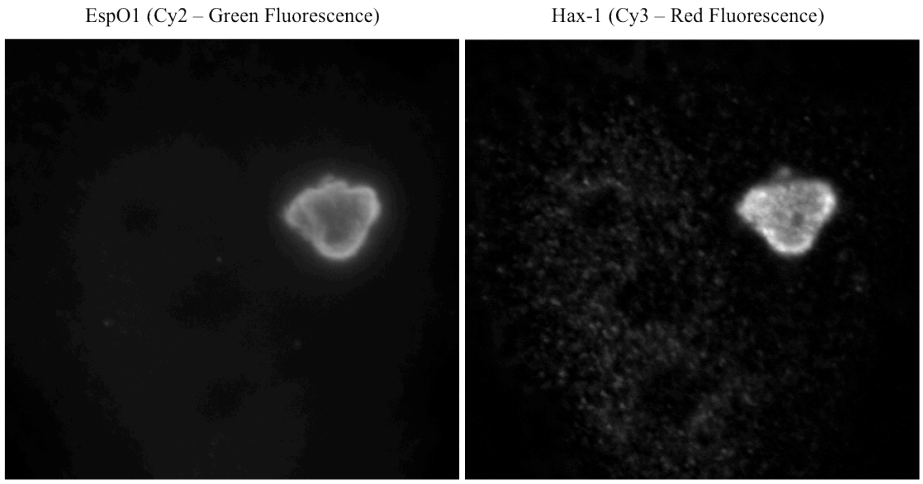

Figure 36. Analysed images
The two channels from the co-localistion experiment were used to perform statistical analysis of the correlation of grey value pixel intensity. The merged dual-channel image in Fig. 36 was split into the individual channels and the two resulting images were used for the statistical analysis done with ImageJ.

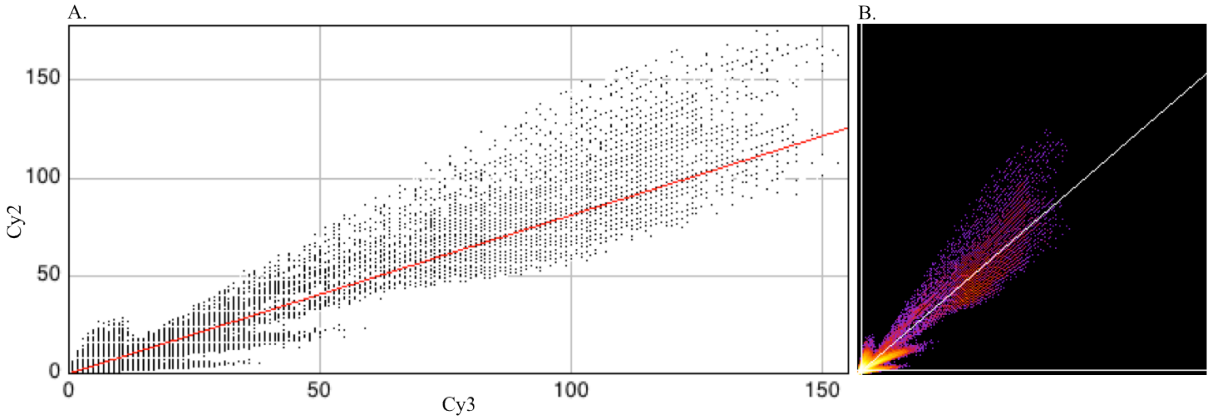

Figure 37. Scatter Plot
The pixel grey values from the images in Fig.37 are plotted against each other on a scatter plot (A) or fluorogram (B) where the x-coordinate shows the intensity of Cy3 (Hax-1) pixels and the y-coordinate represents the intensity of the corresponding Cy2 (EspO1) pixels. The relationship between the intensities of the two images is calculated by linear regression and shown by the fitted line on the plot. The graphs show a complete colocalisation, which is represented by a concentration of the dot cloud along the line. ImageJ was used for the analysis.

The PC value is 0.948, which indicates complete co-localisation. The slope of the line is shifted towards the x-axis, which indicates a difference in the intensities between the two channels with Cy3 being more intense. However, this difference is minimal and does not affect the co-localisation that is still observed but indicates the existence of a small subpopulation of red pixels which has appeared due to a less sensitivity in the green channel. It should be noted that this is different from channel cross-talk or bleed-through, which is represented by a complete shift of the line towards one of the axis on the scatter plot [231].

To confirm co-localisation, the Manders' overlap coefficient (MC) was calculated for each image. This ranges from 0 to 1 with 1 being an indication of 100% co-localisation and 0 indicating no overlap between images. MC defines the proportion of each channel that is

co-localised with the other and for this calculation a threshold is required to exclude any background noise that might exist in each image [232]. The two MC values generated are 0.95 for the fraction of the Cy3 image (Hax-1) overalapping Cy2 image (EspO1) and 0.973 for the opposite fraction (i.e. Cy2 overlapping Cy3).

A statistical confidence of the co-localisation is given by the Costes' approach which is based on image randomisation and further evaluation of PC calculated from thresholded images [233]. The statistical approach compares the PC values from the original non-randomised images with those calculated from the randomised images and a P-value or significance is calculated (given as a percentage). For this, we used 1000 randomisation rounds (200 rounds are proposed to give a significant statistical distribution) to ensure reliable elimination of false positives. The PC is 0.941 and has a P-value of 100% meaning that co-localisation is highly probable.

Additionally, we measured co-localisation according to a cross-correlation function that discriminates between the different co-localisation events by shifting the Hax-1 image pixel per pixel across the x-axis and relative to the EspO1 image [234]. The respective PC is calculated and then plotted as a pixel shift function (δx). A peak at 0 pixel shift (x-value) indicates a complete colocalisation event between the two images as it is shown for EspO1 and Hax-1 (Figure 38). The intensity correlation analysis using Li's correlation coefficient was performed as a last approach to interpret co-localisation on separate graphs for each image that represent normalised intensities (0-1 on y-axis) as a function of the covariance (i.e. relationship between the two variables) of both channels' intensities (x-axis) [235]. If there is co-localisation the pixel cloud has only positive x values and therefore situated on the right side of x=0 line as shown for the EspO1 and Hax-1 images (Figure 39).

In conclusion, the statistical analysis performed with different approaches confirms that the visual estimate of co-localisation observed in Figure 35, is a true positive co-

localisation of EspO1 and Hax-1. However, this is the result taken from one co-localisation experiment and therefore, requires reproducibility.

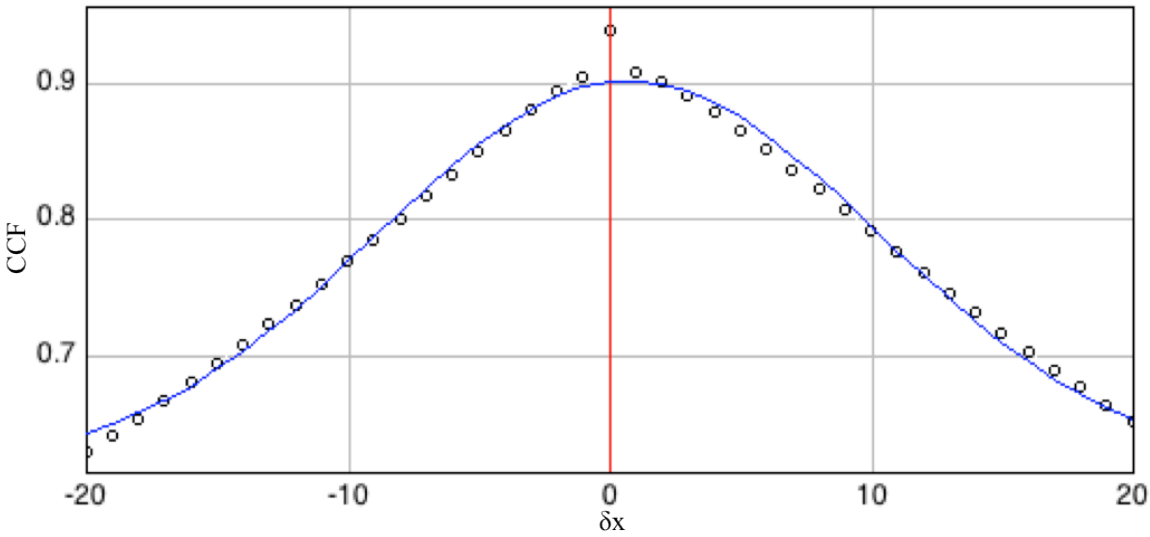

Figure 38. Cross-correlation analysis
Cross-correlation functions (CCF) were determined using a pixel shift of δ=±20. Graph shows complete co-localisation of the EspO1 and Hax-1 images, which is represented by a curve with maximum peak at δ=0. ImageJ was used for the analysis.

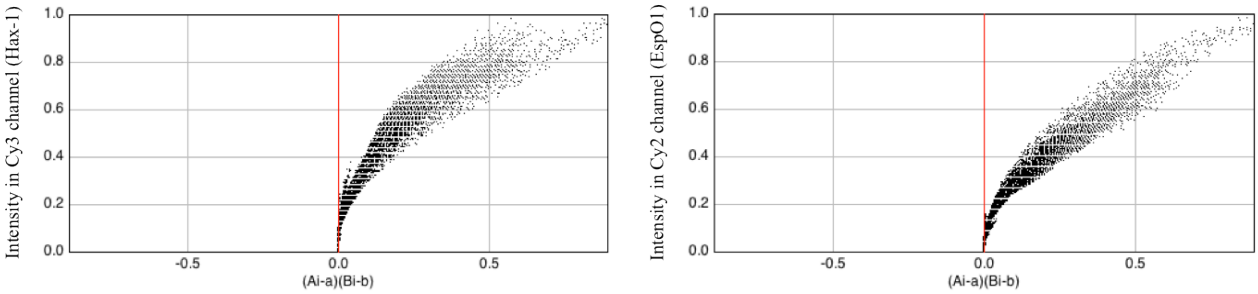

Figure 39. Intensity correlation analysis
Intensity correlation analysis indicates co-localisation between EspO1 and Hax-1. A graph for each channel representing intensity distribution in the channel (y-axis) is plotted against the covariance of both channels (x-axis). Pixels with positive x-values (situated on the right of the x=0 line) show co-localisation. ImageJ was used for the analysis.

5 Chapter 5 : EspO role in Apoptosis and Inflammation

5.1 Inhibition of apoptosis induced by various stimuli

Hax-1 is a potent inhibitor of apoptosis and executes this activity by preventing XIAP degradation and inactivating $SERCA_2$ (hence diminishing ER Ca^{2+} content and protecting the mitochondria from Ca^{2+} overload). Therefore, we investigated the role of the EspO orthologs in apoptosis. We challenged EspO ortholog-transfected HeLa cells with staurosporine (STS), which is a pro-apoptotic agent that inhibits protein kinases. We quantified the number of transfected cells with active caspase-3 (main executioner of apoptosis) and fragmented DNA (late apoptotic feature) by immunofluorescence.

Untransfected or transfected with the *gfp* control STS-treated cells displayed high levels of cleaved caspase-3 and fragmented DNA (70-80%), whereas significantly ($P<0.05$) lower levels (10-20%) were observed in cells transfected with the EspO orthologs (Figure 40). The positive control cells transfected with the already known anti-apoptotic EHEC effector NleH showed low levels (18%) of cleaved caspase-3 similar to the EspO orthologs (Figure 40.A). To determine whether binding to ILK is involved in this anti-apoptotic function, we tested the activity of $EspO1_{W77A}$ and $OspE_{W68A}$. Ectopic expression of the mutant effectors was as effective as the wild type proteins in inhibiting STS-induced apoptosis (10-20%) (Figure 40.A). Importantly, the level of apoptosis in cells ectopically expressing the *S.* Typhi SopO, which cannot interact with Hax-1, was examined by the TUNEL assay and revealed 60-70% apopoptotic nuclei similar to the apoptotic levels shown by negative control cells (70-80%) (Figure 40.B).

To ensure that the effectors on their own do not induce apoptosis, we transfected HeLa cells without the addition of pro-apoptotic agents. The uninduced EspO ortholog transfected cells show similar levels of cleaved caspase-3 (Figure 41.A) and condensed nuclei (Figure 41.B) to the uninduced *gfp* control, which is significantly lower than the STS-treated *gfp* control.

A. EspO inhibition of STS induced apoptosis assessed by cleaved Caspase-3

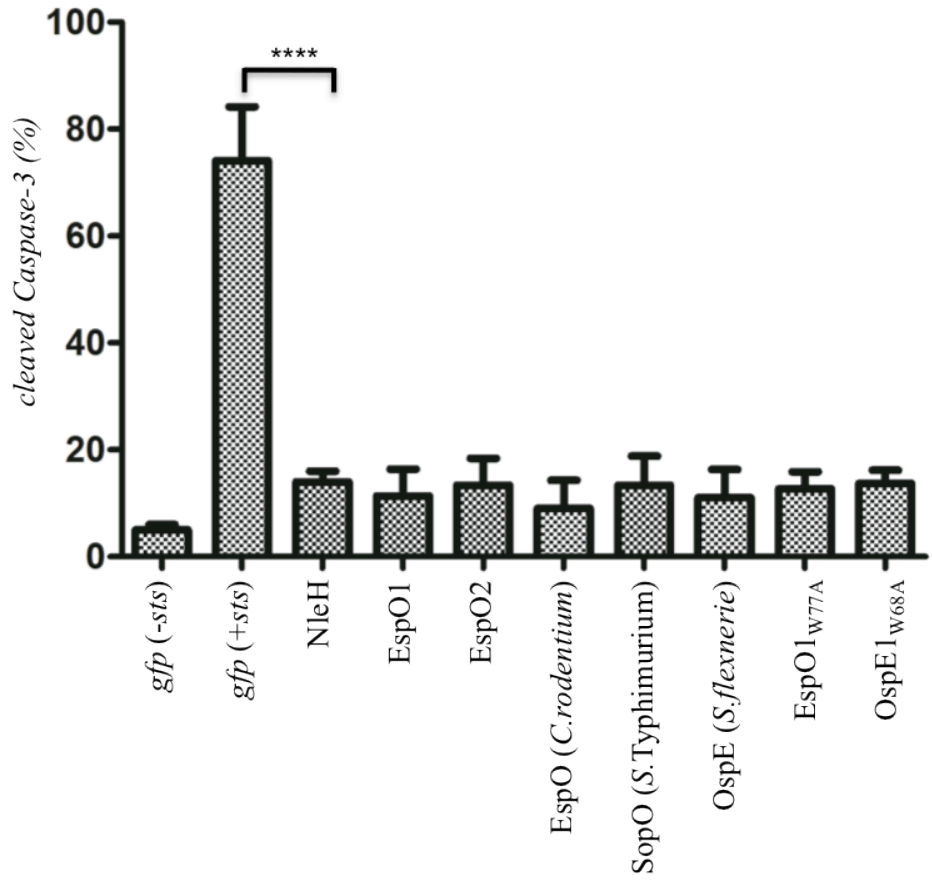

B. EspO inhibition of STS induced apoptosis assessed by TUNEL

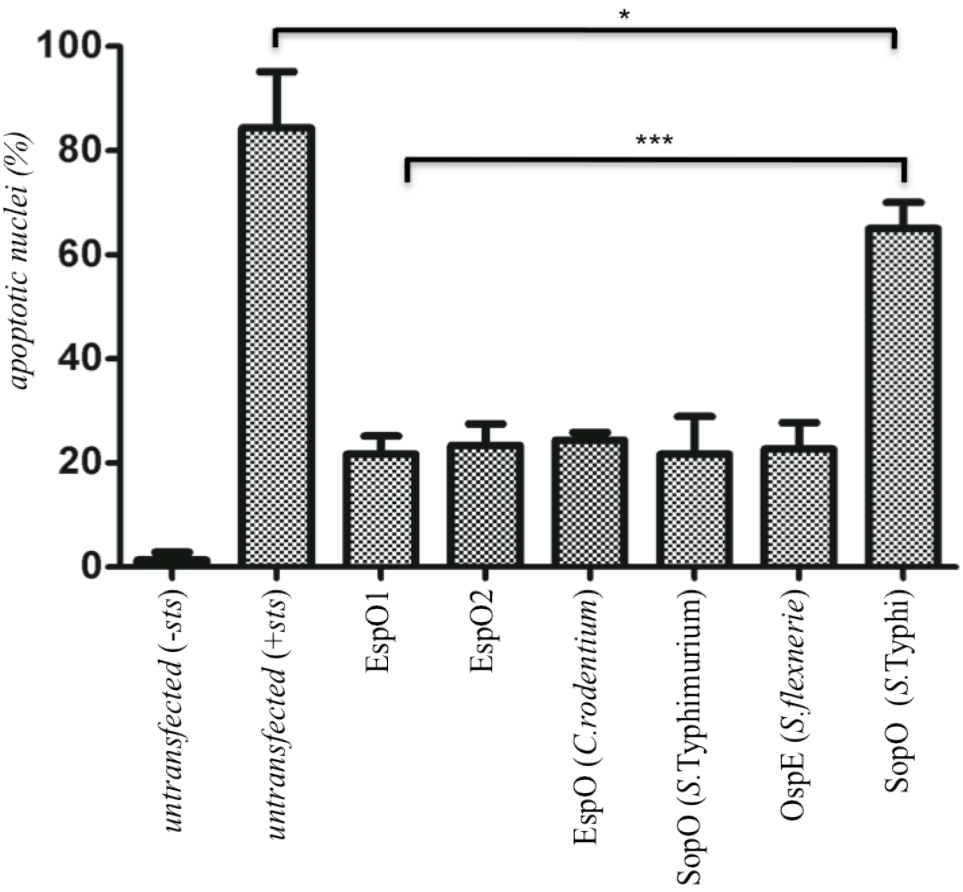

Figure 40. Inhibition of Staurosporine induced apoptosis
EspO orthologs protect against staurosporine (*sts*) induced apoptosis in HeLa cells as measured by cleaved Caspase-3 staining (A) and apoptotic nuclei assessed by TUNEL (B). The levels of cleaved Caspase-3 (A) and apoptotic nuclei (B) were significantly reduced in cells transfected with the NleH positive control and the EspO orthologs (10-20%) compared to the untransfected or transfected with the *gfp* control STS-treated cells (70-80%). The level of apoptosis in cells transfected with the *S.* Typhi SopO showed increased levels of apoptotic nuclei (60%) (B). Three biological replicates with two technical replicates each (100 transfected cells counted per technical replicate) were analysed for statistical significance with the two-tailed unpaired *t*-test with equal SD. **P*<0.05.

A. Levels of cleaved Caspase-3 in STS treated and untreated EspO transfected HeLa cells

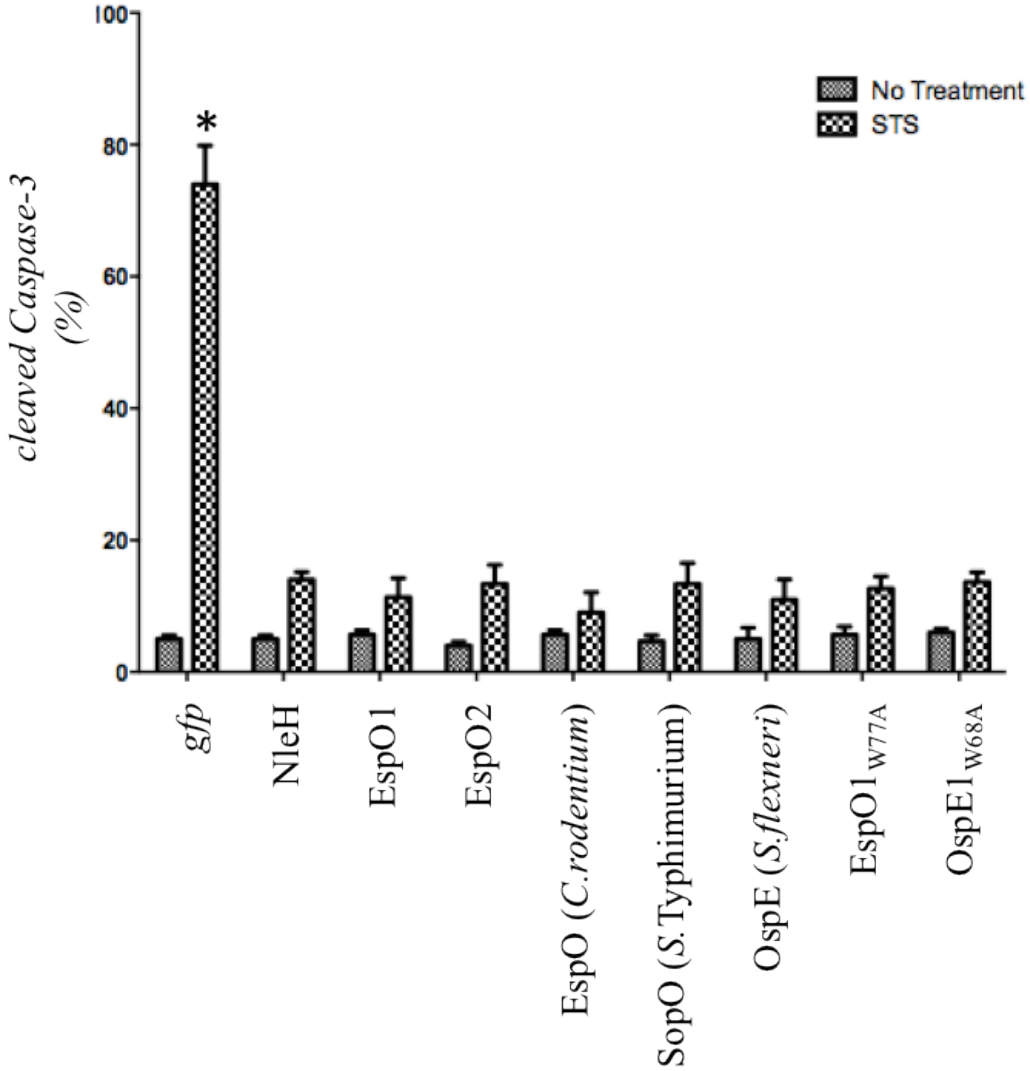

B. Levels of condensed nuclei in STS treated and untreated EspO transfected HeLa cells

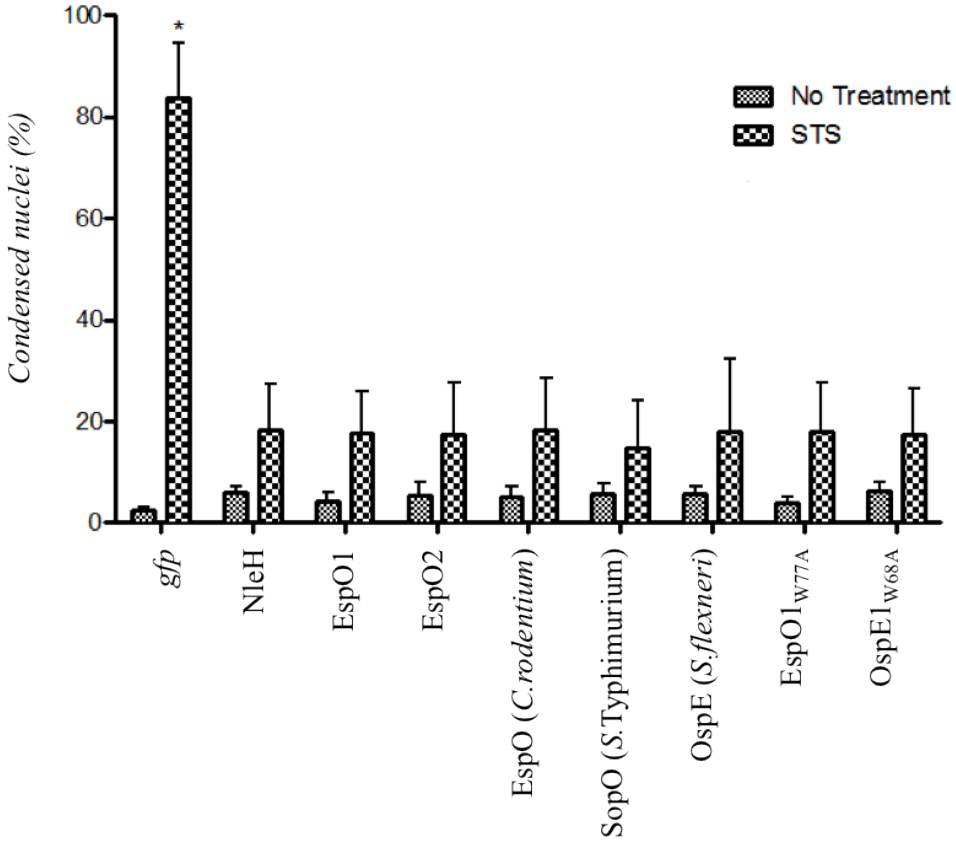

Figure 41. STS treated and untreated EspO transfected cells
Uninduced EspO ortholog transfected cells are non-apoptotic with similar low levels (5-10%) of cleaved caspase-3 (A) and condensed nuclei (B) compared to the *gfp* control cells without treatment (0-5%). The level of apoptosis is significantly higher in *gfp* control cells induced with staurosporine (70-80%) compared to the untreated control cells (0-5%). Three biological replicates with two technical replicates each (100 transfected cells counted per technical replicate) were analysed for statistical significance with the two-tailed unpaired *t*-test with equal SD. **P*<0.05.

To investigate the ability of EspO orthologs to inhibit apoptosis triggered by other stimuli, we challenged EspO transfected cells with tunicamycin (TUN), which disrupts the function of the ER leading to unfolded protein responses and thapsigargin (TG), an inducer of apoptosis through specific inhibition of the Ca^{2+} ATPase $SERCA_2$ pump. Quantification of transfected cells by immunofluoresence revealed that tunicamycin-treated HeLa cells transfected with either EspO1 or $EspO1_{W77A}$ showed low levels (10-20%) of cleaved caspase-3, similar to the NleH positive control (10-20%) and untreated *gfp* control (0-5%) ((Figure 42.A).

Furthermore, we found low levels of apoptosis (20-30%) in thapsigargin treated cells transfected with EspO1, SopO and OspE compared to the untransfected control (80-90%) (Figure 42.B). The uninduced EspO ortholog transfected cells show similar levels (0-5%) of cleaved caspase-3 (Figure 43.A) and condensed nuclei (Figure 43.B) to the uninduced *gfp* control (0-5%), which is significantly lower than the TUN-treated *gfp* control (70-80%). Taken together these results show that EspO orthologs, irrespective of the ILK binding, interfere with numerous cellular pathways leading to inhibition of apoptosis triggered by various inducers.

A. EspO inhibition of TUN induced apoptosis assessed by cleaved Caspase-3

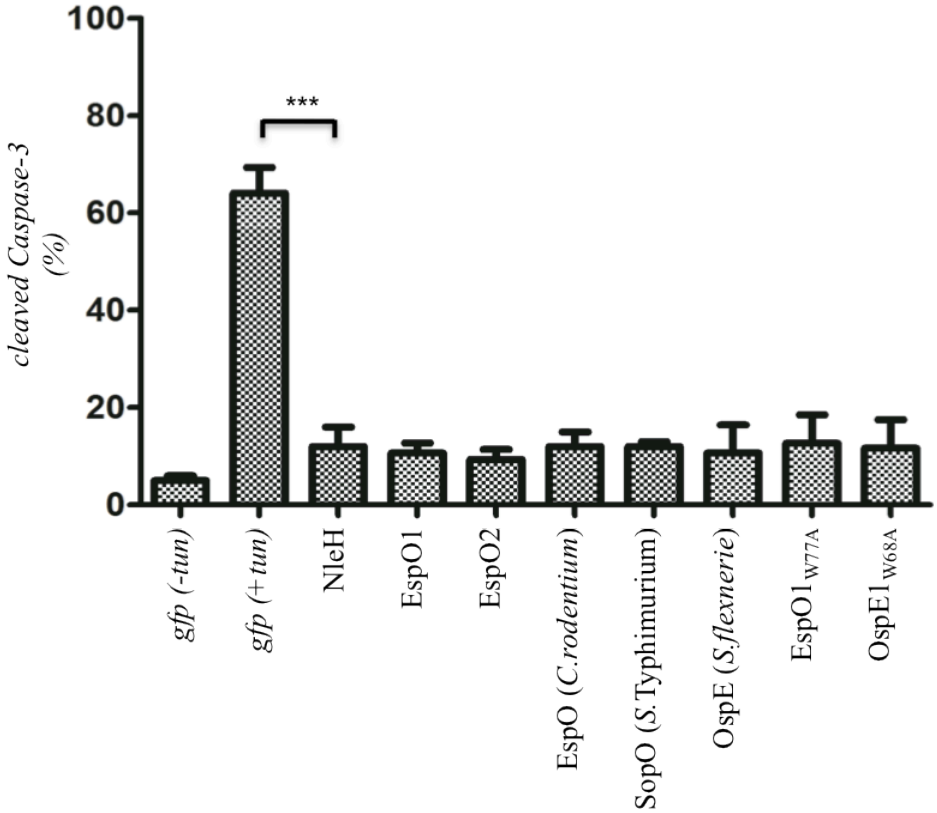

B. EspO inhibition of TG induced apoptosis assessed by TUNEL

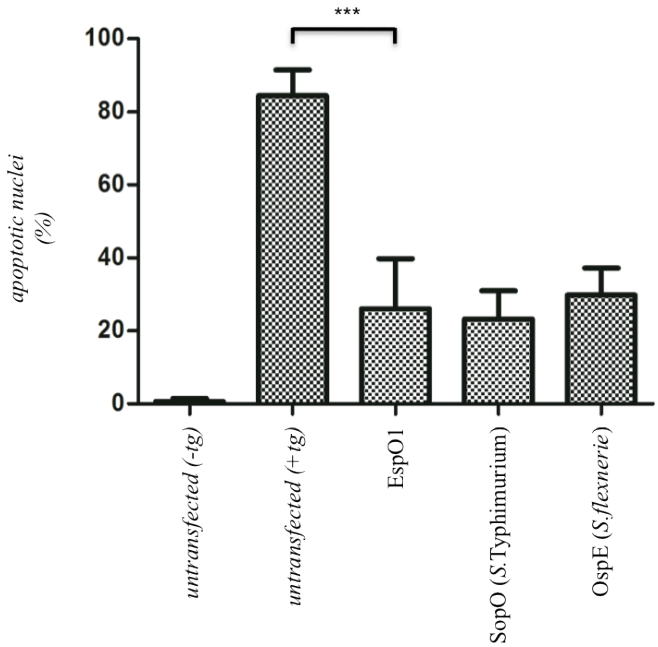

Figure 42. Inhibition of apoptosis induced by ER stress
EspO orthologs protect against tunicamycin (*tun*) induced apoptosis in HeLa cells as measured by cleaved caspase-3 staining (A) and thapsigargin (*tg*) induced apoptosis measured by apoptotic nuclei assessed by TUNEL (B). The levels of cleaved Caspase-3 (A) and apoptotic nuclei (B) were significantly reduced in cells transfected with the NleH positive control and the EspO orthologs (10-20%) compared to the untransfected or transfected with the *gfp* control treated cells (70-80%). Three biological replicates with two technical replicates each (100 transfected cells counted per technical replicate) were analysed for statistical significance with the two-tailed unpaired *t*-test with equal SD. **P*<0.05.

A. Levels of cleaved Caspase-3 in TUN treated and untreated EspO transfected HeLa cells

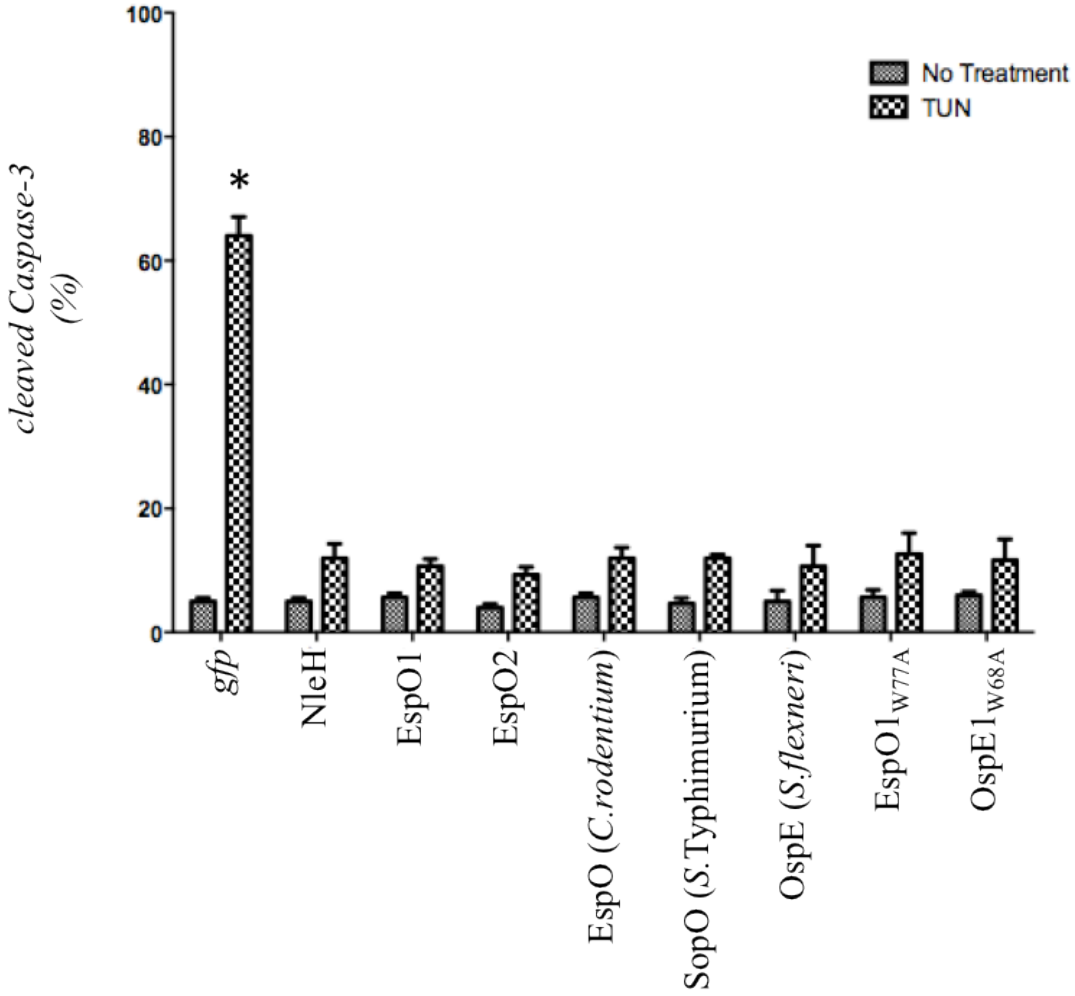

B. Levels of condensed nuclei in TUN treated and untreated EspO transfected HeLa cells

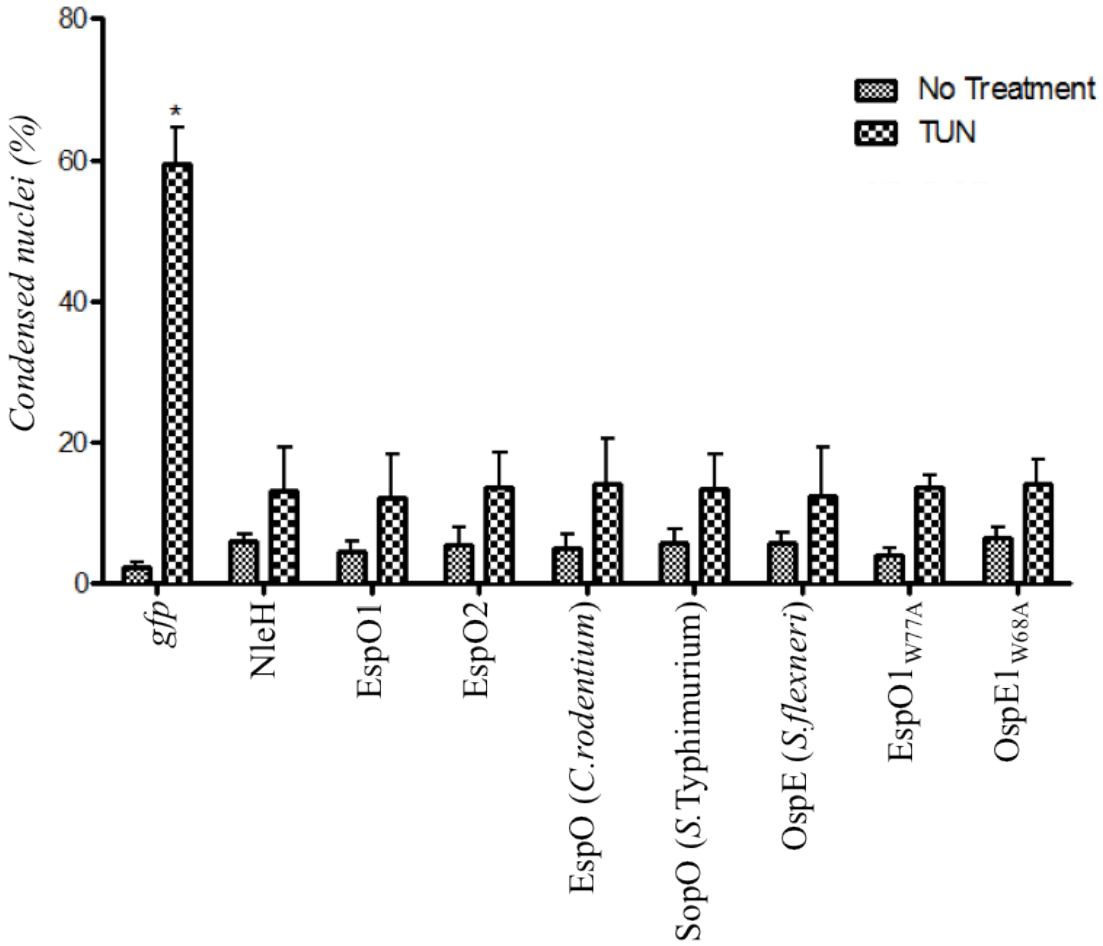

Figure 43. TUN treated and untreated EspO transfected cells
Untreated EspO ortholog transfected cells are non-apoptotic with similar low levels (5-10%) of cleaved caspase-3 (A) and condensed nuclei (B) compared to the *gfp* control cells without treatment (0-5%). The level of apoptosis is significantly higher in *gfp* control cells induced with staurosporine (70-80%) compared to the untreated control cells (0-5%). Three biological replicates with two technical replicates each (100 transfected cells counted per technical replicate) were analysed for statistical significance with the two-tailed unpaired *t*-test with equal SD. **P*<0.05.

5.2 EspO1 inhibits apoptosis during infections

Work in the Frankel group has previously reported that infection of HeLa cells with EPEC and EHEC *nleH* mutants leads to apoptosis and cell detachment that could be prevented by pre-treatment with the global caspase inhibitor, Z-Vad-fmk [48]. To investigate if EspO can substitute for Z-Vad-fmk, we transformed EPEC E2348/69 (which is naturally *espO* negative) Δ*nleH* with plasmids encoding untagged (to allow EspO:Hax-1 interaction) full length EspO1 or EspO1$_{W77A}$.

HeLa cells were seeded 48 hours prior to infection at a density of $5x10^4$ to have 80-90% cell confluency in 24-well plates on the day of infection. The lower level of adherent cells remaining in plates infected with EPEC E2348/69 Δ*nleH1* Δ*nleH2* was obvious under the microscope (10-20%) when compared to the EPEC E69 wild-type (80%) and the double *nleH* mutant expressing either full-length EspO1 or W77A EspO1 (80%). For every condition, the remaining adherent cells were examined by immunofluorescence for membrane blebbing indicated by cell shrinkage and rounding and apoptotic stress in mitochondria labelled with anti Cytochrome – *c*. Cell detachment, membrane blebbing or changes in the mitochondrial network were not obvious in the wild-type or the double *nleH* mutant expressing either full-length EspO1 or W77A EspO1 meaning that EspO1 was able to inhibit the apoptosis induced by the *nleH*-mutant (Figure 44). Taken together these results show that the EspO orthologs are potent inhibitors of apoptosis in HeLa cells and execute this function in an ILK-independent manner.

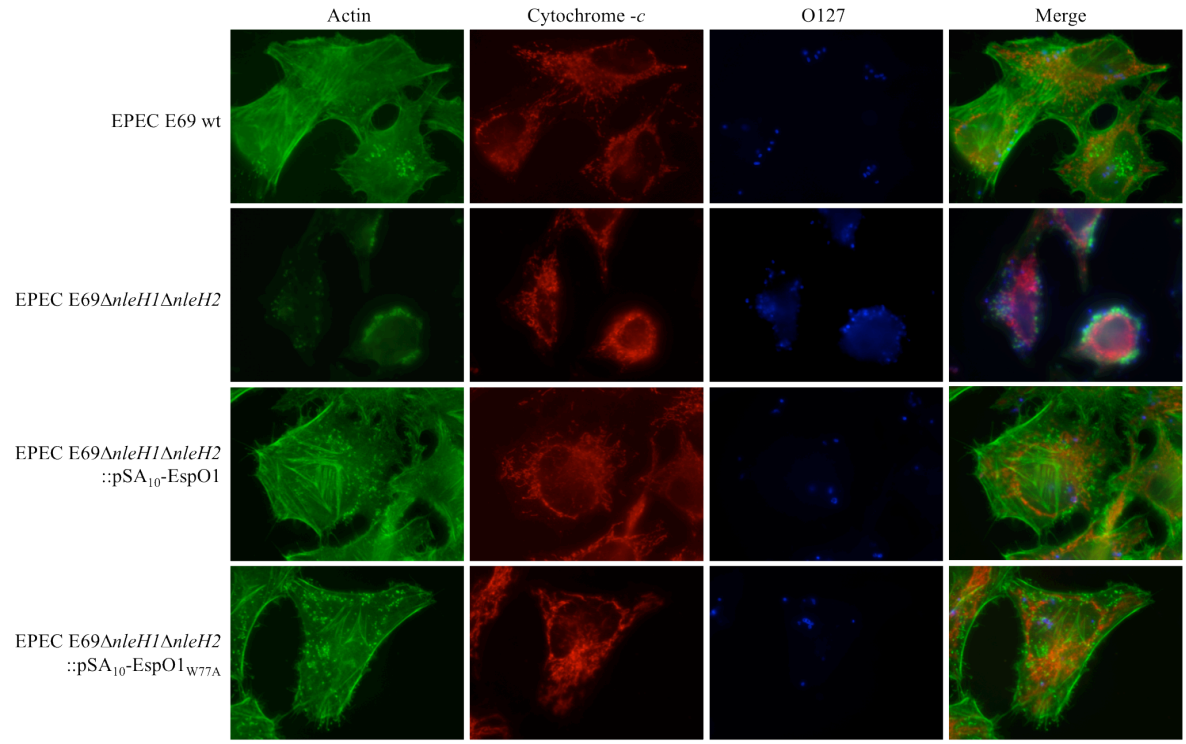

Figure 44. An ILK-independent EspO inhibition of apoptosis in EPEC infections
EspO1 or EspO1$_{W77A}$ complemented EPEC E2348/69 double *nleH* mutant inhibit membrane blebbing and cell detachment induced by the *nleH*-mutant. 50 adherent cells were examined by immunofluorescence for each condition. Actin was stained with Phalloidin Green, mitochondria labelled with anti – Cytochrome – *c* (Red) and an anti-O127 antibody (Blue) for EPEC bacteria.

5.3 EspO inhibition of apoptosis is Hax-1 dependent

To investigate whether Hax-1 is directly involved in the anti apoptotic activity of the EspO orthologs, we treated HeLa cells with Hax-1 siRNA and induced apoptosis with STS. Silenced Hax-1 expression was confirmed by Western blotting (Figure 45). Hax-1 depleted and untransfected cells did not trigger apoptosis without STS treatment. HeLa cells depleted of Hax-1 were then transfected with EspO1, SopO or OspE, treated with STS and assessed by TUNEL. The EspO ortholog-transfected cells showed high levels of apoptosis (60-80%) similar to the control untransfected cells (Figure 45). Taken together, these results show that EspO orthologs protect cells from apoptosis in a Hax-1 dependent manner.

Furthermore, we investigated whether Hax-1 is also directly involved in the EspO ability to inhibit the apoptosis, induced specifically by ER stress. As previously described, we treated HeLa cells with siRNA and silenced Hax-1 expression was confirmed by Western blotting (Figure 46). In this case, we induced apoptosis using the ER-stress inducer, TUN. Hax-1 depleted and untransfected cells did not trigger apoptosis without STS treatment. HeLa cells depleted of Hax-1 were then transfected with EspO1, SopO or OspE, treated with STS and assessed by TUNEL. The EspO ortholog-transfected cells showed high levels of apoptosis (60-80%) similar to the control untransfected cells (Figure 46).

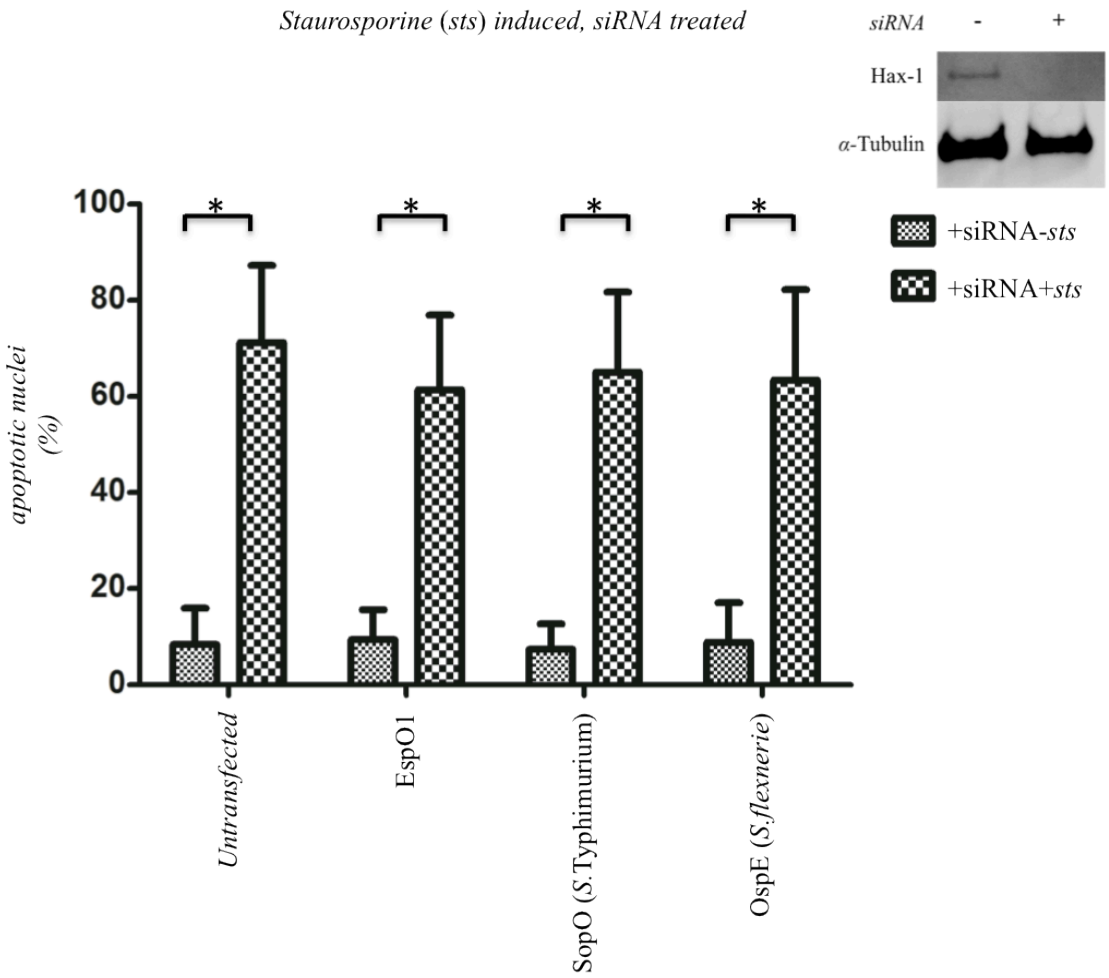

Figure 45. Hax-1 dependent EspO inhibition of apoptosis
EspO orthologs cannot protect against staurosporine induced apoptosis in Hax-1 depleted HeLa cells. Apoptotic nuclei assessed by TUNEL. The level of apoptosis is significantly higher in untransfected control cells and EspO ortholog transfected cells induced with Staurosporine (60-70%) compared to the untreated control cells (5-10%). Three biological replicates with two technical replicates each (100 transfected cells counted per technical replicate) were analysed for statistical significance with the two-tailed unpaired *t*-test with equal SD. **P*<0.05.

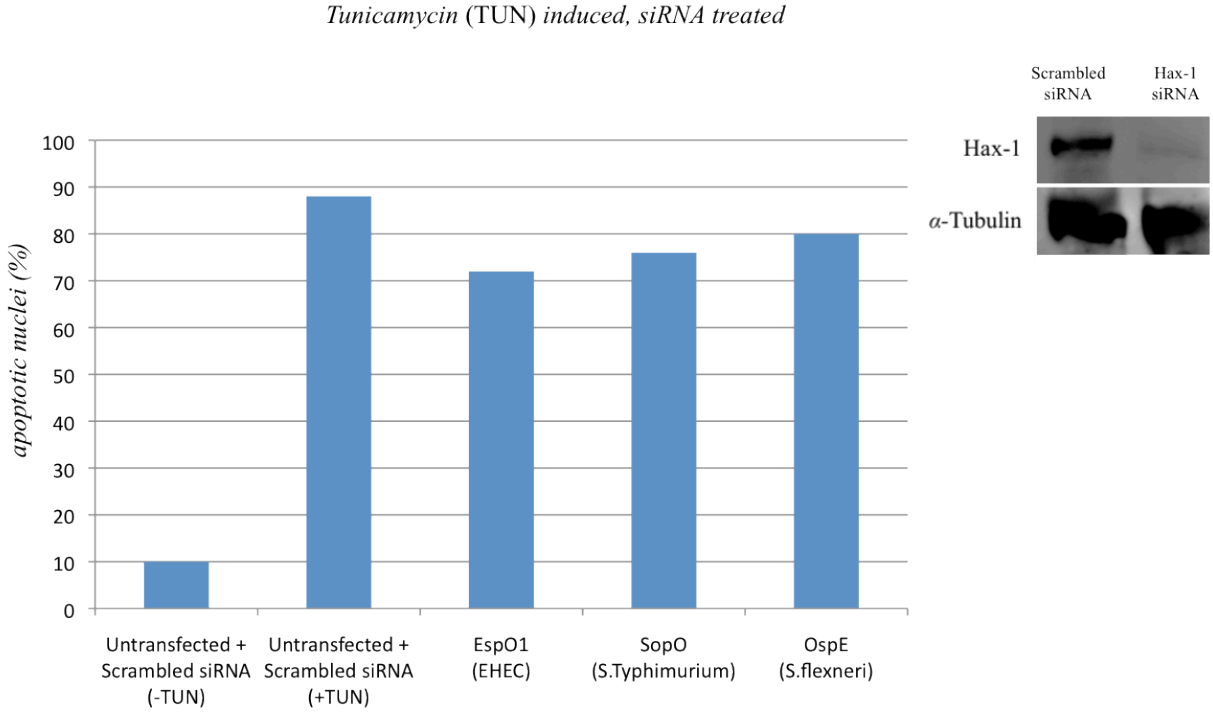

Figure 46. EspO inhibition of ER stress is Hax-1 dependent
EspO orthologs cannot protect against tunicamycin induced apoptosis in Hax-1 depleted HeLa cells. Apoptotic nuclei assessed by TUNEL. The level of apoptosis is significantly higher in untransfected control cells and EspO ortholog transfected cells induced with Tunicamycin (70-90%) compared to the untreated control cells (10%). One biological replicate with two technical replicates (50 transfected cells counted per technical replicate) are shown.

5.4 Preliminary *in-vivo* study of EspO : Histopathology

In order to investigate the role of EspO in the *in-vivo* pathogenesis of *C. rodentium* (CR), we generated an *espO* deletion mutant. As mentioned earlier, this is a commonly used model of EPEC or EHEC infection in mice but there are certain limitations. Although, the EHEC EspO effectors were previously confirmed as T3SS effectors, Deng *et al.* have shown in an *in-vitro* study on *C. rodentium* T3SS effectors that CR EspO might not be secreted by the type III secretion system [213, 236]. However, the homology shared between EHEC and CR EspO but also the common behaviour shared in the *in-vitro* experimental work discussed in previous chapters, induced us to examine the role of EspO in a physiological setting.

We orally infected C57BL/6 mice with wild-type CR (ICC169), the *espO* mutant and the mutant complemented with full-length EspO or $EspO_{W77A}$ (to abolish the EspO:ILK interaction) and monitored CR by enumerating the number of colony forming units per gram of stools (cfu g-1) collected at regular intervals following inoculation. All strains were peaked at day 8 and although at different rates, all strains started to clear from day 11 post-inoculation. Differences were observed in the rate of clearance for *espO* deletion mutant, which appears to be more persistent in comparison to the EspO complemented strain or wt CR (Figure 47). To ensure the *in-vivo* plasmid stability in the complemented strain we performed differential antibiotic plating and showed that the plasmid was fully stable over the course of the infection (Figure 48).

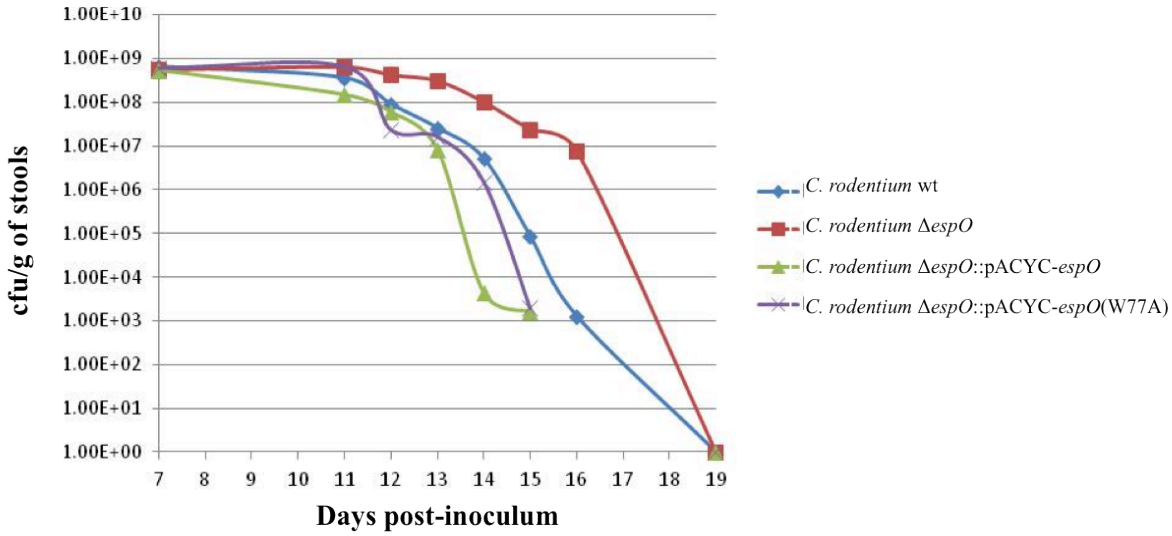

Figure 47. Colonisation rates of *C. rodentium* infection *in-vivo*
C. rodentium wt strain showing similar colonisation with EspO mutant and complemented strains up to day 11. Clearance rates are similar between the wt and complemented strains but the EspO mutant appears more persistent. Full clearance is seen at day 19 post-inoculation for all strains. Graph shows the mean value from 8 mice per condition. Courtesy of Dr V. Crepin-Sevenou.

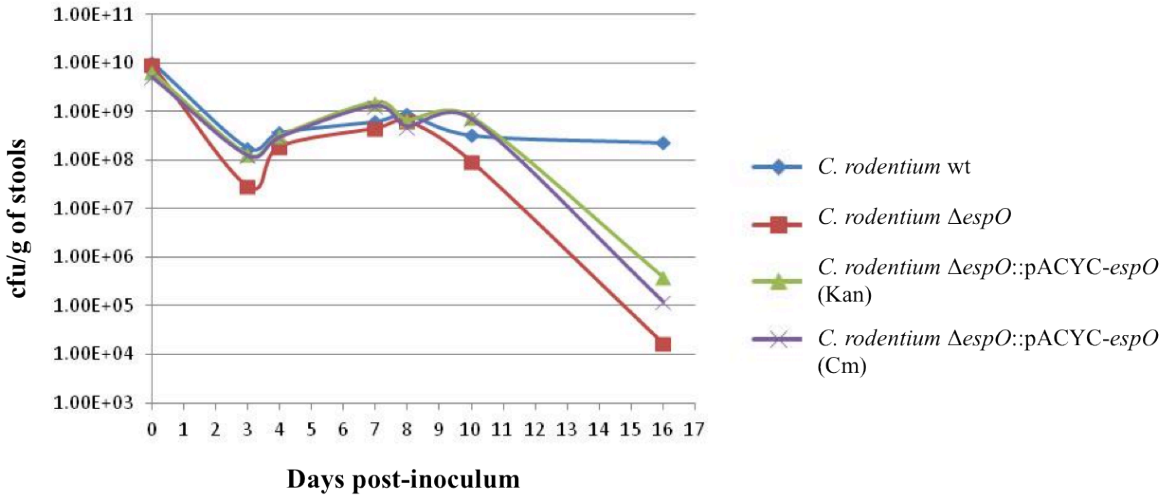

Figure 48. Plasmid complementation stability *in-vivo*
The stability of the plasmids used for complementation was confirmed by differential antibiotic plating during the course of infection. Stool samples taken during the course of infection were plated with antibiotics to ensure the presence of the transformed plasmid. Differential antibiotic plating was used to select for both the *espO* mutation (kanamycin) and the complementation plasmid (chlorampenicol). Courtesy of Dr V. Crepin-Sevenou.

Light microscopy analysis of colonic sections from mice infected with the *espO* mutant showed a statistically significant reduction in hyperplasia levels (measured by length of crypt per condition) compared to the wild type and complemented strains (Figure 49). Colonic mucosal hyperplasia is the hallmark of CR infection and is characterized by elongation of the colonic crypts, goblet cell depletion, mucosal erosion, increased mitotic activity or cell proliferation and increased infiltration of immune cells. The decreased levels observed with the *espO* mutant were similar to the uninfected control. We additionally tested the mutant strain complemented with EspO(W77A) to abolish the ILK interaction and this showed similar levels to the wild type and EspO complemented strain (Personal communication with Dr V. Crepin-Sevenou). Furthermore, we examined the tissue sections for protein expression by Western blot analysis, which revealed that Hax-1 is signigicantly up-regulated in *C. rodentium* infection (Figure 49.C). Therefore, ILK remains independent, which suggests that an EspO:Hax-1 interaction might be regulating crypt epithelial proliferation and apoptosis to promote the hyperplastic phenotype in CR *in-vivo* model of EHEC/EPEC infection.

A. Hyperplasia Graph

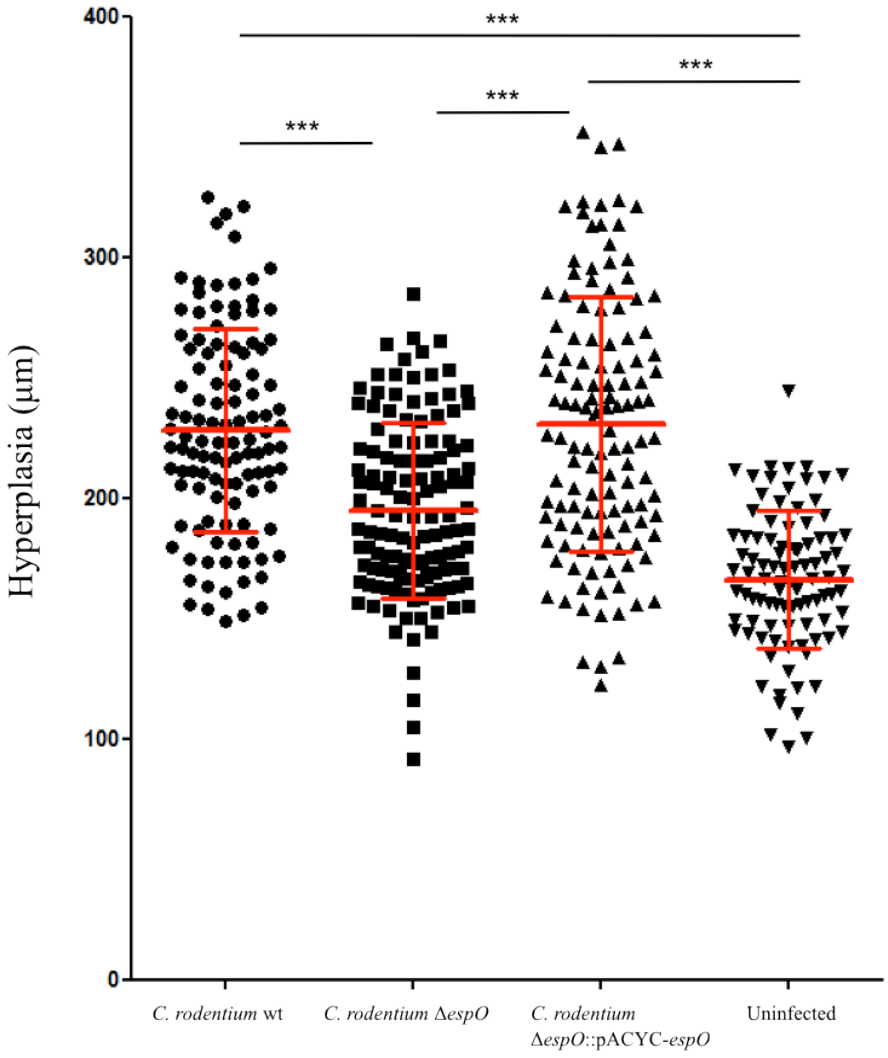

B. H & E staining of tissue sections

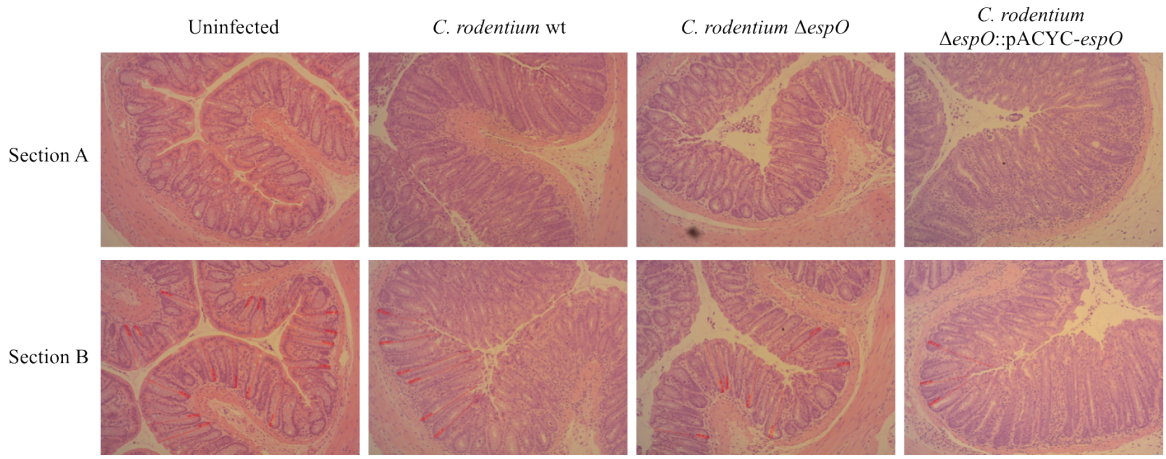

C. Hax-1 expression levels

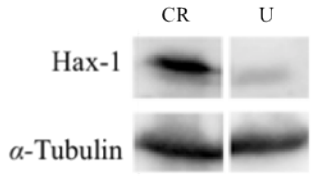

Figure 49. Histopathology of EspO *in-vivo*

A. Hyperplasia as measured by crypt length from H &E staining of tissue sections is reduced in the EspO mutant compared to the wild type and the complemented mutant strain. Data is shown as mean +/- SD. B. H & E staining of tissue sections used to measure colonic hyperplasia. C. Western blot analysis showing increased Hax-1 expression levels in *C.rodentium* (CR) infected mice compared to the uninfected control reveals a possible role of Hax-1 in CR infections. Courtesy of Dr V. Crepin-Sevenou.

5.5 EspO regulates inflammation *in-vivo*

Hyperplasia is the hallmark of CR infections and this is presented partly by mucosal inflammation. Therefore, we investigated whether the ability to recruit immune cells to the site of bacterial infection could be, at least to a certain extend, attributed to EspO. We employed fluorescence microscopy to examine neutrophil and CD4+T cell recruitment on colonic cryosections. Ly6G surface antigen and CD4 (respectively) positive cells were detected following infection with CR wild type, *espO* mutant and complemented with EspO. Both neutrophil and CD4+-T cell recruitment was higher in colonic sections from mice infected with the EspO complemented mutant whereas *espO* deletion mutant shows marginally reduced levels compared to wild-type CR (Figure 50). These data suggest that EspO plays a direct role in recruiting neutrophils and CD4+-T cells to the site of bacterial infection. In addition, the decreased levels of inflammatory cell infiltration could further explain the reduction of hyperplasia observed following mice infected with *espO* deletion mutant.

A. Neutrophil Counts

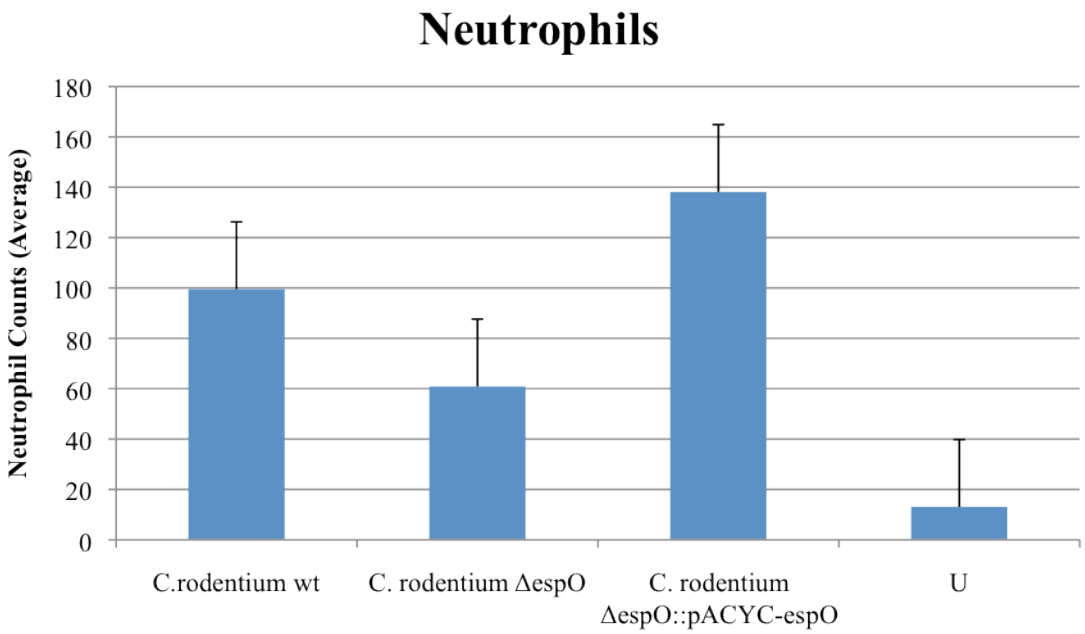

B. CD4+T cell Counts

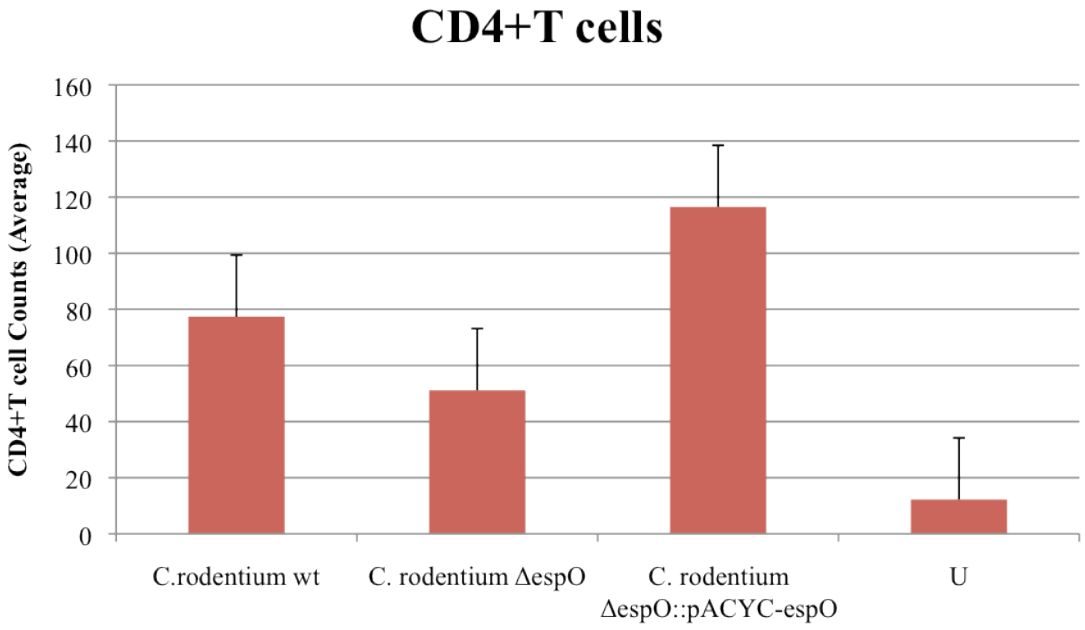

C. Neutrophil Ly6G staining of frozen sections

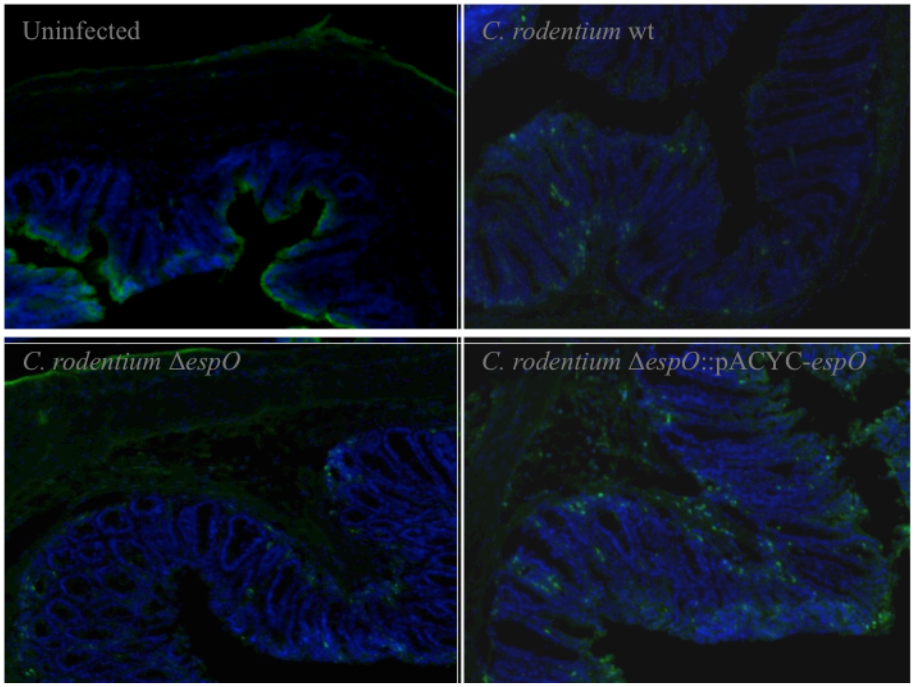

Figure 50. Neutrophil and CD4+T cell Counts
A. The EspO mutant strain shows lower levels of neutrophil infiltration compared to the wild type and EspO complemented mutant strain. B. CD4+T cell infiltration is less in mice infected with the mutant compared to the wild type and EspO complemented strain. Neutrophils and CD4+T cells counts presented as a mean of counts from two tissue sections from four different mice per condition. C. Increased neutrophil infiltration in wild type and EspO complemented strain compared to the uninfected control or mutant strain are shown by Ly6G stainings of frozen sections. Immunofluorescent stainings were kindly performed by Dr V. Crepin-Sevenou.

6 Chapter 6 : Discussion

In this work, we present a T3SS effector paradigm illustrating an orchestrated influence of multiple signalling pathways leading to cell survival. As previously reported, the EspO orthologs interact with ILK at FA sites to stabilise host cell attachment on the extracellular matrix [130]. Our results show that EspO orthologs also interact with Hax-1 to additionally protect host cells from apoptosis and regulate inflammation. We propose a novel EspO mechanism that might be employed by enteric bacteria and involves the protection of Hax-1 from degradation, which is normally executed by caspase-3 and Omi/HtrA2 [199, 206]. Potentially this enables EspO orthologs to regulate a key anti apoptotic Hax-1 interactome, which may include the potent inhibitor of apoptosis XIAP [197]. Figure 51 illustrates a suggested model for the T3SS EspO orthologs within the context of an infection with enteric bacteria.

Microbial intrusion of the intestinal environment is sensed by pattern recognition receptors (PRRs) mainly bound at the cell surface but can also localise in the cytosol or even internalised in vesicles [237]. The PRR families associated with bacterial recognition include the well-characterised Toll-like receptors (TLRs) and the nucleotide binding oligomerisation domain (NOD)-like receptors (NLRs) [238, 239]. In a heathly intestine, TLRs and NLRs interact with the naturally available ligands often provided by the commensal microbiota. Their action maintains the intestinal epithelial barrier by regulating signalling pathways involved in cell survival [240]. The TLR- and NLR- specific ligands are known as pathogen associate molecular patterns or PAMPs and include lipopolysaccharides, peptidoglycan (e.g. muramyl dipeptide – MDP), flagellin and nucleic acids. PAMPs enable the pathogen to manipulate the first line of host defence and evade the intestinal barrier [241].

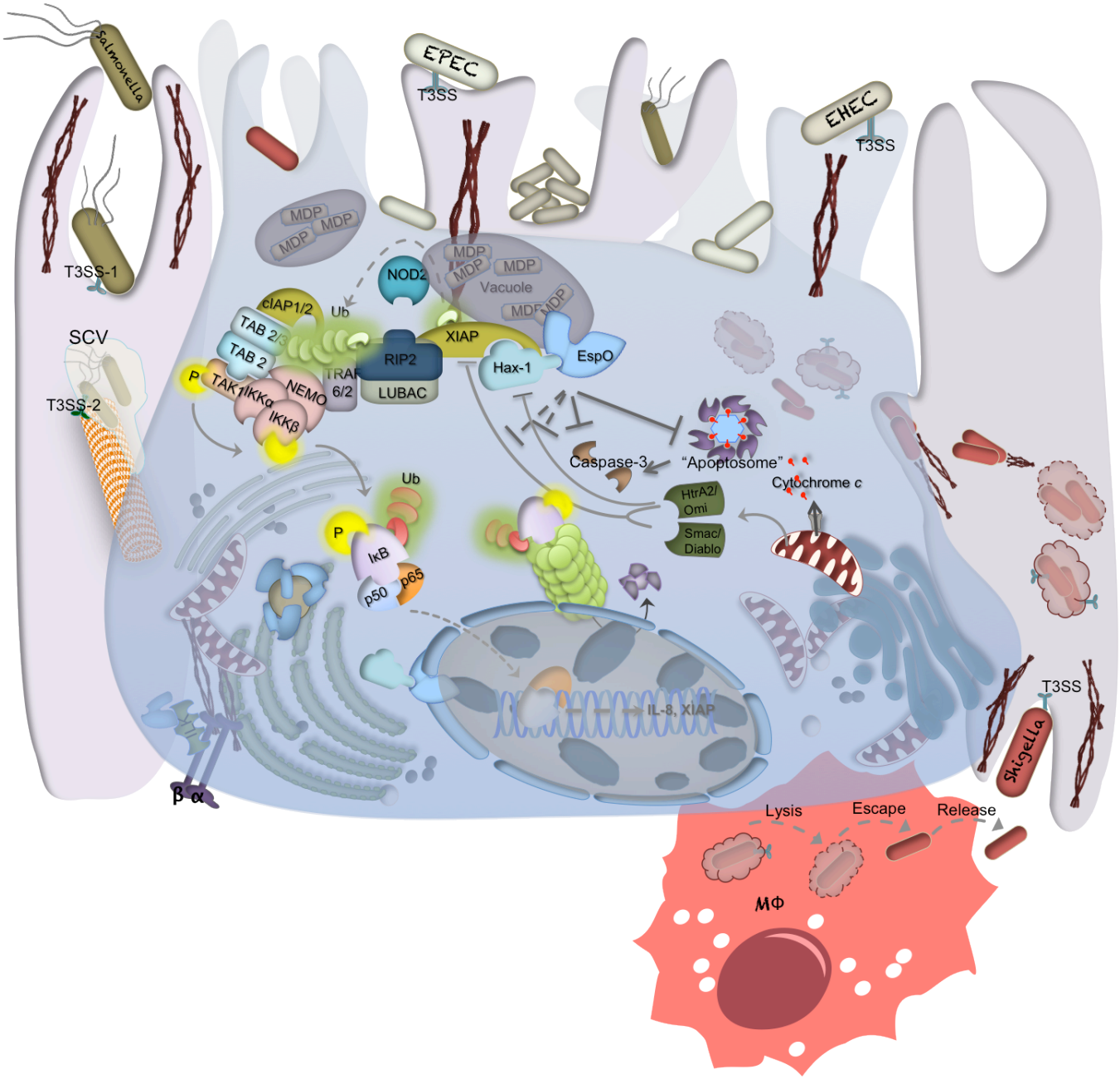

Figure 51. Illustrating a novel EspO model (Designed by author)
In a hypothetical model, EspO orthologs from EPEC / EHEC, Shigella and Salmonella may interact with Hax-1 to regulate the onset of apoptosis but also the inflammatory response initiated by the NOD signalling, upon bacterial recognition. Illustration was designed by the author for this study.

MDPs in epithelial cells are endocytosed in a clathrin-dependent internalisation within vesicles, which communicate with members of the NLR signalling [242]. Interestingly, the two main players of the NLR family, known as NOD1 and NOD2, are homologues of the apoptotic protease-activating factor (APAF1) and also regulate inflammation through NF-κB [239]. Once stimulated, they form multimeric complexes by recruiting protein kinases (RIP2, TAK1:TAB1 complex, TAB2 and the most essential IKKα-IKKβ-NEMO complex for NF-κB activation), ubiquitin recruiters (TNF receptor associated factors TRAF6 and TRAF2) and the inhibitors of apoptosis XIAP and cIAP. An intriguing study by Krieg *et al.* showed that XIAP interacts with the receptor-interacting protein kinase 2 (RIP2) to regulate downstream NOD signalling [243]. Recently, Damgaard *et al*. demonstrated that RIP2 ubiquitination is a XIAP-dependent E_3 ubiquitin ligase action that recruits LUBAC, another important member of the ubiquitination system to regulate the NOD2 only signalling cascade [244]. When XIAP is absent, the NOD2 signalling is not facilitated and this results in decreased production of NF-κB targets (e.g. IL-8) [244].

The ubiquitination system in eukaryotic cells is a key mechanism used to separate proteins required to maintain their function (e.g. Lys-63 or M1) from those assigned for elimination (Lys-48 or U-48 in Fig. 5) by the 26S proteasome [245, 246]. Both XIAP and the LUBAC complex promote linear M1-linked ubiquitination in NOD2-RIP2 signalling [244]. The process of ubiquititnation attracts enteric bacteria and T3SS effectors like NleG from EHEC / EPEC, IpaH from Shigella or SopA, SlrP and SspH from Salmonella have been shown to function as E_3 ubiquitin ligases [247-251]. Additionally, the SPI-2 T3SS deubiquitinase SseL counteracts the ubiquitin ligase-functioning effectors in Salmonella [114]. In this study, we showed that EspO orthologs exhibit an anti-apoptotic activity that depends on Hax-1. Once Hax-1 is protected from degradation, the formation of a binding complex with XIAP might be promoted.

The Hax-1:XIAP interaction was shown to suppress XIAP polyubiquitination and thus, protect it from being degraded by the ubiquitin / proteasome system [197]. Regulation of XIAP is fascilitated by HtrA2/Omi and Smac/Diablo, which are mitochondrial proteases released in the cytosol upon induction of apoptosis [176]. XIAP consists of 3 baculovirus IAP repeats (BIRs) which are commonly found in IAPs to confer the anti-apoptotic ability, one ubiquitin binding domain (UBA) and a C-terminal RING domain which functions as an E_3 ubiquitin ligase [252]. The N-terminal BIR domain 1 is required for TAK1:TAB1 complex that allows XIAP to regulate NF-κB activation whereas BIRs 2 and 3 are involved in the inhibition of caspases -3, -7 and -9. HtrA2/Omi and Smac/Diablo interact with BIRs 2 and 3, which can be additionally occupied by Hax-1 [197]. The latter prevents the interaction of pro-apoptotic proteases with XIAP and therefore, promotes its intracellular stability. Additionally, the RING domain functions as an auto-survival mechanism, which ubiquitinates proteases like Smac/Diablo [253].

In this study, we also show a co-localisation of EspO and Hax-1 with cytosolic vacuoles, which might be a result of a XIAP-dependent recruitment of the Hax-1:EspO complex to the MDP-containing vesicles that stimulate NOD2 signalling. However, since our observation is restricted to ectopically expressed EspO and endogenous Hax-1, the vacuole formation might also be a Hax-1 participation in clathrin-mediated endocytosis due to its integrin β6-binding site [254]. The vacuoles formed in EspO transfected cells also co-localise with the ER marker $CREB_3$ (a transcription factor residing at the ER and once activated, it travels to the nucleus to enhance cell proliferation). Consistently, multiple viral proteins also target Hax-1 to interfere with apoptotic pathways and both ER and nuclear redistribution of Hax-1 was reported [209, 211, 212]. We further confirm a nuclear localisation of both ectopically expressed EspO1 and endogenous Hax-1. The consensus HeLa cell localization of Hax-1 includes mitochondria, ER and nuclear membrane [255].

Once enteric bacteria evade the first line of defence, they work towards establishing an infection by utilising their T3SS effector repertoire. In a *C. rodentium* model the T3SS effector NleE was shown to alter colonization and disease severity when absent [256]. In addition, the EHEC / EPEC T3SS NleB along with NleE and its Shigella homologue OspZ are able to block NF-κB activation and nuclear translocation of the p65 subunit [50]. In EPEC infections, the action of NleE and NleB affect interleukin-8 (IL-8) secretion and this allows transepithelial migration of neutrophils from the submucosa to the lumen [257]. Shigella was shown to use this neutrophil migration as a port of entry towards the basolateral membrane [258, 259]. Furthermore, the Shigella effectors $IpaH_{9.8}$, OspB and OspF but also SspH1, the $IpaH_{9.8}$ homologue in Salmonella are targeted to the nucleus to supress the production of IL-8 [111-113].

Bacteria also block NF-κB activation by targeting the NOD signalling and depletion of NOD2 worsens *S.* Typhimurium and *L. monocytogenes* infections [260-262]. The intracellular action of EspO orthologs might also promote bacterial survival through an interaction with Hax-1, which in turn binds XIAP to prevent its degradation. However, whether the RING domain of XIAP, which is essential for NOD2 signalling, is still functional within the Hax-1:EspO conformational complex would require further investigation. Possibly by testing the M1-specific ubiquitination of XIAP in the presence of EspO orthologs. A non-functional RING domain in XIAP is known to cause X-linked lymphoproliferative disease (XLP) and mainly affects the immune system [263, 264]. Additionally, non-functional NOD2 has been identified as a cause of the prolonged bacterial infection in inflammatory bowel diseases like ulcerative colitis or Crohn's [241, 265, 266]. The latter is a disease characterised by diminished neutrophil and T cell function caused by pro-inflammatory cytokines, like the potent neutrophil chemoattractant IL-8, which are being severely affected by defects in NF-κB activation [267]. Importantly, a non-functional

Hax-1 has been identified as an important genetic marker for severe congenital neutropenia or Kostmann disease, which describes an immunodeficiency syndrome with increased apoptosis in neutrophils [268].

Once infected however, the intestinal environment is forced to battle for survival. This involves cellular communication governed by Ca^{2+}, a key ionic messenger that coordinates cellular development and activity but also triggers their death [185]. Whether a cell is irreversibly committed to suicide is also dependent upon a homeostatic crosstalk governed by Ca^{2+} signalling [185]. Attenuated homeostasis allows Ca^{2+} to orchestrate apoptosis, which is considerably regulated by the interaction of Hax-1 with the active ER-specific Ca^{2+} importer, $SERCA_2$ [193, 205]. Cells over expressing Hax-1 exhibit down regulation of $SERCA_2$ and this presents an inhibition of apoptosis through diminished ER Ca^{2+} content.

Apart from $SERCA_2$, Hax-1 participation in Ca^{2+} homeostasis may also include its interaction with the ER localised polycystic kidney disease type II, PKD2 or TRPP2 [201]. In a dimeric complex, PKD1 and PKD2 form cationic channels that permit a two-way direction Ca^{2+} flux [202]. The PKD2 channels were shown to inhibit apoptosis by permitting less ER Ca^{2+} export to the cytosol and mitochondria in association with the ER Ca^{2+} efflux channels, inositol triphosphate receptors (IP3Rs) [203, 204]. In EHEC / EPEC infection the action of IP3Rs is also targeted by the T3SS NleH, which inhibits apoptosis through a direct interaction with Bax inhibitor-1 (BI-1). Interestingly, specific C-terminal conformational changes additionally localise PKD2 at the nucleus to activate transcription factors regulating genes involved in cell proliferation [269, 270].

In addition, silencing of PKD2 in a human colonic epithelial cell line results in decreased activation of NF-κB and IL-8 production [271]. Non-functional *pkd1* and *pkd2*

genes cause autosomal dominant polycystic kidney disease (ADPKD), which is characterised by enlarged kidneys due to increased proliferation and apoptosis [272]. Additionally, the *lcn2* expressed human neutrophil lipocalin (NGAL) or oncogene 24p3 is a potent genetic marker for ADPKD [273, 274]. Neutrophils release NGAL at sites of infection to bind bacterial ferric siderophores [275, 276]. The complexes are then endocytosed within cytosolic vesicles, which subsequently release the siderophores to activate iron-dependent inflammatory pathways. Intriguingly, NGAL is now considered as a potent biomarker for renal failure in children suffering from HUS commonly caused by Shiga toxin-producing EHEC infections [277-279].

The preliminary *in-vivo* data shown in this study, indicate a significant role of EspO in the regulation of inflammatory responses mediated by IL-8 and presented by an increase in both neutrophil and CD4+ T cell infiltration in mice infected with wild type *C. rodentium* and the complemented strains but not in the *espO* mutant. Therefore, EspO orthologues might be able to control IL-8 production through their interaction with Hax-1, which maintains a stable intracellular XIAP. This in turn, might lead to an inhibition of apoptosis but also a control of host cell inflammation through the NF-κB regulation of IL-8.

Although, there is an abundance of elements suggesting an important EspO contribution in bacterial survival within the infected host, it is still speculative to say that it is included in the auxiliary T3SS effector proteins that worsen the outcome of infection. Whether the *in-vitro* EspO:Hax-1 interaction has a physiological meaning is currently being further investigated with the *C. rodentium* model employed for *in-vivo* studies of EHEC / EPEC infection. Our current understanding introduces a T3SS effector commonly expressed in enteric bacteria to promote their infective life inside the host and its presence within the effector repertoire might be a determinant of disease severity in certain pathogenic strains.

7 References

1. Chen, H.D. and G. Frankel, *Enteropathogenic Escherichia coli: unravelling pathogenesis.* FEMS Microbiol Rev, 2005. **29**(1): p. 83-98.
2. Nakazato, G., et al., *Attaching and effacing Escherichia coli isolated from dogs in Brazil: characteristics and serotypic relationship to human enteropathogenic E. coli (EPEC).* Vet Microbiol, 2004. **101**(4): p. 269-77.
3. Leomil, L., et al., *Characterization of two major groups of diarrheagenic Escherichia coli O26 strains which are globally spread in human patients and domestic animals of different species.* FEMS Microbiol Lett, 2005. **249**(2): p. 335-42.
4. Wenzel, C., et al., *Invasive ductal carcinoma and invasive lobular carcinoma of breast differ in response following neoadjuvant therapy with epidoxorubicin and docetaxel + G-CSF.* Breast Cancer Res Treat, 2007. **104**(1): p. 109-14.
5. Majowicz, S.E., et al., *The global burden of nontyphoidal Salmonella gastroenteritis.* Clin Infect Dis, 2010. **50**(6): p. 882-9.
6. Westrell, T., et al., *Zoonotic infections in Europe in 2007: a summary of the EFSA-ECDC annual report.* Euro Surveill, 2009. **14**(3).
7. Weinberger, M. and N. Keller, *Recent trends in the epidemiology of non-typhoid Salmonella and antimicrobial resistance: the Israeli experience and worldwide review.* Curr Opin Infect Dis, 2005. **18**(6): p. 513-21.
8. Laupland, K.B., et al., *Salmonella enterica bacteraemia: a multi-national population-based cohort study.* BMC Infect Dis, 2010. **10**: p. 95.
9. Wassef, J.S., D.F. Keren, and J.L. Mailloux, *Role of M cells in initial antigen uptake and in ulcer formation in the rabbit intestinal loop model of shigellosis.* Infect Immun, 1989. **57**(3): p. 858-63.
10. Sansonetti, P.J., et al., *Infection of rabbit Peyer's patches by Shigella flexneri: effect of adhesive or invasive bacterial phenotypes on follicle-associated epithelium.* Infect Immun, 1996. **64**(7): p. 2752-64.
11. Man, A.L., M.E. Prieto-Garcia, and C. Nicoletti, *Improving M cell mediated transport across mucosal barriers: do certain bacteria hold the keys?* Immunology, 2004. **113**(1): p. 15-22.
12. Islam, D., et al., *In situ characterization of inflammatory responses in the rectal mucosae of patients with shigellosis.* Infect Immun, 1997. **65**(2): p. 739-49.
13. Zychlinsky, A., M.C. Prevost, and P.J. Sansonetti, *Shigella flexneri induces apoptosis in infected macrophages.* Nature, 1992. **358**(6382): p. 167-9.
14. Zychlinsky, A., et al., *In vivo apoptosis in Shigella flexneri infections.* Infect Immun, 1996. **64**(12): p. 5357-65.
15. Bernardini, M.L., et al., *Identification of icsA, a plasmid locus of Shigella flexneri that governs bacterial intra- and intercellular spread through interaction with F-actin.* Proc Natl Acad Sci U S A, 1989. **86**(10): p. 3867-71.
16. Monack, D.M. and J.A. Theriot, *Actin-based motility is sufficient for bacterial membrane protrusion formation and host cell uptake.* Cell Microbiol, 2001. **3**(9): p. 633-47.

17. Stevens, J.M., E.E. Galyov, and M.P. Stevens, *Actin-dependent movement of bacterial pathogens.* Nat Rev Microbiol, 2006. **4**(2): p. 91-101.
18. Sansonetti, P.J., et al., *Multiplication of Shigella flexneri within HeLa cells: lysis of the phagocytic vacuole and plasmid-mediated contact hemolysis.* Infect Immun, 1986. **51**(2): p. 461-9.
19. Kaper, J.B., J.P. Nataro, and H.L. Mobley, *Pathogenic Escherichia coli.* Nat Rev Microbiol, 2004. **2**(2): p. 123-40.
20. Nataro, J.P. and J.B. Kaper, *Diarrheagenic Escherichia coli.* Clin Microbiol Rev, 1998. **11**(1): p. 142-201.
21. Shaw, R.K., et al., *Enterohemorrhagic Escherichia coli exploits EspA filaments for attachment to salad leaves.* Appl Environ Microbiol, 2008. **74**(9): p. 2908-14.
22. Pennington, H., *Escherichia coli O157.* Lancet, 2010. **376**(9750): p. 1428-35.
23. Kaper, J.B. and M.A. Karmali, *The continuing evolution of a bacterial pathogen.* Proc Natl Acad Sci U S A, 2008. **105**(12): p. 4535-6.
24. Thorpe, C.M., *Shiga toxin-producing Escherichia coli infection.* Clin Infect Dis, 2004. **38**(9): p. 1298-303.
25. Donnenberg, M.S. and T.S. Whittam, *Pathogenesis and evolution of virulence in enteropathogenic and enterohemorrhagic Escherichia coli.* J Clin Invest, 2001. **107**(5): p. 539-48.
26. Garmendia, J., G. Frankel, and V.F. Crepin, *Enteropathogenic and enterohemorrhagic Escherichia coli infections: translocation, translocation, translocation.* Infect Immun, 2005. **73**(5): p. 2573-85.
27. Petty, N.K., et al., *The Citrobacter rodentium genome sequence reveals convergent evolution with human pathogenic Escherichia coli.* J Bacteriol, 2010. **192**(2): p. 525-38.
28. Wong, A.R., et al., *Enteropathogenic and enterohaemorrhagic Escherichia coli: even more subversive elements.* Mol Microbiol, 2011. **80**(6): p. 1420-38.
29. Jerse, A.E., et al., *A genetic locus of enteropathogenic Escherichia coli necessary for the production of attaching and effacing lesions on tissue culture cells.* Proc Natl Acad Sci U S A, 1990. **87**(20): p. 7839-43.
30. McDaniel, T.K., et al., *A genetic locus of enterocyte effacement conserved among diverse enterobacterial pathogens.* Proc Natl Acad Sci U S A, 1995. **92**(5): p. 1664-8.
31. Kenny, B., et al., *Enteropathogenic E. coli (EPEC) transfers its receptor for intimate adherence into mammalian cells.* Cell, 1997. **91**(4): p. 511-20.
32. Touze, T., et al., *Self-association of EPEC intimin mediated by the beta-barrel-containing anchor domain: a role in clustering of the Tir receptor.* Mol Microbiol, 2004. **51**(1): p. 73-87.
33. Robinson, C.M., et al., *Shiga toxin of enterohemorrhagic Escherichia coli type O157:H7 promotes intestinal colonization.* Proc Natl Acad Sci U S A, 2006. **103**(25): p. 9667-72.
34. Phillips, A.D., et al., *Enterohaemorrhagic Escherichia coli O157:H7 target Peyer's patches in humans and cause attaching/effacing lesions in both human and bovine intestine.* Gut, 2000. **47**(3): p. 377-81.
35. Naylor, S.W., et al., *Lymphoid follicle-dense mucosa at the terminal rectum is the principal site of colonization of enterohemorrhagic Escherichia coli O157:H7 in the bovine host.* Infect Immun, 2003. **71**(3): p. 1505-12.
36. Phillips, A.D. and G. Frankel, *Intimin-mediated tissue specificity in enteropathogenic Escherichia coli interaction with human intestinal organ cultures.* J Infect Dis, 2000. **181**(4): p. 1496-500.

37. Fitzhenry, R.J., et al., *Human intestinal tissue tropism of intimin epsilon O103 Escherichia coli.* FEMS Microbiol Lett, 2003. **218**(2): p. 311-6.
38. Cornelis, G.R., *The type III secretion injectisome.* Nat Rev Microbiol, 2006. **4**(11): p. 811-25.
39. Galan, J.E. and H. Wolf-Watz, *Protein delivery into eukaryotic cells by type III secretion machines.* Nature, 2006. **444**(7119): p. 567-573.
40. Daniell, S.J., et al., *The filamentous type III secretion translocon of enteropathogenic Escherichia coli.* Cell Microbiol, 2001. **3**(12): p. 865-71.
41. Buttner, D. and U. Bonas, *Port of entry--the type III secretion translocon.* Trends Microbiol, 2002. **10**(4): p. 186-92.
42. Galan, J.E. and A. Collmer, *Type III secretion machines: bacterial devices for protein delivery into host cells.* Science, 1999. **284**(5418): p. 1322-8.
43. Pace, J., M.J. Hayman, and J.E. Galan, *Signal transduction and invasion of epithelial cells by S. typhimurium.* Cell, 1993. **72**(4): p. 505-14.
44. Clerc, P.L., et al., *Internalization of Shigella flexneri into HeLa cells occurs without an increase in cytosolic Ca2+ concentration.* Infect Immun, 1989. **57**(9): p. 2919-22.
45. Hueck, C.J., *Type III protein secretion systems in bacterial pathogens of animals and plants.* Microbiol Mol Biol Rev, 1998. **62**(2): p. 379-433.
46. Iguchi, A., et al., *Complete genome sequence and comparative genome analysis of enteropathogenic Escherichia coli O127:H6 strain E2348/69.* J Bacteriol, 2009. **191**(1): p. 347-54.
47. Hayashi, T., et al., *Complete genome sequence of enterohemorrhagic Escherichia coli O157:H7 and genomic comparison with a laboratory strain K-12.* DNA Res, 2001. **8**(1): p. 11-22.
48. Hemrajani, C., et al., *NleH effectors interact with Bax inhibitor-1 to block apoptosis during enteropathogenic Escherichia coli infection.* Proc Natl Acad Sci U S A, 2010. **107**(7): p. 3129-34.
49. Dahan, S., et al., *EspJ is a prophage-carried type III effector protein of attaching and effacing pathogens that modulates infection dynamics.* Infect Immun, 2005. **73**(2): p. 679-86.
50. Newton, H.J., et al., *The type III effectors NleE and NleB from enteropathogenic E. coli and OspZ from Shigella block nuclear translocation of NF-kappaB p65.* PLoS Pathog, 2010. **6**(5): p. e1000898.
51. Kalman, D., et al., *Enteropathogenic E-coli acts through WASP and Arp2/3 complex to form actin pedestals.* Nature Cell Biology, 1999. **1**(6): p. 389-391.
52. Frankel, G. and A.D. Phillips, *Attaching effacing Escherichia coli and paradigms of Tir-triggered actin polymerization: getting off the pedestal.* Cell Microbiol, 2008. **10**(3): p. 549-56.
53. Gruenheid, S., et al., *Enteropathogenic E. coli Tir binds Nck to initiate actin pedestal formation in host cells.* Nat Cell Biol, 2001. **3**(9): p. 856-9.
54. Phillips, N., R.D. Hayward, and V. Koronakis, *Phosphorylation of the enteropathogenic E. coli receptor by the Src-family kinase c-Fyn triggers actin pedestal formation.* Nat Cell Biol, 2004. **6**(7): p. 618-25.
55. Campellone, K.G., et al., *Clustering of Nck by a 12-residue Tir phosphopeptide is sufficient to trigger localized actin assembly.* J Cell Biol, 2004. **164**(3): p. 407-16.
56. Campellone, K.G., D. Robbins, and J.M. Leong, *EspFU is a translocated EHEC effector that interacts with Tir and N-WASP and promotes Nck-independent actin assembly.* Dev Cell, 2004. **7**(2): p. 217-28.

57. Garmendia, J., et al., *TccP is an enterohaemorrhagic Escherichia coli O157:H7 type III effector protein that couples Tir to the actin-cytoskeleton.* Cell Microbiol, 2004. **6**(12): p. 1167-83.
58. Cheng, H.C., et al., *Structural mechanism of WASP activation by the enterohaemorrhagic E. coli effector EspF(U).* Nature, 2008. **454**(7207): p. 1009-13.
59. McGhie, E.J., R.D. Hayward, and V. Koronakis, *Control of actin turnover by a salmonella invasion protein.* Mol Cell, 2004. **13**(4): p. 497-510.
60. Chang, J., J. Chen, and D. Zhou, *Delineation and characterization of the actin nucleation and effector translocation activities of Salmonella SipC.* Mol Microbiol, 2005. **55**(5): p. 1379-89.
61. Zhou, D. and J. Galan, *Salmonella entry into host cells: the work in concert of type III secreted effector proteins.* Microbes Infect, 2001. **3**(14-15): p. 1293-8.
62. Schlumberger, M.C. and W.D. Hardt, *Salmonella type III secretion effectors: pulling the host cell's strings.* Curr Opin Microbiol, 2006. **9**(1): p. 46-54.
63. Terebiznik, M.R., et al., *Elimination of host cell PtdIns(4,5)P(2) by bacterial SigD promotes membrane fission during invasion by Salmonella.* Nature Cell Biology, 2002. **4**(10): p. 766-73.
64. Hernandez, L.D., et al., *Salmonella modulates vesicular traffic by altering phosphoinositide metabolism.* Science, 2004. **304**(5678): p. 1805-7.
65. Srikanth, C.V., et al., *Salmonella pathogenesis and processing of secreted effectors by caspase-3.* Science, 2010. **330**(6002): p. 390-3.
66. Garcia-del Portillo, F., et al., *Salmonella induces the formation of filamentous structures containing lysosomal membrane glycoproteins in epithelial cells.* Proc Natl Acad Sci U S A, 1993. **90**(22): p. 10544-8.
67. Stein, M.A., et al., *Identification of a Salmonella virulence gene required for formation of filamentous structures containing lysosomal membrane glycoproteins within epithelial cells.* Mol Microbiol, 1996. **20**(1): p. 151-64.
68. Beuzon, C.R., et al., *Salmonella maintains the integrity of its intracellular vacuole through the action of SifA.* EMBO J, 2000. **19**(13): p. 3235-49.
69. Hilbi, H., *Host responses to secreted Shigella virulence factors.* Curr Opin Infect Dis, 1999. **12**(3): p. 221-8.
70. Skoudy, A., et al., *CD44 binds to the Shigella IpaB protein and participates in bacterial invasion of epithelial cells.* Cell Microbiol, 2000. **2**(1): p. 19-33.
71. Watarai, M., S. Funato, and C. Sasakawa, *Interaction of Ipa proteins of Shigella flexneri with alpha5beta1 integrin promotes entry of the bacteria into mammalian cells.* J Exp Med, 1996. **183**(3): p. 991-9.
72. Tran Van Nhieu, G., et al., *IpaC induces actin polymerization and filopodia formation during Shigella entry into epithelial cells.* EMBO J, 1999. **18**(12): p. 3249-62.
73. Ohya, K., et al., *IpgB1 is a novel Shigella effector protein involved in bacterial invasion of host cells. Its activity to promote membrane ruffling via Rac1 and Cdc42 activation.* J Biol Chem, 2005. **280**(25): p. 24022-34.
74. Alto, N.M., et al., *Identification of a bacterial type III effector family with G protein mimicry functions.* Cell, 2006. **124**(1): p. 133-45.
75. Bourdet-Sicard, R., et al., *Binding of the Shigella protein IpaA to vinculin induces F-actin depolymerization.* EMBO J, 1999. **18**(21): p. 5853-62.
76. Yoshida, S., et al., *Shigella deliver an effector protein to trigger host microtubule destabilization, which promotes Rac1 activity and efficient bacterial internalization.* EMBO J, 2002. **21**(12): p. 2923-35.

77. High, N., et al., *IpaB of Shigella flexneri causes entry into epithelial cells and escape from the phagocytic vacuole.* EMBO J, 1992. **11**(5): p. 1991-9.
78. Fernandez-Prada, C.M., et al., *Shigella flexneri IpaH(7.8) facilitates escape of virulent bacteria from the endocytic vacuoles of mouse and human macrophages.* Infect Immun, 2000. **68**(6): p. 3608-19.
79. Niebuhr, K., et al., *Conversion of PtdIns(4,5)P(2) into PtdIns(5)P by the S.flexneri effector IpgD reorganizes host cell morphology.* EMBO J, 2002. **21**(19): p. 5069-78.
80. Goldberg, M.B. and J.A. Theriot, *Shigella flexneri surface protein IcsA is sufficient to direct actin-based motility.* Proc Natl Acad Sci U S A, 1995. **92**(14): p. 6572-6.
81. Egile, C., et al., *Activation of the CDC42 effector N-WASP by the Shigella flexneri IcsA protein promotes actin nucleation by Arp2/3 complex and bacterial actin-based motility.* J Cell Biol, 1999. **146**(6): p. 1319-32.
82. Suzuki, T., et al., *Neural Wiskott-Aldrich syndrome protein is implicated in the actin-based motility of Shigella flexneri.* EMBO J, 1998. **17**(10): p. 2767-76.
83. Suzuki, T., et al., *Neural Wiskott-Aldrich syndrome protein (N-WASP) is the specific ligand for Shigella VirG among the WASP family and determines the host cell type allowing actin-based spreading.* Cell Microbiol, 2002. **4**(4): p. 223-33.
84. Ogawa, M., et al., *Escape of intracellular Shigella from autophagy.* Science, 2005. **307**(5710): p. 727-31.
85. Yoshida, S., et al., *Microtubule-severing activity of Shigella is pivotal for intercellular spreading.* Science, 2006. **314**(5801): p. 985-9.
86. Bulgin, R., et al., *Bacterial guanine nucleotide exchange factors SopE-like and WxxxE effectors.* Infect Immun, 2010. **78**(4): p. 1417-25.
87. Hall, A., *Rho GTPases and the actin cytoskeleton.* Science, 1998. **279**(5350): p. 509-14.
88. Huang, Z., et al., *Structural insights into host GTPase isoform selection by a family of bacterial GEF mimics.* Nat Struct Mol Biol, 2009. **16**(8): p. 853-60.
89. Jaffe, A.B. and A. Hall, *Rho GTPases: biochemistry and biology.* Annu Rev Cell Dev Biol, 2005. **21**: p. 247-69.
90. Kenny, B., et al., *Co-ordinate regulation of distinct host cell signalling pathways by multifunctional enteropathogenic Escherichia coli effector molecules.* Mol Microbiol, 2002. **44**(4): p. 1095-1107.
91. Arbeloa, A., et al., *EspM2 is a RhoA guanine nucleotide exchange factor.* Cell Microbiol, 2010. **12**(5): p. 654-64.
92. Bulgin, R., et al., *The T3SS effector EspT defines a new category of invasive enteropathogenic E. coli (EPEC) which form intracellular actin pedestals.* PLoS Pathog, 2009. **5**(12): p. e1000683.
93. Tu, X., et al., *EspH, a new cytoskeleton-modulating effector of enterohaemorrhagic and enteropathogenic Escherichia coli.* Mol Microbiol, 2003. **47**(3): p. 595-606.
94. Dong, N., L. Liu, and F. Shao, *A bacterial effector targets host DH-PH domain RhoGEFs and antagonizes macrophage phagocytosis.* EMBO J, 2010. **29**(8): p. 1363-76.
95. Shaw, R.K., et al., *Enteropathogenic Escherichia coli type III effectors EspG and EspG2 disrupt the microtubule network of intestinal epithelial cells.* Infect Immun, 2005. **73**(7): p. 4385-90.
96. Boyle, E.C., N.F. Brown, and B.B. Finlay, *Salmonella enterica serovar Typhimurium effectors SopB, SopE, SopE2 and SipA disrupt tight junction structure and function.* Cell Microbiol, 2006. **8**(12): p. 1946-57.
97. Schuller, S., et al., *The ex vivo response of human intestinal mucosa to enteropathogenic Escherichia coli infection.* Cell Microbiol, 2009. **11**(3): p. 521-30.

98. Ruchaud-Sparagano, M.H., M. Maresca, and B. Kenny, *Enteropathogenic Escherichia coli (EPEC) inactivate innate immune responses prior to compromising epithelial barrier function.* Cell Microbiol, 2007. **9**(8): p. 1909-21.
99. Nadler, C., et al., *The type III secretion effector NleE inhibits NF-kappaB activation.* PLoS Pathog, 2010. **6**(1): p. e1000743.
100. Pearson, J.S., et al., *A type III effector protease NleC from enteropathogenic Escherichia coli targets NF-kappaB for degradation.* Mol Microbiol, 2011. **80**(1): p. 219-30.
101. Baruch, K., et al., *Metalloprotease type III effectors that specifically cleave JNK and NF-kappaB.* EMBO J, 2011. **30**(1): p. 221-31.
102. Hemrajani, C., et al., *Role of NleH, a type III secreted effector from attaching and effacing pathogens, in colonization of the bovine, ovine, and murine gut.* Infect Immun, 2008. **76**(11): p. 4804-13.
103. Royan, S.V., et al., *Enteropathogenic E. coli non-LEE encoded effectors NleH1 and NleH2 attenuate NF-kappaB activation.* Mol Microbiol, 2010. **78**(5): p. 1232-45.
104. Gao, X., et al., *Bacterial effector binding to ribosomal protein s3 subverts NF-kappaB function.* PLoS Pathog, 2009. **5**(12): p. e1000708.
105. Wan, F., et al., *IKKbeta phosphorylation regulates RPS3 nuclear translocation and NF-kappaB function during infection with Escherichia coli strain O157:H7.* Nat Immunol, 2011. **12**(4): p. 335-43.
106. Raymond, B., et al., *The WxxxE effector EspT triggers expression of immune mediators in an Erk/JNK and NF-kappaB-dependent manner.* Cell Microbiol, 2011. **13**(12): p. 1881-93.
107. Arbibe, L., et al., *An injected bacterial effector targets chromatin access for transcription factor NF-kappaB to alter transcription of host genes involved in immune responses.* Nat Immunol, 2007. **8**(1): p. 47-56.
108. Li, H., et al., *The phosphothreonine lyase activity of a bacterial type III effector family.* Science, 2007. **315**(5814): p. 1000-3.
109. Kramer, R.W., et al., *Yeast functional genomic screens lead to identification of a role for a bacterial effector in innate immunity regulation.* PLoS Pathog, 2007. **3**(2): p. e21.
110. Kim, D.W., et al., *The Shigella flexneri effector OspG interferes with innate immune responses by targeting ubiquitin-conjugating enzymes.* Proc Natl Acad Sci U S A, 2005. **102**(39): p. 14046-51.
111. Rohde, J.R., et al., *Type III secretion effectors of the IpaH family are E3 ubiquitin ligases.* Cell Host Microbe, 2007. **1**(1): p. 77-83.
112. Okuda, J., et al., *Shigella effector IpaH9.8 binds to a splicing factor U2AF(35) to modulate host immune responses.* Biochem Biophys Res Commun, 2005. **333**(2): p. 531-9.
113. Zurawski, D.V., et al., *Shigella flexneri type III secretion system effectors OspB and OspF target the nucleus to downregulate the host inflammatory response via interactions with retinoblastoma protein.* Mol Microbiol, 2009. **71**(2): p. 350-68.
114. Rytkonen, A., et al., *SseL, a Salmonella deubiquitinase required for macrophage killing and virulence.* Proc Natl Acad Sci U S A, 2007. **104**(9): p. 3502-7.
115. Worley, M.J., et al., *Salmonella typhimurium disseminates within its host by manipulating the motility of infected cells.* Proc Natl Acad Sci U S A, 2006. **103**(47): p. 17915-20.
116. Quitard, S., et al., *The enteropathogenic Escherichia coli EspF effector molecule inhibits PI-3 kinase-mediated uptake independently of mitochondrial targeting.* Cell Microbiol, 2006. **8**(6): p. 972-81.

117. Iizumi, Y., et al., *The enteropathogenic E. coli effector EspB facilitates microvillus effacing and antiphagocytosis by inhibiting myosin function.* Cell Host Microbe, 2007. **2**(6): p. 383-92.
118. Marches, O., et al., *EspJ of enteropathogenic and enterohaemorrhagic Escherichia coli inhibits opsono-phagocytosis.* Cell Microbiol, 2008. **10**(5): p. 1104-15.
119. Vazquez-Torres, A., et al., *Salmonella pathogenicity island 2-dependent evasion of the phagocyte NADPH oxidase.* Science, 2000. **287**(5458): p. 1655-8.
120. Chakravortty, D., I. Hansen-Wester, and M. Hensel, *Salmonella pathogenicity island 2 mediates protection of intracellular Salmonella from reactive nitrogen intermediates.* J Exp Med, 2002. **195**(9): p. 1155-66.
121. Hersh, D., et al., *The Salmonella invasin SipB induces macrophage apoptosis by binding to caspase-1.* Proc Natl Acad Sci U S A, 1999. **96**(5): p. 2396-401.
122. Hilbi, H., et al., *Shigella-induced apoptosis is dependent on caspase-1 which binds to IpaB.* J Biol Chem, 1998. **273**(49): p. 32895-900.
123. Zychlinsky, A., et al., *IpaB mediates macrophage apoptosis induced by Shigella flexneri.* Mol Microbiol, 1994. **11**(4): p. 619-27.
124. Sansonetti, P.J., et al., *Caspase-1 activation of IL-1beta and IL-18 are essential for Shigella flexneri-induced inflammation.* Immunity, 2000. **12**(5): p. 581-90.
125. Zychlinsky, A., et al., *Interleukin 1 is released by murine macrophages during apoptosis induced by Shigella flexneri.* J Clin Invest, 1994. **94**(3): p. 1328-32.
126. Crane, J.K., S. Majumdar, and D.F. Pickhardt, 3rd, *Host cell death due to enteropathogenic Escherichia coli has features of apoptosis.* Infect Immun, 1999. **67**(5): p. 2575-84.
127. Barnett Foster, D., et al., *Enterohemorrhagic Escherichia coli induces apoptosis which augments bacterial binding and phosphatidylethanolamine exposure on the plasma membrane outer leaflet.* Infect Immun, 2000. **68**(6): p. 3108-15.
128. Nougayrede, J.P. and M.S. Donnenberg, *Enteropathogenic Escherichia coli EspF is targeted to mitochondria and is required to initiate the mitochondrial death pathway.* Cell Microbiol, 2004. **6**(11): p. 1097-111.
129. Samba-Louaka, A., et al., *The enteropathogenic Escherichia coli effector Cif induces delayed apoptosis in epithelial cells.* Infect Immun, 2009. **77**(12): p. 5471-7.
130. Kim, M., et al., *Bacteria hijack integrin-linked kinase to stabilize focal adhesions and block cell detachment.* Nature, 2009. **459**(7246): p. 578-82.
131. Shames, S.R., et al., *The pathogenic E. coli type III effector EspZ interacts with host CD98 and facilitates host cell prosurvival signalling.* Cell Microbiol, 2010. **12**(9): p. 1322-39.
132. Clerc, P.L., et al., *Plasmid-mediated early killing of eucaryotic cells by Shigella flexneri as studied by infection of J774 macrophages.* Infect Immun, 1987. **55**(3): p. 521-7.
133. Monack, D.M., et al., *Salmonella typhimurium invasion induces apoptosis in infected macrophages.* Proc Natl Acad Sci U S A, 1996. **93**(18): p. 9833-8.
134. Hueffer, K. and J.E. Galan, *Salmonella-induced macrophage death: multiple mechanisms, different outcomes.* Cell Microbiol, 2004. **6**(11): p. 1019-25.
135. Hernandez, L.D., et al., *A Salmonella protein causes macrophage cell death by inducing autophagy.* J Cell Biol, 2003. **163**(5): p. 1123-31.
136. Jesenberger, V., et al., *Salmonella-induced caspase-2 activation in macrophages: a novel mechanism in pathogen-mediated apoptosis.* J Exp Med, 2000. **192**(7): p. 1035-46.

137. Collazo, C.M. and J.E. Galan, *The invasion-associated type III system of Salmonella typhimurium directs the translocation of Sip proteins into the host cell.* Mol Microbiol, 1997. **24**(4): p. 747-56.
138. van der Velden, A.W., et al., *Salmonella pathogenicity island 1-independent induction of apoptosis in infected macrophages by Salmonella enterica serotype typhimurium.* Infect Immun, 2000. **68**(10): p. 5702-9.
139. Monack, D.M., C.S. Detweiler, and S. Falkow, *Salmonella pathogenicity island 2-dependent macrophage death is mediated in part by the host cysteine protease caspase-1.* Cell Microbiol, 2001. **3**(12): p. 825-37.
140. Paesold, G., et al., *Genes in the Salmonella pathogenicity island 2 and the Salmonella virulence plasmid are essential for Salmonella-induced apoptosis in intestinal epithelial cells.* Cell Microbiol, 2002. **4**(11): p. 771-81.
141. Chen, Y., et al., *A bacterial invasin induces macrophage apoptosis by binding directly to ICE.* EMBO J, 1996. **15**(15): p. 3853-60.
142. Knodler, L.A., B.B. Finlay, and O. Steele-Mortimer, *The Salmonella effector protein SopB protects epithelial cells from apoptosis by sustained activation of Akt.* J Biol Chem, 2005. **280**(10): p. 9058-64.
143. Pendaries, C., et al., *PtdIns5P activates the host cell PI3-kinase/Akt pathway during Shigella flexneri infection.* EMBO J, 2006. **25**(5): p. 1024-34.
144. Kennedy, S.G., et al., *Akt/Protein kinase B inhibits cell death by preventing the release of cytochrome c from mitochondria.* Mol Cell Biol, 1999. **19**(8): p. 5800-10.
145. Clark, C.S. and A.T. Maurelli, *Shigella flexneri inhibits staurosporine-induced apoptosis in epithelial cells.* Infect Immun, 2007. **75**(5): p. 2531-9.
146. Mavris, M., et al., *Regulation of transcription by the activity of the Shigella flexneri type III secretion apparatus.* Mol Microbiol, 2002. **43**(6): p. 1543-53.
147. Parsot, C., et al., *A secreted anti-activator, OspD1, and its chaperone, Spa15, are involved in the control of transcription by the type III secretion apparatus activity in Shigella flexneri.* Mol Microbiol, 2005. **56**(6): p. 1627-35.
148. Kane, C.D., et al., *MxiE regulates intracellular expression of factors secreted by the Shigella flexneri 2a type III secretion system.* J Bacteriol, 2002. **184**(16): p. 4409-19.
149. Brennan, P.C., et al., *Citrobacter Freundii Associated with Diarrhea in a Laboratory Mice.* Lab Anim Care, 1965. **15**: p. 266-75.
150. Muto, T., et al., *Infectious megaenteron of mice. I. Manifestation and pathological observation.* Jpn J Med Sci Biol, 1969. **22**(6): p. 363-74.
151. Ediger, R.D., R.M. Kovatch, and M.M. Rabstein, *Colitis in mice with a high incidence of rectal prolapse.* Lab Anim Sci, 1974. **24**(3): p. 488-94.
152. Schauer, D.B., et al., *Genetic and biochemical characterization of Citrobacter rodentium sp. nov.* J Clin Microbiol, 1995. **33**(8): p. 2064-8.
153. Luperchio, S.A., et al., *Citrobacter rodentium, the causative agent of transmissible murine colonic hyperplasia, exhibits clonality: synonymy of C. rodentium and mouse-pathogenic Escherichia coli.* J Clin Microbiol, 2000. **38**(12): p. 4343-50.
154. Mundy, R., et al., *Citrobacter rodentium of mice and man.* Cell Microbiol, 2005. **7**(12): p. 1697-706.
155. Deng, W., et al., *Citrobacter rodentium translocated intimin receptor (Tir) is an essential virulence factor needed for actin condensation, intestinal colonization and colonic hyperplasia in mice.* Mol Microbiol, 2003. **48**(1): p. 95-115.
156. Mundy, R., et al., *Identification of a novel type IV pilus gene cluster required for gastrointestinal colonization of Citrobacter rodentium.* Mol Microbiol, 2003. **48**(3): p. 795-809.

157. Mundy, R., et al., *Distribution of espI among clinical enterohaemorrhagic and enteropathogenic Escherichia coli isolates.* J Med Microbiol, 2004. **53**(Pt 11): p. 1145-9.
158. Deng, W., et al., *Dissecting virulence: systematic and functional analyses of a pathogenicity island.* Proc Natl Acad Sci U S A, 2004. **101**(10): p. 3597-602.
159. Majno, G. and I. Joris, *Apoptosis, oncosis, and necrosis. An overview of cell death.* Am J Pathol, 1995. **146**(1): p. 3-15.
160. Kroemer, G., et al., *Classification of cell death: recommendations of the Nomenclature Committee on Cell Death 2009.* Cell Death Differ, 2009. **16**(1): p. 3-11.
161. Saikumar, P., et al., *Apoptosis: definition, mechanisms, and relevance to disease.* Am J Med, 1999. **107**(5): p. 489-506.
162. Fink, S.L. and B.T. Cookson, *Apoptosis, pyroptosis, and necrosis: mechanistic description of dead and dying eukaryotic cells.* Infect Immun, 2005. **73**(4): p. 1907-16.
163. Rudel, T., O. Kepp, and V. Kozjak-Pavlovic, *Interactions between bacterial pathogens and mitochondrial cell death pathways.* Nat Rev Microbiol, 2010. **8**(10): p. 693-705.
164. Taylor, R.C., S.P. Cullen, and S.J. Martin, *Apoptosis: controlled demolition at the cellular level.* Nat Rev Mol Cell Biol, 2008. **9**(3): p. 231-41.
165. Elmore, S., *Apoptosis: a review of programmed cell death.* Toxicol Pathol, 2007. **35**(4): p. 495-516.
166. Willingham, S.B., et al., *Microbial pathogen-induced necrotic cell death mediated by the inflammasome components CIAS1/cryopyrin/NLRP3 and ASC.* Cell Host Microbe, 2007. **2**(3): p. 147-59.
167. Chwieralski, C.E., T. Welte, and F. Buhling, *Cathepsin-regulated apoptosis.* Apoptosis, 2006. **11**(2): p. 143-9.
168. Hitomi, J., et al., *Identification of a molecular signaling network that regulates a cellular necrotic cell death pathway.* Cell, 2008. **135**(7): p. 1311-23.
169. Galluzzi, L. and G. Kroemer, *Necroptosis: a specialized pathway of programmed necrosis.* Cell, 2008. **135**(7): p. 1161-3.
170. Degterev, A., et al., *Identification of RIP1 kinase as a specific cellular target of necrostatins.* Nat Chem Biol, 2008. **4**(5): p. 313-21.
171. Yu, S.W., et al., *Mediation of poly(ADP-ribose) polymerase-1-dependent cell death by apoptosis-inducing factor.* Science, 2002. **297**(5579): p. 259-63.
172. Andrabi, S.A., T.M. Dawson, and V.L. Dawson, *Mitochondrial and nuclear cross talk in cell death: parthanatos.* Ann N Y Acad Sci, 2008. **1147**: p. 233-41.
173. Zong, W.X., et al., *Alkylating DNA damage stimulates a regulated form of necrotic cell death.* Genes Dev, 2004. **18**(11): p. 1272-82.
174. Nicholson, D.W. and N.A. Thornberry, *Caspases: killer proteases.* Trends Biochem Sci, 1997. **22**(8): p. 299-306.
175. Cohen, G.M., *Caspases: the executioners of apoptosis.* Biochem J, 1997. **326 (Pt 1)**: p. 1-16.
176. Riedl, S.J. and Y. Shi, *Molecular mechanisms of caspase regulation during apoptosis.* Nat Rev Mol Cell Biol, 2004. **5**(11): p. 897-907.
177. Wang, X., *The expanding role of mitochondria in apoptosis.* Genes Dev, 2001. **15**(22): p. 2922-33.
178. Green, D.R., *Apoptotic pathways: ten minutes to dead.* Cell, 2005. **121**(5): p. 671-4.
179. Youle, R.J. and A. Strasser, *The BCL-2 protein family: opposing activities that mediate cell death.* Nat Rev Mol Cell Biol, 2008. **9**(1): p. 47-59.

180. Huang, D.C. and A. Strasser, *BH3-Only proteins-essential initiators of apoptotic cell death.* Cell, 2000. **103**(6): p. 839-42.
181. Willis, S.N. and J.M. Adams, *Life in the balance: how BH3-only proteins induce apoptosis.* Curr Opin Cell Biol, 2005. **17**(6): p. 617-25.
182. Cullen, S.P. and S.J. Martin, *Mechanisms of granule-dependent killing.* Cell Death Differ, 2008. **15**(2): p. 251-62.
183. Danial, N.N. and S.J. Korsmeyer, *Cell death: critical control points.* Cell, 2004. **116**(2): p. 205-19.
184. Brini, M. and E. Carafoli, *Calcium pumps in health and disease.* Physiol Rev, 2009. **89**(4): p. 1341-78.
185. Berridge, M.J., M.D. Bootman, and P. Lipp, *Calcium--a life and death signal.* Nature, 1998. **395**(6703): p. 645-8.
186. Rizzuto, R., et al., *Close contacts with the endoplasmic reticulum as determinants of mitochondrial Ca2+ responses.* Science, 1998. **280**(5370): p. 1763-6.
187. Berridge, M.J., *The endoplasmic reticulum: a multifunctional signaling organelle.* Cell Calcium, 2002. **32**(5-6): p. 235-49.
188. Clapham, D.E., *Calcium signaling.* Cell, 2007. **131**(6): p. 1047-58.
189. Michelangeli, F., O.A. Ogunbayo, and L.L. Wootton, *A plethora of interacting organellar Ca2+ stores.* Curr Opin Cell Biol, 2005. **17**(2): p. 135-40.
190. Carafoli, E., *Calcium signaling: a tale for all seasons.* Proc Natl Acad Sci U S A, 2002. **99**(3): p. 1115-22.
191. Wei, M.C., et al., *Proapoptotic BAX and BAK: a requisite gateway to mitochondrial dysfunction and death.* Science, 2001. **292**(5517): p. 727-30.
192. Foyouzi-Youssefi, R., et al., *Bcl-2 decreases the free Ca2+ concentration within the endoplasmic reticulum.* Proc Natl Acad Sci U S A, 2000. **97**(11): p. 5723-8.
193. Demaurex, N. and C. Distelhorst, *Cell biology. Apoptosis--the calcium connection.* Science, 2003. **300**(5616): p. 65-7.
194. Suzuki, Y., et al., *HAX-1, a novel intracellular protein, localized on mitochondria, directly associates with HS1, a substrate of Src family tyrosine kinases.* J Immunol, 1997. **158**(6): p. 2736-44.
195. Fadeel, B. and E. Grzybowska, *HAX-1: a multifunctional protein with emerging roles in human disease.* Biochim Biophys Acta, 2009. **1790**(10): p. 1139-48.
196. Yap, S.V., et al., *HAX-1: a multifaceted antiapoptotic protein localizing in the mitochondria and the sarcoplasmic reticulum of striated muscle cells.* J Mol Cell Cardiol, 2010. **48**(6): p. 1266-79.
197. Kang, Y.J., et al., *Molecular interaction between HAX-1 and XIAP inhibits apoptosis.* Biochem Biophys Res Commun, 2010. **393**(4): p. 794-9.
198. Han, Y., et al., *Overexpression of HAX-1 protects cardiac myocytes from apoptosis through caspase-9 inhibition.* Circ Res, 2006. **99**(4): p. 415-23.
199. Lee, A.Y., et al., *HS 1-associated protein X-1 is cleaved by caspase-3 during apoptosis.* Mol Cells, 2008. **25**(1): p. 86-90.
200. Han, J., et al., *Deregulation of mitochondrial membrane potential by mitochondrial insertion of granzyme B and direct Hax-1 cleavage.* J Biol Chem, 2010. **285**(29): p. 22461-72.
201. Gallagher, A.R., et al., *The polycystic kidney disease protein PKD2 interacts with Hax-1, a protein associated with the actin cytoskeleton.* Proc Natl Acad Sci U S A, 2000. **97**(8): p. 4017-22.
202. Koulen, P., et al., *Polycystin-2 is an intracellular calcium release channel.* Nat Cell Biol, 2002. **4**(3): p. 191-7.

203. Wegierski, T., et al., *TRPP2 channels regulate apoptosis through the Ca2+ concentration in the endoplasmic reticulum.* EMBO J, 2009. **28**(5): p. 490-9.
204. Sammels, E., et al., *Polycystin-2 activation by inositol 1,4,5-trisphosphate-induced Ca2+ release requires its direct association with the inositol 1,4,5-trisphosphate receptor in a signaling microdomain.* J Biol Chem, 2010. **285**(24): p. 18794-805.
205. Vafiadaki, E., et al., *The anti-apoptotic protein HAX-1 interacts with SERCA2 and regulates its protein levels to promote cell survival.* Mol Biol Cell, 2009. **20**(1): p. 306-18.
206. Cilenti, L., et al., *Regulation of HAX-1 anti-apoptotic protein by Omi/HtrA2 protease during cell death.* J Biol Chem, 2004. **279**(48): p. 50295-301.
207. Bouwmeester, T., et al., *A physical and functional map of the human TNF-alpha/NF-kappa B signal transduction pathway.* Nat Cell Biol, 2004. **6**(2): p. 97-105.
208. Yedavalli, V.S., et al., *Human immunodeficiency virus type 1 Vpr interacts with antiapoptotic mitochondrial protein HAX-1.* J Virol, 2005. **79**(21): p. 13735-46.
209. Modem, S. and T.R. Reddy, *An anti-apoptotic protein, Hax-1, inhibits the HIV-1 rev function by altering its sub-cellular localization.* J Cell Physiol, 2008. **214**(1): p. 14-9.
210. Kawaguchi, Y., et al., *Interaction of Epstein-Barr virus nuclear antigen leader protein (EBNA-LP) with HS1-associated protein X-1: implication of cytoplasmic function of EBNA-LP.* J Virol, 2000. **74**(21): p. 10104-11.
211. Dufva, M., M. Olsson, and L. Rymo, *Epstein-Barr virus nuclear antigen 5 interacts with HAX-1, a possible component of the B-cell receptor signalling pathway.* J Gen Virol, 2001. **82**(Pt 7): p. 1581-7.
212. Johns, H.L., et al., *The classical swine fever virus N-terminal protease N(pro) binds to cellular HAX-1.* J Gen Virol, 2010. **91**(Pt 11): p. 2677-86.
213. Tobe, T., et al., *An extensive repertoire of type III secretion effectors in Escherichia coli O157 and the role of lambdoid phages in their dissemination.* Proceedings of the National Academy of Sciences of the United States of America, 2006. **103**(40): p. 14941-14946.
214. Morita-Ishihara, T., et al., *EspO1-2 regulates EspM2-mediated RhoA activity to stabilize formation of focal adhesions in enterohemorrhagic Escherichia coli-infected host cells.* PLoS One, 2013. **8**(2): p. e55960.
215. Datsenko, K.A. and B.L. Wanner, *One-step inactivation of chromosomal genes in Escherichia coli K-12 using PCR products.* Proc Natl Acad Sci U S A, 2000. **97**(12): p. 6640-5.
216. Gietz, R.D. and R.H. Schiestl, *Quick and easy yeast transformation using the LiAc/SS carrier DNA/PEG method.* Nat Protoc, 2007. **2**(1): p. 35-7.
217. Gietz, R.D. and R.H. Schiestl, *Frozen competent yeast cells that can be transformed with high efficiency using the LiAc/SS carrier DNA/PEG method.* Nat Protoc, 2007. **2**(1): p. 1-4.
218. Levine, M.M., et al., *Escherichia coli strains that cause diarrhoea but do not produce heat-labile or heat-stable enterotoxins and are non-invasive.* Lancet, 1978. **1**(8074): p. 1119-22.
219. Schlosser-Silverman, E., et al., *Characterization of Escherichia coli DNA lesions generated within J774 macrophages.* J Bacteriol, 2000. **182**(18): p. 5225-30.
220. Hageman, J., et al., *A DNAJB chaperone subfamily with HDAC-dependent activities suppresses toxic protein aggregation.* Mol Cell, 2010. **37**(3): p. 355-69.
221. De Bock, C.E., et al., *Interaction between urokinase receptor and heat shock protein MRJ enhances cell adhesion.* Int J Oncol, 2010. **36**(5): p. 1155-63.

222. Watson, E.D., et al., *The Mrj co-chaperone mediates keratin turnover and prevents the formation of toxic inclusion bodies in trophoblast cells of the placenta.* Development, 2007. **134**(9): p. 1809-17.
223. Dey, S., P. Banerjee, and P. Saha, *Cell cycle specific expression and nucleolar localization of human J-domain containing co-chaperone Mrj.* Mol Cell Biochem, 2009. **322**(1-2): p. 137-42.
224. Hurst, D.R., et al., *Breast cancer metastasis suppressor 1 (BRMS1) is stabilized by the Hsp90 chaperone.* Biochem Biophys Res Commun, 2006. **348**(4): p. 1429-35.
225. Zhang, Y., *I-TASSER server for protein 3D structure prediction.* BMC Bioinformatics, 2008. **9**: p. 40.
226. Roy, A., A. Kucukural, and Y. Zhang, *I-TASSER: a unified platform for automated protein structure and function prediction.* Nat Protoc, 2010. **5**(4): p. 725-38.
227. Knodler, L.A. and O. Steele-Mortimer, *The Salmonella effector PipB2 affects late endosome/lysosome distribution to mediate Sif extension.* Mol Biol Cell, 2005. **16**(9): p. 4108-23.
228. Knodler, L.A., et al., *Salmonella type III effectors PipB and PipB2 are targeted to detergent-resistant microdomains on internal host cell membranes.* Mol Microbiol, 2003. **49**(3): p. 685-704.
229. Henry, T., et al., *The Salmonella effector protein PipB2 is a linker for kinesin-1.* Proc Natl Acad Sci U S A, 2006. **103**(36): p. 13497-502.
230. Sharp, T.V., et al., *K15 protein of Kaposi's sarcoma-associated herpesvirus is latently expressed and binds to HAX-1, a protein with antiapoptotic function.* J Virol, 2002. **76**(2): p. 802-16.
231. Bolte, S. and F.P. Cordelieres, *A guided tour into subcellular colocalization analysis in light microscopy.* J Microsc, 2006. **224**(Pt 3): p. 213-32.
232. Manders, E.M., et al., *Dynamics of three-dimensional replication patterns during the S-phase, analysed by double labelling of DNA and confocal microscopy.* J Cell Sci, 1992. **103 (Pt 3)**: p. 857-62.
233. Costes, S.V., et al., *Automatic and quantitative measurement of protein-protein colocalization in live cells.* Biophys J, 2004. **86**(6): p. 3993-4003.
234. van Steensel, B., et al., *Partial colocalization of glucocorticoid and mineralocorticoid receptors in discrete compartments in nuclei of rat hippocampus neurons.* J Cell Sci, 1996. **109 (Pt 4)**: p. 787-92.
235. Li, Q., et al., *A syntaxin 1, Galpha(o), and N-type calcium channel complex at a presynaptic nerve terminal: analysis by quantitative immunocolocalization.* J Neurosci, 2004. **24**(16): p. 4070-81.
236. Deng, W., et al., *A comprehensive proteomic analysis of the type III secretome of Citrobacter rodentium.* J Biol Chem, 2010. **285**(9): p. 6790-800.
237. Kawai, T. and S. Akira, *Innate immune recognition of viral infection.* Nat Immunol, 2006. **7**(2): p. 131-7.
238. Abreu, M.T., *Toll-like receptor signalling in the intestinal epithelium: how bacterial recognition shapes intestinal function.* Nat Rev Immunol, 2010. **10**(2): p. 131-44.
239. Shaw, M.H., et al., *NOD-like receptors (NLRs): bona fide intracellular microbial sensors.* Curr Opin Immunol, 2008. **20**(4): p. 377-82.
240. Rakoff-Nahoum, S., et al., *Recognition of commensal microflora by toll-like receptors is required for intestinal homeostasis.* Cell, 2004. **118**(2): p. 229-41.
241. Cario, E., *Bacterial interactions with cells of the intestinal mucosa: Toll-like receptors and NOD2.* Gut, 2005. **54**(8): p. 1182-93.

242. Marina-Garcia, N., et al., *Pannexin-1-mediated intracellular delivery of muramyl dipeptide induces caspase-1 activation via cryopyrin/NLRP3 independently of Nod2.* J Immunol, 2008. **180**(6): p. 4050-7.
243. Krieg, A., et al., *XIAP mediates NOD signaling via interaction with RIP2.* Proc Natl Acad Sci U S A, 2009. **106**(34): p. 14524-9.
244. Damgaard, R.B., et al., *The ubiquitin ligase XIAP recruits LUBAC for NOD2 signaling in inflammation and innate immunity.* Mol Cell, 2012. **46**(6): p. 746-58.
245. Chen, Z.J., *Ubiquitin signalling in the NF-kappaB pathway.* Nature Cell Biology, 2005. **7**(8): p. 758-65.
246. Ye, Y. and M. Rape, *Building ubiquitin chains: E2 enzymes at work.* Nat Rev Mol Cell Biol, 2009. **10**(11): p. 755-64.
247. Wu, B., et al., *NleG Type 3 effectors from enterohaemorrhagic Escherichia coli are U-Box E3 ubiquitin ligases.* PLoS Pathog, 2010. **6**(6): p. e1000960.
248. Singer, A.U., et al., *Structure of the Shigella T3SS effector IpaH defines a new class of E3 ubiquitin ligases.* Nat Struct Mol Biol, 2008. **15**(12): p. 1293-301.
249. Miao, E.A., et al., *Salmonella typhimurium leucine-rich repeat proteins are targeted to the SPI1 and SPI2 type III secretion systems.* Mol Microbiol, 1999. **34**(4): p. 850-64.
250. Bernal-Bayard, J. and F. Ramos-Morales, *Salmonella type III secretion effector SlrP is an E3 ubiquitin ligase for mammalian thioredoxin.* J Biol Chem, 2009. **284**(40): p. 27587-95.
251. Diao, J., et al., *Crystal structure of SopA, a Salmonella effector protein mimicking a eukaryotic ubiquitin ligase.* Nat Struct Mol Biol, 2008. **15**(1): p. 65-70.
252. Galban, S. and C.S. Duckett, *XIAP as a ubiquitin ligase in cellular signaling.* Cell Death Differ, 2010. **17**(1): p. 54-60.
253. Huang, Y., et al., *Requirement of both the second and third BIR domains for the relief of X-linked inhibitor of apoptosis protein (XIAP)-mediated caspase inhibition by Smac.* J Biol Chem, 2003. **278**(49): p. 49517-22.
254. Ramsay, A.G., et al., *HS1-associated protein X-1 regulates carcinoma cell migration and invasion via clathrin-mediated endocytosis of integrin alphavbeta6.* Cancer Res, 2007. **67**(11): p. 5275-84.
255. Yap, S.V., J.M. Koontz, and A. Kontrogianni-Konstantopoulos, *HAX-1: A family of apoptotic regulators in health and disease.* J Cell Physiol, 2011.
256. Zurawski, D.V., et al., *The NleE/OspZ family of effector proteins is required for polymorphonuclear transepithelial migration, a characteristic shared by enteropathogenic Escherichia coli and Shigella flexneri infections.* Infect Immun, 2008. **76**(1): p. 369-79.
257. Savkovic, S.D., A. Koutsouris, and G. Hecht, *Attachment of a noninvasive enteric pathogen, enteropathogenic Escherichia coli, to cultured human intestinal epithelial monolayers induces transmigration of neutrophils.* Infect Immun, 1996. **64**(11): p. 4480-7.
258. McCormick, B.A., A.M. Siber, and A.T. Maurelli, *Requirement of the Shigella flexneri virulence plasmid in the ability to induce trafficking of neutrophils across polarized monolayers of the intestinal epithelium.* Infect Immun, 1998. **66**(9): p. 4237-43.
259. Perdomo, J.J., P. Gounon, and P.J. Sansonetti, *Polymorphonuclear leukocyte transmigration promotes invasion of colonic epithelial monolayer by Shigella flexneri.* J Clin Invest, 1994. **93**(2): p. 633-43.
260. Hisamatsu, T., et al., *CARD15/NOD2 functions as an antibacterial factor in human intestinal epithelial cells.* Gastroenterology, 2003. **124**(4): p. 993-1000.

261. Kobayashi, K.S., et al., *Nod2-dependent regulation of innate and adaptive immunity in the intestinal tract.* Science, 2005. **307**(5710): p. 731-4.
262. Chin, A.I., et al., *Involvement of receptor-interacting protein 2 in innate and adaptive immune responses.* Nature, 2002. **416**(6877): p. 190-4.
263. Rigaud, S., et al., *XIAP deficiency in humans causes an X-linked lymphoproliferative syndrome.* Nature, 2006. **444**(7115): p. 110-4.
264. Rigaud, S., et al., *Human X-linked variable immunodeficiency caused by a hypomorphic mutation in XIAP in association with a rare polymorphism in CD40LG.* Blood, 2011. **118**(2): p. 252-61.
265. Ogura, Y., et al., *A frameshift mutation in NOD2 associated with susceptibility to Crohn's disease.* Nature, 2001. **411**(6837): p. 603-6.
266. Hugot, J.P., et al., *Association of NOD2 leucine-rich repeat variants with susceptibility to Crohn's disease.* Nature, 2001. **411**(6837): p. 599-603.
267. Li, J., et al., *Regulation of IL-8 and IL-1beta expression in Crohn's disease associated NOD2/CARD15 mutations.* Hum Mol Genet, 2004. **13**(16): p. 1715-25.
268. Klein, C., et al., *HAX1 deficiency causes autosomal recessive severe congenital neutropenia (Kostmann disease).* Nat Genet, 2007. **39**(1): p. 86-92.
269. von Blume, J., et al., *Phosphorylation at Ser244 by CK1 determines nuclear localization and substrate targeting of PKD2.* EMBO J, 2007. **26**(22): p. 4619-33.
270. Papazyan, R., E. Rozengurt, and O. Rey, *The C-terminal tail of protein kinase D2 and protein kinase D3 regulates their intracellular distribution.* Biochem Biophys Res Commun, 2006. **342**(3): p. 685-9.
271. Chiu, T.T., et al., *Protein kinase D2 mediates lysophosphatidic acid-induced interleukin 8 production in nontransformed human colonic epithelial cells through NF-kappaB.* Am J Physiol Cell Physiol, 2007. **292**(2): p. C767-77.
272. Boucher, C. and R. Sandford, *Autosomal dominant polycystic kidney disease (ADPKD, MIM 173900, PKD1 and PKD2 genes, protein products known as polycystin-1 and polycystin-2).* Eur J Hum Genet, 2004. **12**(5): p. 347-54.
273. Coca, S.G., et al., *Biomarkers for the diagnosis and risk stratification of acute kidney injury: a systematic review.* Kidney Int, 2008. **73**(9): p. 1008-16.
274. Parikh, C.R., et al., *Evaluation of urine biomarkers of kidney injury in polycystic kidney disease.* Kidney Int, 2012. **81**(8): p. 784-90.
275. Flo, T.H., et al., *Lipocalin 2 mediates an innate immune response to bacterial infection by sequestrating iron.* Nature, 2004. **432**(7019): p. 917-21.
276. Schmidt-Ott, K.M., et al., *Dual action of neutrophil gelatinase-associated lipocalin.* J Am Soc Nephrol, 2007. **18**(2): p. 407-13.
277. Bolignano, D., et al., *Neutrophil gelatinase-associated lipocalin (NGAL) as a marker of kidney damage.* Am J Kidney Dis, 2008. **52**(3): p. 595-605.
278. Trachtman, H., et al., *Urinary neutrophil gelatinase-associated lipocalcin in D+HUS: a novel marker of renal injury.* Pediatr Nephrol, 2006. **21**(7): p. 989-94.
279. Wasilewska, A., et al., *KIM-1 and NGAL: new markers of obstructive nephropathy.* Pediatr Nephrol, 2011. **26**(4): p. 579-86.